

The Pennsylvania State University  
The Graduate School  
Department of Mechanical and Nuclear Engineering

**COMPUTER AIDED DESIGN, SIMULATION AND TRANSMISSION  
ERROR ANALYSIS OF A FACE GEAR PAIR**

A Thesis in  
Mechanical Engineering

by  
Erick W. Froede

© 2013 Erick W. Froede

Submitted in Partial Fulfillment  
of the Requirements  
for the Degree of

Master of Science

August 2013

The thesis of Erick W. Froede was reviewed and approved\* by the following:

Martin Trethewey  
Professor of Mechanical Engineering  
Thesis Co-Advisor

Suren Rao  
Senior Scientist  
Thesis Co-Advisor

H.J. Sommer III  
Professor of Mechanical Engineering  
Thesis Reader

Karen A. Thole  
Professor of Mechanical Engineering  
Head of Department of Mechanical Engineering

\*Signatures are on file in the Graduate School

## ABSTRACT

In recent years, there has been significant interest in the development of new and innovative rotorcraft gearboxes. Future helicopter transmissions aim to reduce overall gear train weight while maintaining efficiency and reliability. The Pericyclic Mechanical Transmission (PMT) is one of the compelling candidates that can achieve these goals. It consists of a high reduction ratio, high tooth contact ratio, and nutating/rotating mechanism which incorporates meshing conjugate face gear (FG) pairs. The use of a FG pair is novel for aerospace applications, and represents a new area of research. Accordingly, there is a distinct knowledge gap that must be bridged for this technology to become a reality. With the intention of supporting that effort, this investigation consisted of three key areas: 1) applying commercial modeling and simulation software; 2) conducting transmission error (TE) analysis, and; 3) exploring the performance of a FG pair. The first objective was achieved by generating the FG models with SolidWorks 2012-2013 and then introducing them to the commercial simulation package Abaqus 6.12-2 to evaluate static transmission error (TE). A novel three-dimensional expression of TE was specifically developed for use in a FG pair. When the simulation data was post processed it showed that the FG pair is capable of a peak-to-peak static TE of 0.382  $\mu\text{m}$ . This result is significantly less than typical values found in industry, which bodes well for future applications. In addition, the physics of the system were well represented, with fluctuations in TE corresponding to teeth entering and leaving the FG mesh, stress concentrations on the inner tooth radius, and clearly visible contact lines (as a function of contact pressure) along a plane of contact. All of these behaviors were predicted by previous literature, and helped build confidence in the simulation. Lastly, the entire process was documented, providing a complete evaluation package for the future. These results represent original contributions to the understanding of a FG pair, which will be integral to developing the PMT as a viable next-generation solution for demanding aerospace applications.

## TABLE OF CONTENTS

LIST OF FIGURES .....	vi
LIST OF TABLES.....	x
LIST OF EQUATIONS .....	xi
LIST OF SYMBOLS.....	xii
LIST OF ABBREVIATIONS.....	xiii
ACKNOWLEDGEMENTS.....	xiv
Chapter 1 Introduction .....	1
1.1 Fundamentals of Gear Design.....	2
1.2 Overview of the Pericyclic Mechanical Transmission.....	6
1.3 Problem Statement .....	9
1.4 Research Objectives .....	10
1.5 Scope and Assumptions .....	12
1.6 Outline of Thesis.....	12
Chapter 2 Literature Review .....	15
2.1 Transmission Error.....	15
2.2 Gear Performance Simulation .....	16
Chapter 3 Face Gear Model Assembly .....	19
3.1 A Note on Contact Line Generation.....	20
3.2 Step #1: Create Tooth Surface .....	22
3.3 Step #2: Develop Tooth Features .....	24
3.4 Step #3: Generate Complete Gear.....	27
3.4.1 Optional Feature Refinement .....	28
3.5 Summary .....	29
Chapter 4 Face Gear Simulation Development.....	31
4.1 A Note on Abaqus Implementation.....	32
4.2 Step #1: Import Part .....	34
4.3 Step #2: Apply Properties .....	35
4.4 Step #3: Create Assembly .....	37
4.5 Step #4: Define Steps .....	41
4.6 Step #5: Add Interactions.....	43
4.7 Step #6: Create Loads .....	46
4.8 Step #7: Develop Mesh .....	48
4.9 Step #8: Run Job .....	50

4.9.1 Optional Cluster Simulation.....	51
4.10 Summary .....	53
Chapter 5 Post Processing and Results .....	58
5.1 Analysis.....	71
5.2 Summary .....	80
Chapter 6 Conclusion.....	82
6.1 Future Work .....	84
Appendix A SolidWorks: FeatureManager Design Tree .....	86
Appendix B SolidWorks: Detailed Menu Items .....	87
Appendix C FG Design Parameters .....	97
Appendix D Spur Gear Test.....	99
Appendix E Abaqus: Model Tree .....	101
Appendix F Abaqus: Detailed Menu Items.....	102
Appendix G PBS Script .....	110
Appendix H Computational Comparison Model and Parameters .....	111
Appendix I Sample Simulation Data .....	112
Appendix J MATLAB Transmission Error Analysis Code .....	113
Appendix K MATLAB Stiffness Analysis Code.....	120
References.....	121

## LIST OF FIGURES

Figure 1: Common Gear Terminology [9].....	5
Figure 2: FG with an Intersected Axis Spur Pinion [11] .....	6
Figure 3: Basic Cross Section of the PMT [5].....	7
Figure 4: Pitch Cones of the External and Internal FG [5] .....	8
Figure 5: Twin PMT Design [5] .....	8
Figure 6: Summary of Research Objectives .....	11
Figure 7: Flow Chart for FG Analysis .....	14
Figure 8: Summary of Modeling Procedures Used for FG Generation in SolidWorks .....	19
Figure 9: MATLAB Generated FG Tooth Form .....	21
Figure 10: MATLAB Generated Assembly.....	21
Figure 11: Contact Lines after Import (Isometric View) .....	22
Figure 12: Boundary Surfaces Created from the Mirrored Contact Lines .....	23
Figure 13: Root Form Developed Using Ruled Surfaces .....	24
Figure 14: Bulk of the Tooth Created Through an Extrusion .....	25
Figure 15: Trimmed Tooth Form after a Revolved Cut.....	26
Figure 16: A Complete Single Tooth.....	27
Figure 17: The Resulting FG Model (Internal).....	28
Figure 18: Detailed View of Fillets and Chamfers (Outer FG Radii Not Shown).....	29
Figure 19: Summary of Simulation Procedures Used for FG Generation in Abaqus .....	32
Figure 20: Internal FG after Abaqus Part Import.....	35
Figure 21: Outermost Point of the External FG.....	39
Figure 22: Completed FG Assembly .....	40
Figure 23: Detail View of Assembly Features.....	40

Figure 24: Points Available for Selection .....	41
Figure 25: Selection of Tooth Face Surfaces .....	43
Figure 26: Selection of the FG Bore .....	45
Figure 27: Final Form of the FG System .....	46
Figure 28: The Fully Meshed FG Assembly.....	49
Figure 29: Plot of Percent Error between Abaqus Distributed Solution and MATLAB Analytical Solution .....	53
Figure 30: Overall von Mises Stresses.....	59
Figure 31: Closeup of von Mises Stresses .....	60
Figure 32: Closeup of Contact Pressure.....	61
Figure 33: Difference in Angular Position vs. Time.....	63
Figure 34: Difference in Angular Position vs. Rotation .....	63
Figure 35: TE vs. Time .....	65
Figure 36: TE vs. Rotation.....	65
Figure 37: TE vs. Rotation, per Tooth .....	66
Figure 38: Transmission Error Vector Geometry .....	67
Figure 39: Pitch Circle and Associated Relations.....	67
Figure 40: TEVM vs. Time.....	69
Figure 41: TEVM vs. Rotation .....	69
Figure 42: TEVM (Modified) vs. Rotation.....	70
Figure 43: TEVM (Modified) vs. Rotation, per Tooth .....	71
Figure 44: Closeup of Contact Pressure, Early .....	72
Figure 45: Closeup of Contact Pressure, Midpoint.....	72
Figure 46: Closeup of Contact Pressure, Late.....	73
Figure 47: Closeup of Contact Line Progression .....	74

Figure 48: Simulated and Calculated Angular Position vs. Rotation.....	75
Figure 49: $\Delta\theta_2$ vs. Rotation.....	76
Figure 50: TE vs. Rotation with Tooth Period Indicators.....	77
Figure 51: TEVM (Modified) vs. Rotation with Tooth Period Indicators.....	78
Figure 52: SolidWorks FeatureManager Design Tree for FG Generation.....	86
Figure 53: Curve Import Menu Item.....	87
Figure 54: Mirror Menu Item.....	88
Figure 55: Boundary Surface Menu Item.....	89
Figure 56: Ruled Surface Menu Item.....	90
Figure 57: Extrude Menu Item.....	91
Figure 58: Cut Menu Item.....	92
Figure 59: Revolved Boss/Base Menu Item.....	93
Figure 60: Circular Pattern Menu Item.....	94
Figure 61: Combine Menu Item.....	95
Figure 62: Fillet/Chamfer Menu Item.....	96
Figure 63: Spur Gear System, Test Code.....	99
Figure 64: Von Mises Stress, Test Code.....	100
Figure 65: TE Data, Test Code.....	100
Figure 66: Abaqus Model Tree for FG Generation.....	101
Figure 67: Import Part Menu Item.....	102
Figure 68: Sequence for Applying Properties.....	103
Figure 69: Sequence for Creating an Assembly.....	104
Figure 70: Sequence for Defining Steps.....	104
Figure 71: Sequence to Add Interactions.....	105
Figure 72: Create Surface Menu Item.....	106

Figure 73: Create Set Menu Item.....	106
Figure 74: Sequence to Create Loads .....	107
Figure 75: Sequence to Develop Mesh .....	108
Figure 76: Sequence to Run Job .....	108
Figure 77: Sequence to Post Processing .....	109
Figure 78: Report XY Menu Item.....	109
Figure 79: Model Used for Simulation .....	111

**LIST OF TABLES**

Table 1: Steps Taken to Construct a FG Model.....	30
Table 2: Comparison between Abaqus/Standard and Abaqus/Explicit [45, 46].....	33
Table 3: Material Properties for the Simulation [48].....	36
Table 4: Unit System Consistency.....	37
Table 5: Datum Point Coordinates.....	38
Table 6: Summary of Loads and Boundary Conditions.....	48
Table 7: Mesh Characteristics.....	50
Table 8: Lion-LSP Specifications [50] .....	51
Table 9: Steps Taken to Set Up an Abaqus Simulation .....	54
Table 10: Overview of Error Sources .....	79
Table 11: External FG Data .....	97
Table 12: Internal FG Data .....	98
Table 13: Disk Parameters.....	111
Table 14: Rotational Displacements for both the External and Internal FG.....	112

**LIST OF EQUATIONS**

Equation 1: Transmission Error .....	16
Equation 2: Angular Difference Representation of Transmission Error .....	62
Equation 3: Vector Representation of Transmission Error .....	68
Equation 4: Angular Rotation Analysis of the External FG .....	76

**LIST OF SYMBOLS**

$\beta$ : Pitch Cone Angle

$\theta_1$ : Angular Displacement, Input

$\theta_2$ : Angular Displacement, Output

$N_1$ : Number of Teeth, Input

$N_2$ : Number of Teeth, Output

$r_{p1}$ : Pitch Circle Radius, Input

$r_{p2}$ : Pitch Circle Radius, Output

$r_{pV}$ : Pitch Circle Radius (Vector)

$m_p$ : Gear Ratio

## LIST OF ABBREVIATIONS

- DoD: Department of Defense
- FVL: Future Vertical Lift
- JMR-TD: Joint Multi-Role Technology Development
- PMT: Pericyclic Mechanical Transmission
- FG: Face Gear
- PSU: The Pennsylvania State University
- TE: Transmission Error
- CAD: Computer Aided Design
- FE: Finite Element
- BC: Boundary Condition
- PBS: Portable Batch System
- ODB: Output Data Base
- UR: Angular Displacement
- TEA: Transmission Error (Angular)
- TEVM: Transmission Error (Vector Magnitude)

## ACKNOWLEDGEMENTS

Over the last two years, I have been supported by an incredible group of individuals that made this work possible. Foremost among these is Dr. Zihni Saribay, my friend and mentor that spent countless hours teaching me everything I know about the gear world. His words of advice not only made me a better engineer, but his unlimited patience and kindness taught me something about life as well. Also, my thesis advisors Dr. Martin Trethewey and Dr. Suren Rao were integral to my success. Whenever I found myself frustrated, stuck, or without direction (sometimes a combination of all three) their knowledge and insight showed me the path forward. I will always be grateful to them for being the best advisors a student could ask for.

In addition to those mentioned above, there were a number of other people and organizations that were part of this journey. I would like to express my deep appreciation to Anand Singh, Abdul Aziz, and Pierre-Yves Taunay of the Research Computing Group, who were kind enough to help me with a wide array of computational challenges that proved to be instrumental throughout this thesis. Also, Dr. Bill Mark of the Gear Research Institute and Dr. H.J. Sommer III provided their incredible insight and experience at several stages of this effort. Furthermore, I would not have had the opportunity to study at The Pennsylvania State University without the Vertical Lift Research Center of Excellence and those that made the Eric A. Walker Fellowship possible. Thank you for an amazing two years!

Lastly, to my friends and family, I cannot express how much your support has meant to me. You have been there whenever I have needed you, providing motivation and inspiration while asking for nothing in return. Ultimately, I could not have done this without you.

## **Chapter 1**

### **Introduction**

From the first sketches of a “flying machine” by Leonardo Da Vinci and the birth of modern vertical lift with successful flights by Igor Sikorsky in 1939, the helicopter has become an indispensable part of our modern world. These sophisticated, highly complex machines can be found on every continent and in almost any role – at the beginning of this past decade, there were over 40,000 flying worldwide. These perform such diverse tasks as wilderness rescue, firefighting, police surveillance, oil-rig services, troop transport, medical evacuation, and much more. Just the lifesaving capability alone is astounding, accounting for more than a million people to date [1]. According to MedEvac Foundation International, helicopters and associated aircraft carry out approximately half a million transports per year inside the United States today [2]. This is in large part to the technical capabilities of the helicopter, which for even a common civilian model includes top speeds in excess of 200 miles per hour, altitudes of over 10,000 feet, load capacities of 2,000 pounds, and a range of 300 miles or more. However, many of the current designs that serve as the primary fleet are approaching obsolescence, and the fundamental technology has not undergone a major change in several decades [3]. In the hope of addressing this impending service life horizon in its own helicopters, the United States Department of Defense (DoD) has introduced the Future Vertical Lift (FVL) and Joint Multi-Role Technology Development (JMR-TD) programs. Estimated to have a budget of \$100 billion, these initiatives hope to replace the traditional workhorses used by the Army since the 1980’s. The motivation for this effort, slated for completion by 2030, is clear:

Recent study findings concluded that the DoD rotary wing aviation fleet is aging and upgrades to current fleet aircraft will not provide the capabilities required for future operations. Additionally, because of the time in service for currently fielded helicopters, many of the decision points for the future fleet will occur within the next 10 years...[t]he current fleet of DoD rotorcraft cannot continue to be incrementally improved to meet future operational requirements. Significant

improvement in vertical lift, range, speed, payload, survivability, reliability, and reduced logistical footprint are all required to meet future needs and can only be achieved through the application of new technologies and designs. Operational costs must be reduced to a fraction of those for the current fleet. [4]

In order to realize this vision, which will be beneficial not only to the military but also civilian sectors, there must be a selection of next-generation technologies available for adoption. Particularly, due to its influence on a majority of these critical objectives, the propulsion system has been identified as one of the most viable avenues for further development. This is in large part due to the drivetrain's disproportionate contribution to a helicopter's volume and weight. In fact, propulsion systems comprise 25-30% of the empty weight, of which 30% of that value can be attributed to the main gearbox. Therefore, innovative approaches to this component can bring exponential improvements in range, efficiency and payload capacity [5]. At the forefront of these solutions are advances in gear design, which have led to the emergence of a unique system known as the Pericyclic Mechanical Transmission (PMT) based on face gear (FG) technology.

## **1.1 Fundamentals of Gear Design**

Spanning the ancient world to the modern era, gears have been an integral part of mankind's productivity and mobility. Almost universal in their application, they have harnessed the power of wind and water to support early economies in addition to driving the most modern automobiles and aircraft. The uses of a gear are so ubiquitous because of their ability to change the speed, torque and direction of almost any power source to produce mechanical advantage. Two or more gears, when combined, constitute a transmission and are unique from other similar devices due to the use of cut teeth. The location and orientation of this feature largely defines the various types of gears, which consist of four primary classes: spur, bevel, helical, and worm. The

teeth prevent slipping, as is the case with pulley or friction disk systems, and in more advanced applications have the ability to produce smooth uniform angular motion (otherwise known as conjugate action). This resulted from the discovery of the involute curve, and has dramatically reduced the vibration, noise, and wear that had been a defining limitation to gears in the past. Currently, the involute is an industry-wide standard, and nearly all modern teeth feature this shape [6, 7].

In addition to the general concept, there is some specific terminology that serves as the foundation for understanding the geometry of a gear [8]. A selection of key nomenclature includes:

- Gear – The larger of the two gears in contact.
- Pinion – The smaller of the two gears in contact.
- Pitch Circle – A circle with its center coincident and perpendicular to the gear axes that has a perimeter passing through the pitch point.
- Pitch Point – This is a fixed point that lies at the intersection of two pitch circles and the common center line connecting two gear axes.
- Base Circle – A circle that is the basis for the involute curve generation.
- Line of Action – A straight line normal to the profiles of two teeth in contact that passes through the pitch point.
- Pressure Angle – An angle that is formed between the line of action and a tangent line between two pitch circles at the pitch point.
- Addendum – The distance from the pitch circle to the outermost part of the tooth.
- Dedendum – The distance from the pitch circle to the lowest part of the tooth.

- Tooth Face – A surface on the side of the tooth between the pitch circle and top of the tooth.
- Backlash – The extra space between an engaged tooth and its two nearest neighboring teeth on the opposite gear.
- Gear Ratio – A relationship between the number of teeth on the mating gears; typically, the output divided by the input gear.
- Contact Ratio – A representation of the average number of teeth that interact during the period of contact between a tooth entering and leaving the mesh.
- Module – The ratio of pitch circle diameter to the number of teeth.
- Diametral Pitch – The ratio between number of teeth and the pitch circle diameter; inverse of module.
- Circular Pitch – The length of the pitch circle between identical geometric points on two adjacent teeth.

To further illustrate some of these concepts, a detail view of a simple transmission can be seen in Figure 1. Not all terms shown below are included in the previous list, but are readily available in reference [8].

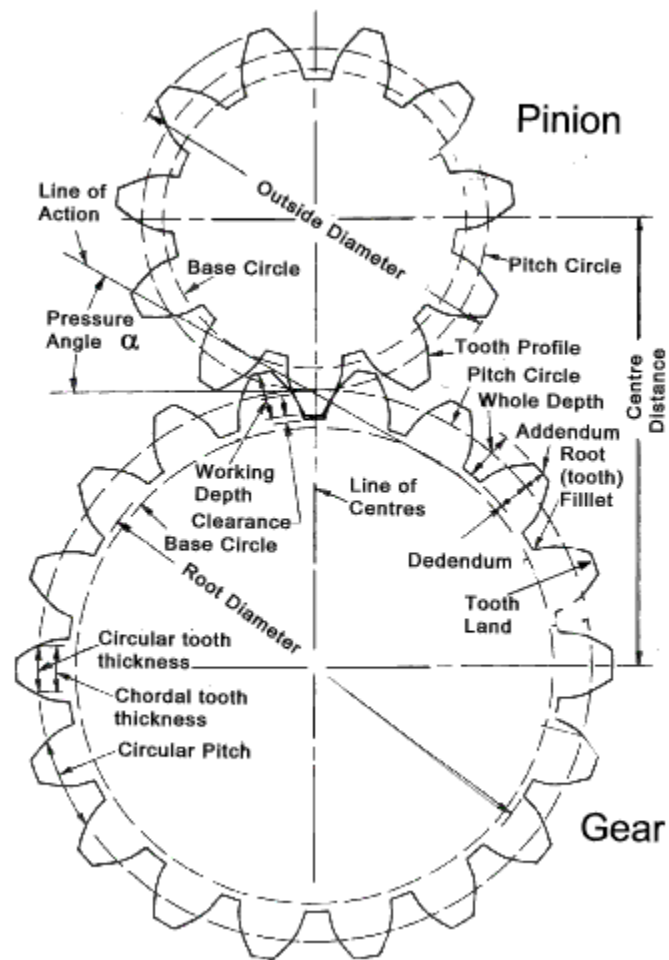
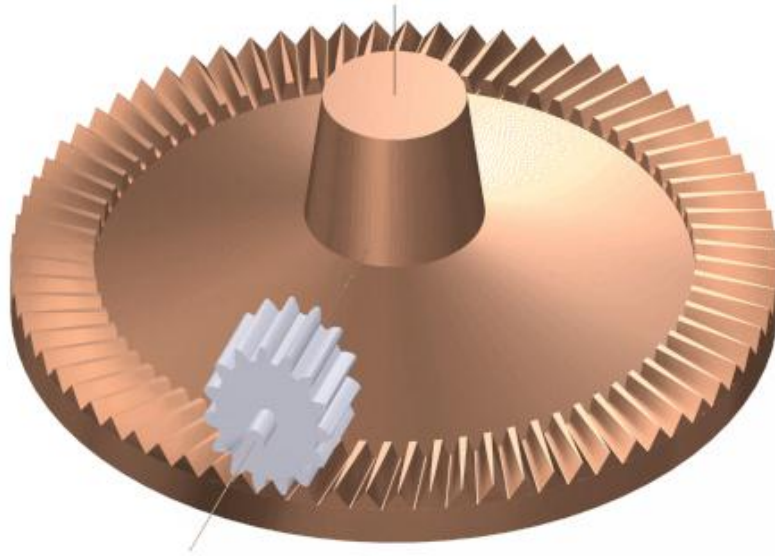


Figure 1: Common Gear Terminology [9]

Another equally important, but less common, gear type is the FG. First proposed by the Fellows Corporation, this component consists of a gear with its teeth cut radially around the interior perimeter. As shown below in Figure 2, the FG has been traditionally mated with a spur pinion in either an intersected or offset axes configuration. The former serves as a replacement for a spiral bevel gear drive, and the latter a hypoid gear drive. The advantages of FG drives include the ability to split torque in a transmission as well as low misalignment sensitivity [10, 11].



**Figure 2: FG with an Intersected Axis Spur Pinion [11]**

## **1.2 Overview of the Pericyclic Mechanical Transmission**

The PMT is a unique gear train system based on the concept of pericyclic motion and advanced meshing conjugate FG pair geometries. The PMT system was first proposed by Lemanski [12], who describes pericyclic motion as a synthesis of rotation, nutation, and oscillation. This, combined with meshing conjugate FGs, allows for high reduction ratios in a compact design. In fact, a single stage reduction ratio of 50:1 is well within the realm of possibility due to almost equally sized gears and high contact ratios. The idea of meshing a FG with another FG is particularly innovative and facilitates the properties of high power density, minimum part count, and high efficiencies that make the PMT effective [13]. This arrangement is ideal for high power, high velocity applications whereas previously, despite the potential in helicopter systems, FGs have been constrained to applications with low torque, low speed due to a lack of experience and research [14-16].

A representative image of the mechanism, highlighting the four primary components (input, reaction control member (RCM), pericyclic motion converter (PMC), and output), can be found below in Figure 3. Note that the RCM and PMC have their teeth at slightly different orientations, representing an external and internal FG respectively. This difference supports the concept of a pitch cone and pitch cone apex, as seen in Figure 4. Also, it can be observed that the PMC is placed at a nutation angle (represented by  $\beta$ ), which is typically between two and five degrees. In addition, the most recent and fully developed PMT concept can be seen in Figure 5, which is the “twin” design that features two conjugate FG pairs that are offset to reduce dynamic loads.

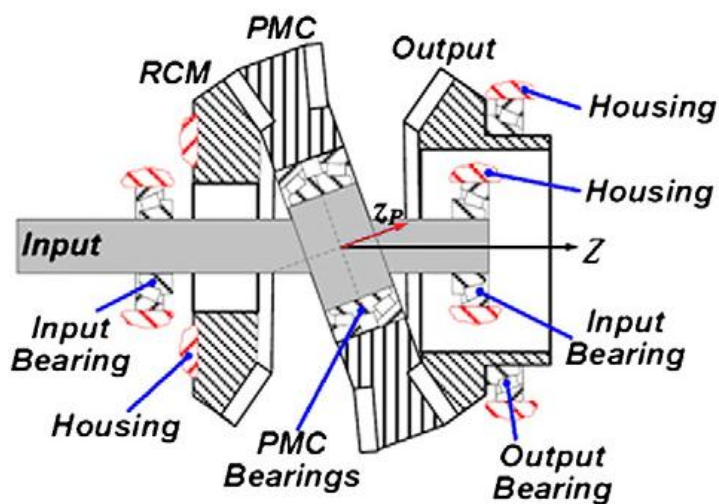


Figure 3: Basic Cross Section of the PMT [5]

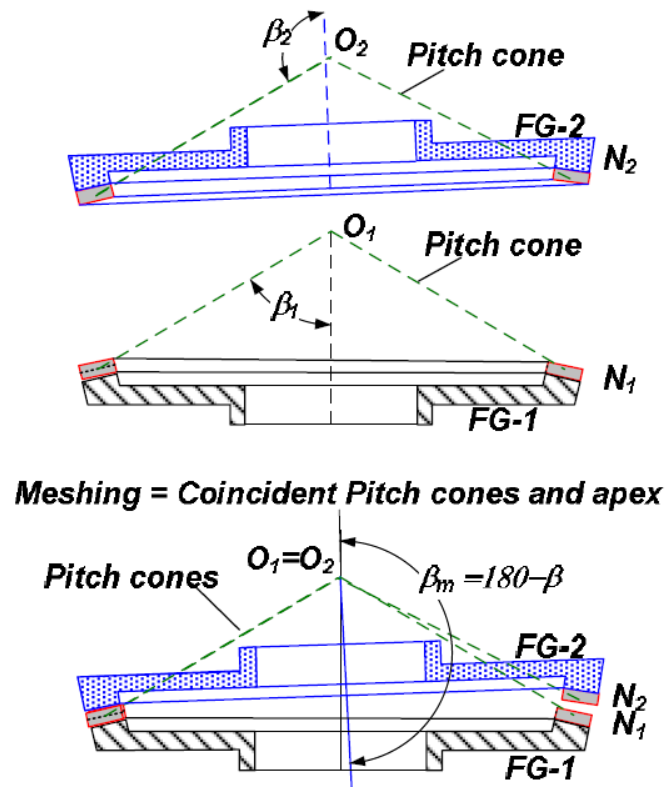


Figure 4: Pitch Cones of the External and Internal FG [5]

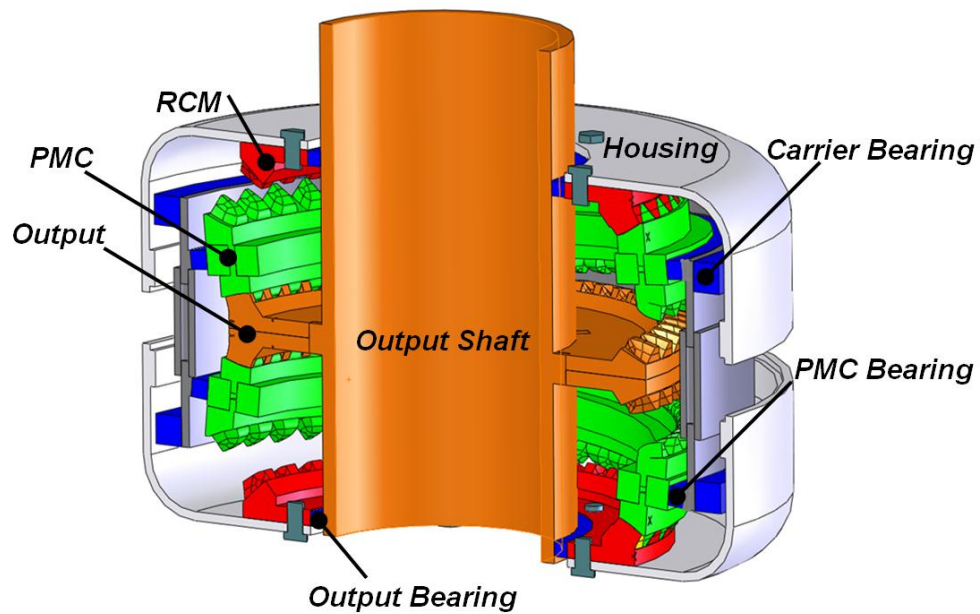


Figure 5: Twin PMT Design [5]

As part of a collaboration with the Vertical Lift Research Center of Excellence at The Pennsylvania State University (PSU), PMT technology has progressed beyond its initial patent to a stage where several analyses and feasibility studies have been conducted. At the core of this partnership is a large scale effort by Saribay [13] that considered the following: kinematics and power flow, mathematical modeling and validation of conjugate meshing FGs, consideration of loaded and unloaded FG cases, coefficient of friction and efficiency prediction, investigation of pericyclic motion, system bearing loads, and FG tooth mesh loads. The results were wide-ranging, but some highlights include numerical and analytical proof of FG conjugacy, analysis of FG performance at helicopter torque levels, and detailed consideration of nutation dynamics for the first time in literature. This work was instrumental to understanding the PMT, and provided the foundation for a variety of follow-up work. For example, Saribay and Bill [5] were able to develop the kinematics, tooth load capacity, bearing load capacity, and mesh efficiency even further than before. Also, the elastohydrodynamic lubrication characteristics and mesh efficiencies were explored with Hertzian contact and non-Newtonian considerations [17]. In addition, the geometry and kinematics were considered further by Saribay et al. with the aim of presenting principal geometric relations, tooth dimensions, meshing kinematics, normal and sliding velocities, and much more [18]. Finally, FG bending stress was investigated for single tooth pairs and compared to analogous spur gear teeth [19]. These studies, examining core concepts from a number of avenues, have the cumulative effect of building an intellectual groundwork and confidence that justifies future effort.

### **1.3 Problem Statement**

Currently, there are a number of technical challenges related to conjugate FG pair technology stemming from its new and novel nature. Previous FG configurations have been

explored and are well understood, such as FG-spur gear and FG-helical gear systems. However, these gear sets are not viable for the critical aerospace applications targeted by the PMT. A theoretical knowledge base must be developed to fill the technology void that may eventually lead to manufacturing and experimental evaluation. Without more practical knowledge, the FG pair will remain firmly rooted in theory rather than progressing to a stage where it can be implemented. Three high priority issues for FG pairs are:

1. Accessible and robust evaluation tools
2. Comprehensive performance knowledge
3. Confirmation of behavior predicted by literature

At the moment, none of these exist and have been identified as integral to the advancement of FG understanding.

#### **1.4 Research Objectives**

Broadly speaking, the primary purpose of this work is to expand the knowledge related to conjugate meshing FG pairs with the intention of supporting the development and eventual adoption of the PMT. To reach this goal, the current problems related to FG theory will be addressed in the following manner:

1. Implement available commercial software packages to capture the fundamental operation of FG pairs
2. Develop the understanding of static transmission error (TE) for FG pairs
3. Explore mesh and tooth dynamics of FG pairs

The first objective consists of applying an advanced computer aided design (CAD) package to model the FGs in combination with a comprehensive simulation package to represent the interactions between them. This will be paired with a detailed instruction set that can guide future efforts. Taken as a whole, these two tools are intended to represent a flexible and straightforward evaluation methodology. Once complete, a realistic simulation must be conducted and system data exported for the application of TE theory in line with the second objective. Using classic TE equations found in literature, as well as any original TE expressions that are specifically developed for this system, the data will be analyzed and evaluated with respect to values found in other gear applications. This can be accomplished with TE processing code specifically developed to perform the entire analysis procedure in a self-contained package. Finally, the simulation software will provide an avenue to consider the mesh and teeth in detail, which can then be compared to the latest FG pair literature. A summary of these objectives can be seen below, in Figure 6.

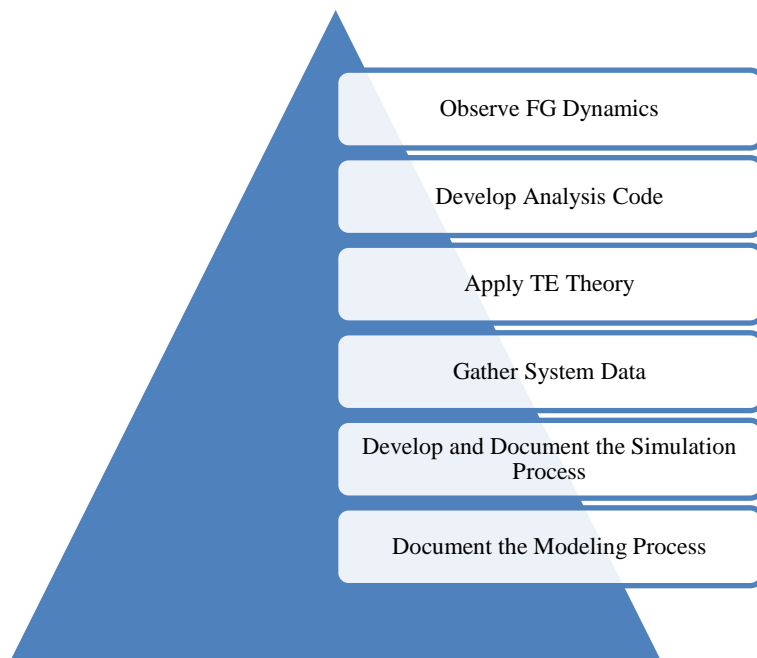


**Figure 6: Summary of Research Objectives**

### **1.5 Scope and Assumptions**

The investigation performed in the following chapters is focused on the tools and methods required to execute a FG pair analysis. While these represent a major component of the PMT, the transmission itself is a much more complex system that will not be considered in this study. For all intents and purposes, the FG pair is treated as free standing, frictionless, free of geometric errors/modifications, and with perfectly rigid shafts/bearings. Also, the numerous factors that would modify the FG performance (such as tip relief, root fillet shape, loads, nutation angles, gear ratios and other factors that constitute a parameter study) will not be explored. These are certainly important, but remain a task left to future work. Essentially, the scope extends to a “proof of concept” standard that confirms the feasibility of the stated objectives to address the primary research problems.

### **1.6 Outline of Thesis**

This work consists of six chapters, starting with the introduction in Chapter 1. Here, a case is made for the PMT based on the current and future state of vertical lift. A functional understanding of gear design and the PMT is also pursued; in the case of the latter, particular attention paid to the research conducted up to this point. Then, the scope and objectives for the following research effort are outlined. In Chapter 2, a literature review is conducted around the key topics of TE and gear performance simulation. In Chapter 3, the FG SolidWorks modeling process is documented from initial point import to full gear assembly. In addition, guidance is provided regarding feature refinements that are applicable to future simulations or prototype manufacture. These instructions are then collected in a “Summary of Actions” that details the action’s intention, its specific menu item, and the subsequent result. In Chapter 4, the individual

modules that comprise a complete Abaqus simulation are explored as well as their detailed parameter values. Furthermore, information regarding both the usage and computational accuracy of distributed clusters at PSU is provided as well. All of this information is again cataloged in a “Summary of Actions” to reinforce understanding and clarity. Next, Chapter 5 begins with exporting the simulation data and then provides the initial results in terms of TEA and TE. A new concept for TE based on vector quantities, referred to as TEVM, is also presented as a more viable alternative in the three dimensional FG context. Relevant values are provided for all of these expressions, along with graphs before and after rotation of the system. These are supported by images of the von Mises stress and contact pressures on the FG, which are then interpreted along with the graphs in an “Analysis” section. Finally, Chapter 6 serves as the conclusion by summarizing key contributions and opportunities for future work. Supplemental information, such as SolidWorks and Abaqus menu images, FG design specifications, and MATLAB code can be found in the Appendices. A summary of this process, spanning all six chapters, can be found below in Figure 7.



Figure 7: Flow Chart for FG Analysis

## Chapter 2

### Literature Review

The ultimate goal for this work is FG performance analysis, but that lies at the intersection of more fundamental concepts that must be understood beforehand. Essentially, this objective can be decomposed into two primary focal points: TE and gear simulation. By focusing on these specific areas, industry and academic insights were available to help guide the project from the onset. In addition, the ability to identify common threads, leverage strengths, and understand weaknesses from each was critical to developing the roadmap for the following chapters.

#### 2.1 Transmission Error

Ideally, a transmission would produce uniform angular motion without any noise or vibration given rigid, geometrically perfect, and equally spaced meshing gears [20]. However, this is not often the case, and a transmission typically suffers from varying degrees of imperfect angular motion and gear wear. Specifically, this results from:

- Deflections (e.g. contact deformations, gear tooth bending, shaft deflections, etc.)
- Geometric errors (e.g. involute deviations, gear tooth bias, pitch errors, etc.)
- Geometric modifications (e.g. profile crowning, tip and root relief, etc.) [21]

The result is undesirable torsional acceleration which causes the bearings to vibrate, and in turn, the transmission casing [22]. This problem is caused by TE, which can be defined as “the deviation in the position of the driven gear (for any given position of the driving gear), relative to

the position that the driven gear would occupy if both gears were geometrically perfect and undeformed” [23, 24]. Another way to express this concept can be seen below in Equation 1, which takes into account the angular displacement ( $\theta_1, \theta_2$ ), number of teeth ( $N_1, N_2$ ) and pitch circle radius ( $rp_1, rp_2$ ) of the driver and driven gear respectively. This expression is formulated so the resulting value represents the displacement along the pitch circle in terms of micrometers ( $\mu\text{m}$ ), also known as “microns”. Typical peak-to-peak values are around 5  $\mu\text{m}$ , independent of tooth size or module, and range from 1  $\mu\text{m}$  for a very precise and 10  $\mu\text{m}$  for a coarse gear. There are several other representations in the literature, including displacement in terms of radians, or using the base circle. Additionally, it is important to distinguish between static TE, which is a low load, low speed condition and dynamic TE that accounts for the gear mass and its rotation [25, 26].

$$TE = rp_1\theta_1 - rp_2\theta_2 = rp_1\theta_1 - rp_1\frac{N_2}{N_1}\theta_2$$

**Equation 1: Transmission Error**

## **2.2 Gear Performance Simulation**

Traditionally, gear performance investigations have required the use of specialty lab equipment, large numbers of custom gear samples, as well as an extensive time investment for setup, testing, and data processing. This type of experimental validation is still invaluable and performed on a regular basis, but the convergence of increasingly accessible processing power with advanced software suites have made it possible to develop high-fidelity digital simulations of the experiment. This has resulted in a paradigm shift which encourages developing a model beforehand, thereby refining current understanding, streamlining the subsequent analysis, and

ultimately saving time and money. This is especially true if there are a large number of parameters to consider or if the gear form is experimental and not readily manufactured.

The most common performance simulation literature focuses on spur gears, due to their widely understood nature. This work, while facilitated by modern tools, has been around in various forms for well over twenty years [27-29]. Generally, there are two unifying themes: the process used to develop and evaluate the model as well as the objectives of the analysis itself. Given the availability of the equations defining an involute curve, each author typically develops an in-house code that defines the tooth profile and gear body. This is interfaced with the simulation package of choice, usually Abaqus or Ansys, and then the system is defined and analyzed. Tooth stress and stiffness investigations, as part of loaded tooth contact analysis, form the majority of cases. In addition, various parameters of interest are often modified to observe their effects; some options include profile modifications, backlash, root crack modeling, and more. For example, Lee examines the stiffness cycle and meshing stiffness of a finite element (FE) transmission model, with an emphasis on tolerance sensitivity, mesh density, and element selection [30]. Also, Sommer et al. considers the influence of backlash and manufacturing errors on the early transient dynamic loading of a transmission [31]. An even more comprehensive study is presented by Li, which takes into account the result of machining errors, assembly errors, and tooth modifications on various stress factors [32]. Other variations on the general theme of study in this area emphasize the difference between static and dynamic simulations [33], or 2D and 3D representations of the gear form [34]. Another key topic of interest is the development of spur gear TE analysis, which was extensively analyzed by a number of authors [35-37]. In particular, an investigation by Tharmakulasingam addressed the question of TE especially well, taking into account both static and dynamic solutions across a wide variety of velocities, tooth ratios, torques, tooth clearances, and pressure angles [25].

This overview cannot take into account the entire breadth and variety of performance simulation literature related to spur gears, which is more readily available in other sources [38], but it is possible to get a sense for the direction that previous authors have pursued. In particular, these studies relate to the current work by outlining the modeling and simulation approach as a whole and, in some cases, provide detailed guidance for the software of choice (Abaqus). Overall, the strengths of the work lay in the sheer variety of cases considered and their validation with real data, indicating the maturity of this effort. However, the weakness is that they are constrained to a very particular gear type which is so ubiquitous that it fails to offer any innovative applications. This presents an opportunity to expand the community's understanding to include a next-generation component such as the FG, a fact which has not been overlooked by those in the field [39]. By using the same context of performance simulation, many of the lessons learned in a spur gear case are still valid while providing a framework to grow into when investigating FGs. Again, Litvin provides insight into this topic with his pioneering studies [10]. Some more recent publications have explored this avenue as well, such as Barone et al. when they looked at the stress state of FG and spur pinion teeth in mate using a combination of 3D modeling and FE code [40]. Another example of loaded contact analysis with the same configuration is provided by Guingand et al., who also validated simulation results with experimental outcomes [41]. Furthermore, the TE produced by such an arrangement was also explored by a number of researchers [42-44]. However, none of these studies have considered the possibility of two conjugate meshing FGs and their associated performance characteristics, which represents a prominent gap in the literature.

## Chapter 3

### Face Gear Model Assembly

The realization of an accurate FG model is the first critical step along the path to successful TE analysis. It is imperative that a high quality tooth form is generated that takes into account the necessary macro and micro features, which will determine the ultimate performance characteristics. With that requirement in mind, specific steps and best practice modeling techniques were applied within the CAD package of choice, SolidWorks 2012-2013. A summary of these procedures can be seen below in Figure 8, which represents the three primary tasks related to this effort and spans initial import to final model.

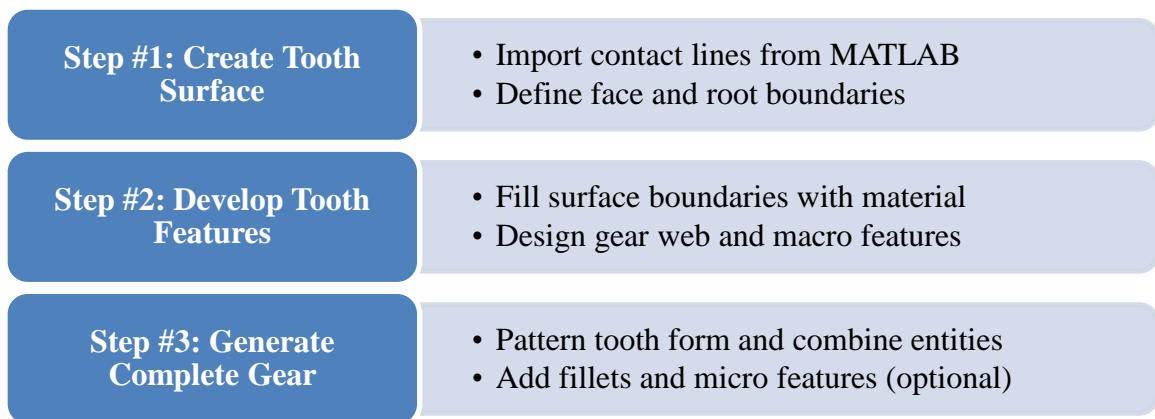


**Figure 8: Summary of Modeling Procedures Used for FG Generation in SolidWorks**

As mentioned, a complete FG system consists of both external and internal components, but despite their unique geometry can be designed with equal success using this method. For a more complete summary in the form of individual FeatureManager Design Tree entries, see Appendix A. In addition, the various modeling actions referenced throughout this chapter have their respective menu item images listed in Appendix B.

### **3.1 A Note on Contact Line Generation**

Resulting from the previous work by Saribay, an in-house MATLAB code was made available to generate both external and internal FG tooth forms. This generation code was based on the idea of a mutually conjugate spur shaper, which develops the contact lines for the gears using simultaneous equations of meshing. In principle, this means each FG is conjugate with the shaper, and therefore conjugate with one another. The generation procedure takes into account a number of relationships, such as the number of teeth on the spur shaper, number of teeth desired on each FG, and the angles formed between them. Furthermore, the theories of gearing and differential geometry were applied to develop this family of surfaces; more details can be found in the supplied reference [13]. An example of a FG tooth generated by this procedure can be seen below in Figure 9, as well as the preliminary alignment of the external and internal FG assembly in Figure 10.

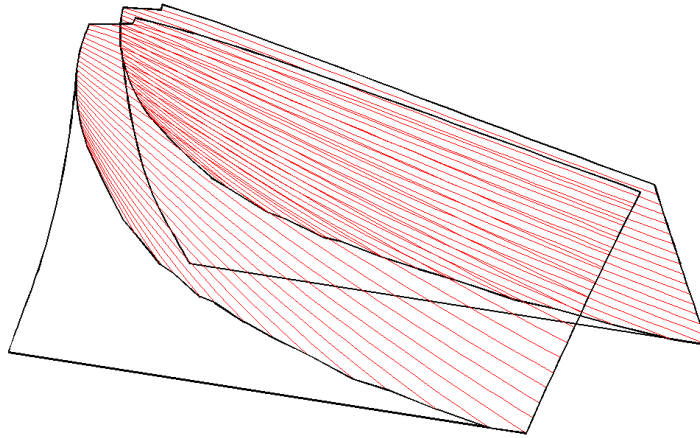


**Figure 9: MATLAB Generated FG Tooth Form**

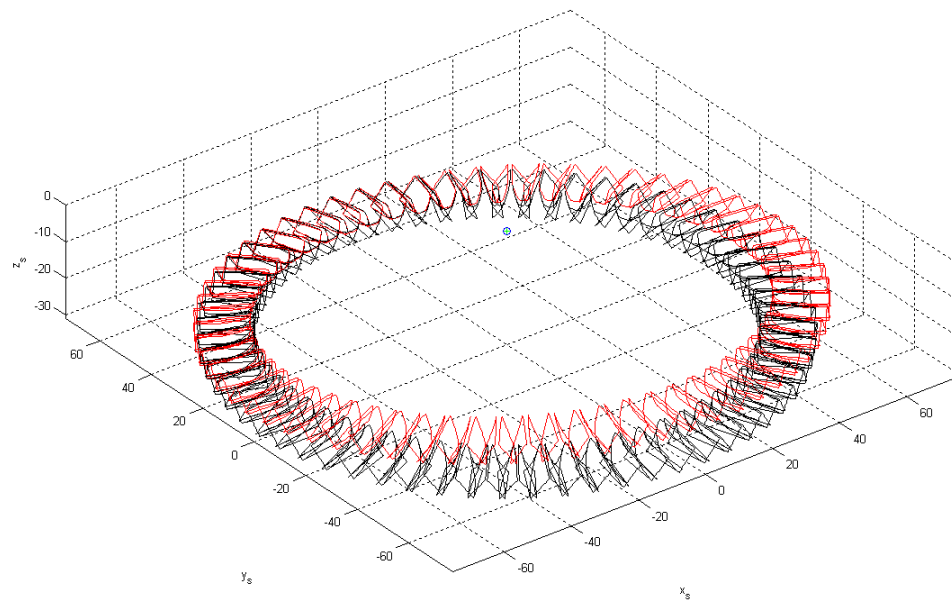


**Figure 10: MATLAB Generated Assembly**

### 3.2 Step #1: Create Tooth Surface

To begin, it is necessary to import conjugate contact lines defining the basic surface shape. These results are logged in a series of text files produced by the MATLAB code described previously, which contain points that can be loaded via the *Curve Through XYZ Points* menu option in a new part document. An individual file contains the spatial and geometric information for a single contact line, so this must be repeated for the entire set of data. Once complete, the result is a cluster of three dimensional sketches that are appropriately located for modeling and assembly as shown in Figure 11.

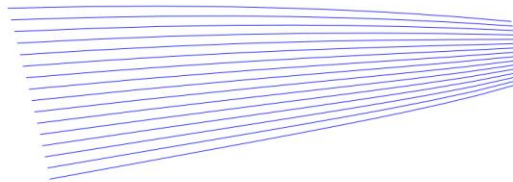


**Figure 11: Contact Lines after Import (Isometric View)**

In order to define the boundaries of the tooth, these contact lines need to be subjected to a *Mirror* and then integrated into a *Boundary Surface* with default settings. Initially, an *Axis of Revolution* is required for this step, which can be created by selecting *Reference Geometry* and

the *Axis* feature. Then, the global *Top Plane* and *Right Plane* can be chosen as the *Reference Entities* to create an *Axis* that runs vertically through the center of the system. This then becomes the rotation point for a plane about which the contact lines should be reflected. Specifically, the angle of this new plane can be determined by dividing 180 degrees by the number of teeth, which will place it on the tooth centerline when measured from the global *Right Plane*. The result of these steps can be seen in Figure 12, which represents the beginning of the overall tooth form.

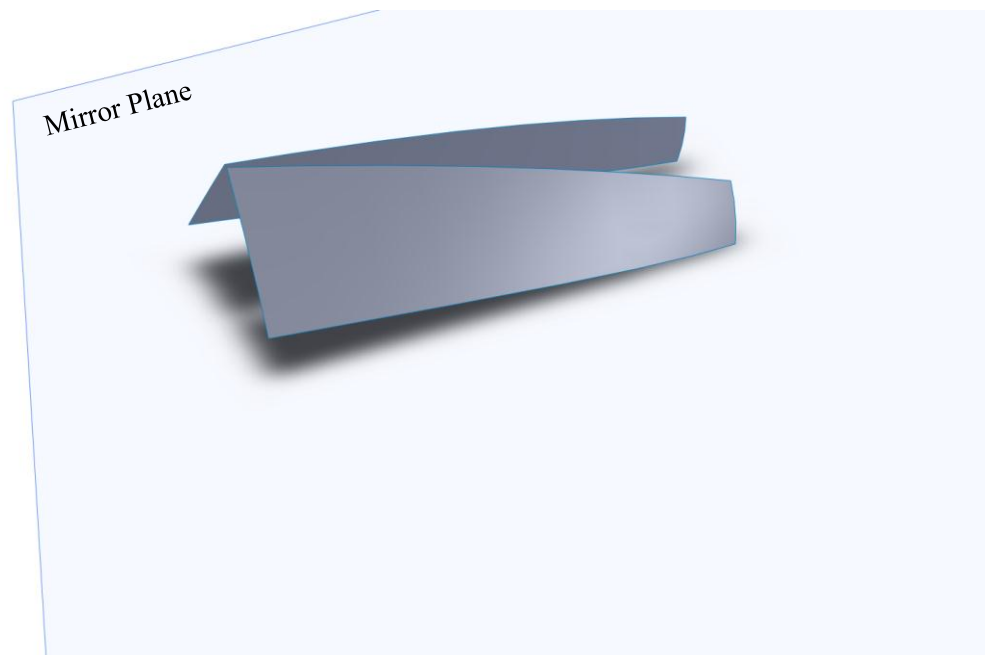


**Figure 12: Boundary Surfaces Created from the Mirrored Contact Lines**

Next, the initial root form can be realized by using a *Ruled Surface*, which will propagate the behavior of the preexisting boundary surface. Specifically, this is achieved through use of the *Tangent to Surface* setting and selecting the dedendum of the tooth. For the purposes of this research, a length of two millimeters as measured from the inner radius was deemed appropriate. The result of these actions can be seen in Figure 13 below.

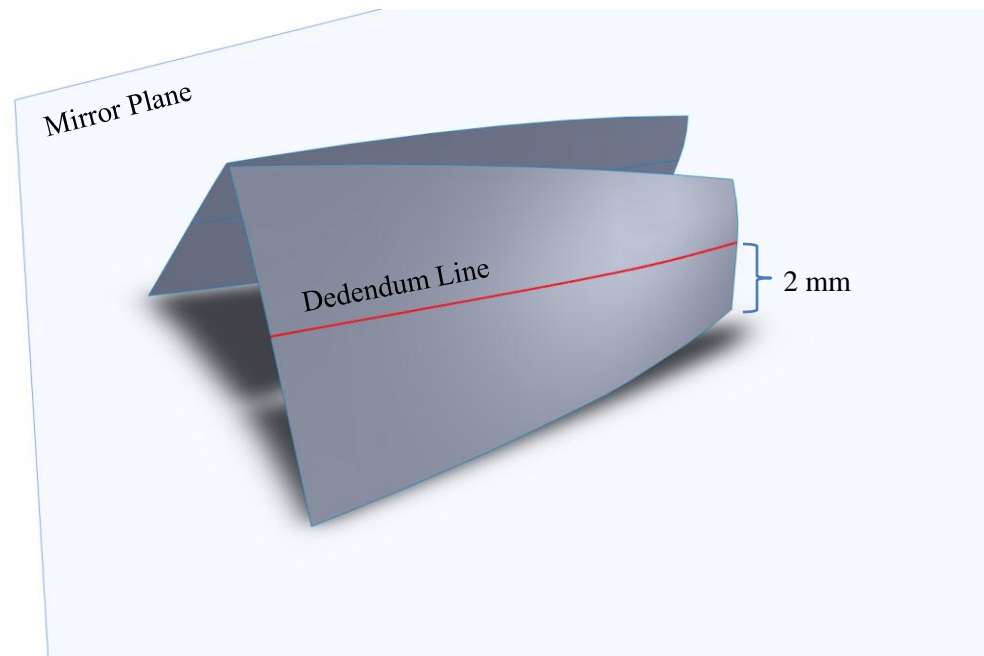


**Figure 13: Root Form Developed Using Ruled Surfaces**

### **3.3 Step #2: Develop Tooth Features**

With the boundaries of the tooth well defined, it is possible to add material between the surfaces. This can be accomplished in a single step by using the *Extruded Boss/Base* tool; however, an initial *Sketch* is required. Specifically, using the mirror plane in combination with the *Convert Entities* feature will create a projected form of the tooth and root surfaces. Once this *Sketch* is present, an *Extrusion* in both directions with the *Up to Surface* setting will create the form seen in Figure 14.

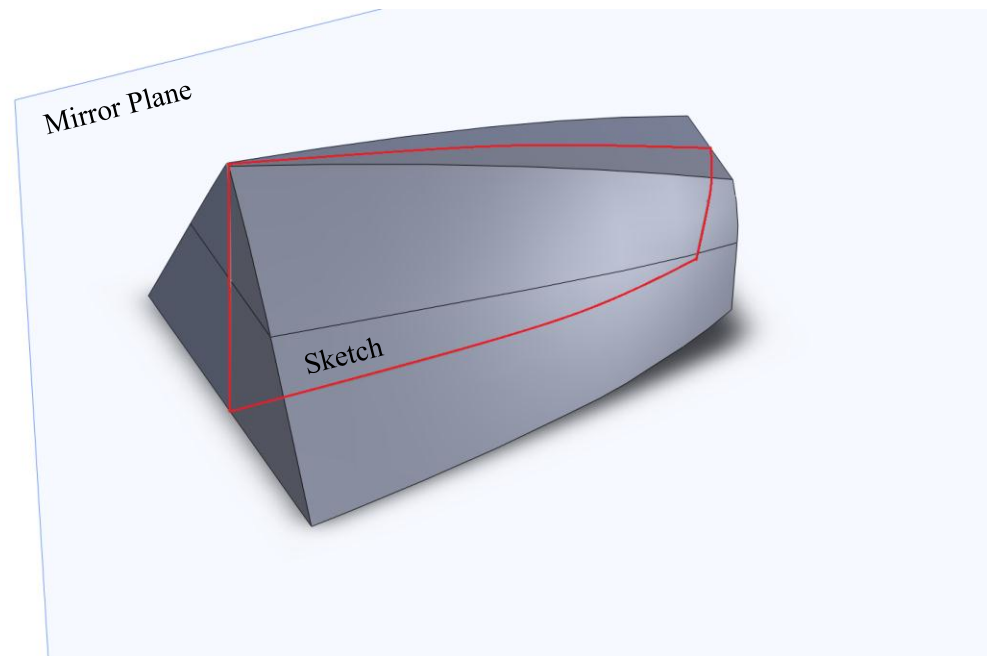


**Figure 14: Bulk of the Tooth Created Through an Extrusion**

Following this action, the tooth needs to be trimmed in order to create a more realistic working surface. This can be achieved by removing material from both the inner and outer radius as well as the dedendum. The exact degree of removal is largely up to the designer's discretion, but the technique used in this case was intended to maximize the face area while keeping the inner and outer radii surfaces parallel. Once again, a *Sketch* on the mirror plane can accomplish this task, followed by a *Revolved Cut* that is based on the preexisting *Axis* created in step one. An ordinary, linear *Extruded Cut* in two directions is not ideal in this case because the curved nature of the inner and outer radius would not be preserved. Note that the *Sketch* used for the *Revolved Cut* should be a closed area of sufficient size to encapsulate the unwanted material (the outer boundary is not shown in the following figure due to arbitrary size). The result of these steps is represented by Figure 15, which retained 67.5% of its original volume.

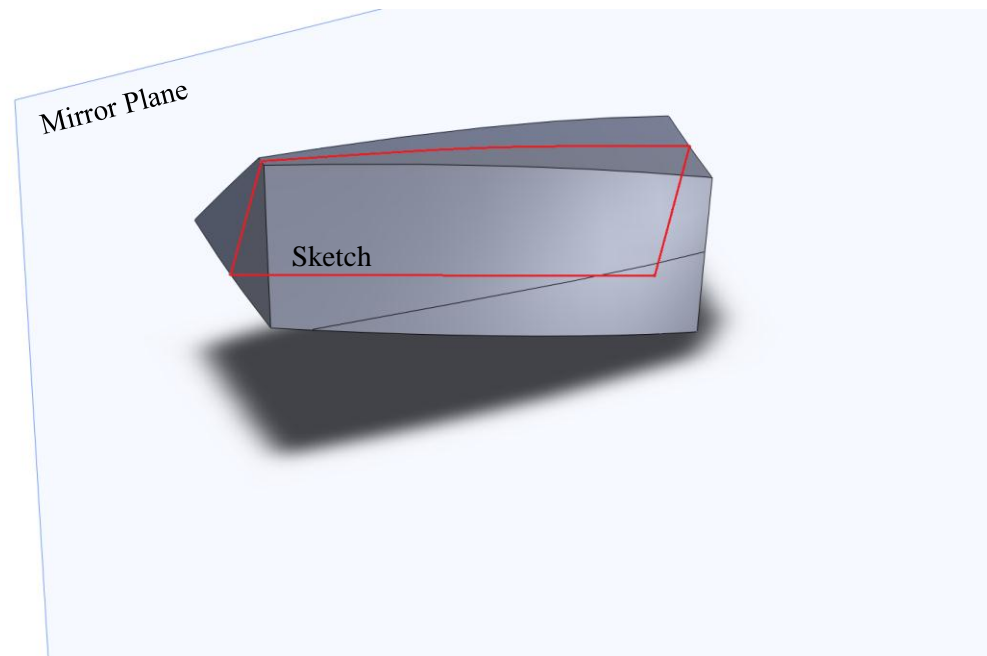


**Figure 15: Trimmed Tooth Form after a Revolved Cut**

Now that the tooth form is essentially complete, the gear web forming the base needs to be realized. As with determining root size and trimming the working surface, the dimensions associated with this step are up to the individual designer to determine. However, in this case it was decided that the web base height would be five millimeters, whereas the width and depth are determined by current geometry. Again, a *Sketch* on the mirror plane was combined with a *Revolved Boss/Base* to create the form desired. When using the latter feature, the direction should be set to *Mid-Plane* and the *Direction Angle* is 360 degrees divided by the number of teeth. This procedure will result in excess root surface that extends beyond both sides of the web, but the material can be removed with an outward facing *Extruded Cut*. The final single tooth is now complete, and can be seen in Figure 16.

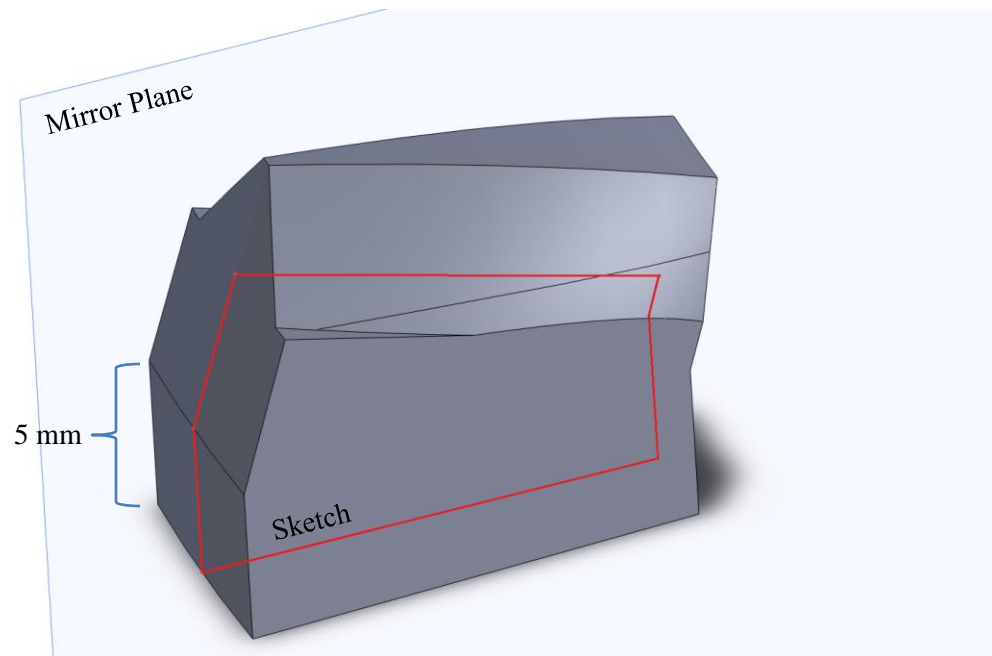


**Figure 16: A Complete Single Tooth**

### **3.4 Step #3: Generate Complete Gear**

Finally, this model can be used to create the entire FG using the *Circular Pattern* feature. This requires a *Pattern Axis* to rotate around, which is already available. In order to realize the full geometry, the *Angle* should be set to 360 degrees and the *Number of Instances* will be equal to the gear teeth desired. Note that these settings should be paired with the *Equal Spacing* option, present in the same *Parameters* menu, to work properly. Once this action is executed, the model must undergo a *Combine* in order to create a single volume and eliminate partition lines. The *Operation Type* that should be chosen for this feature is *Add*, and *Bodies to Combine* will consist of the *Circular Pattern* results. In the end, the complete form of either an external or internal FG will take shape, as seen in Figure 17. The technical details of these gears are also available in Appendix C for further reference.

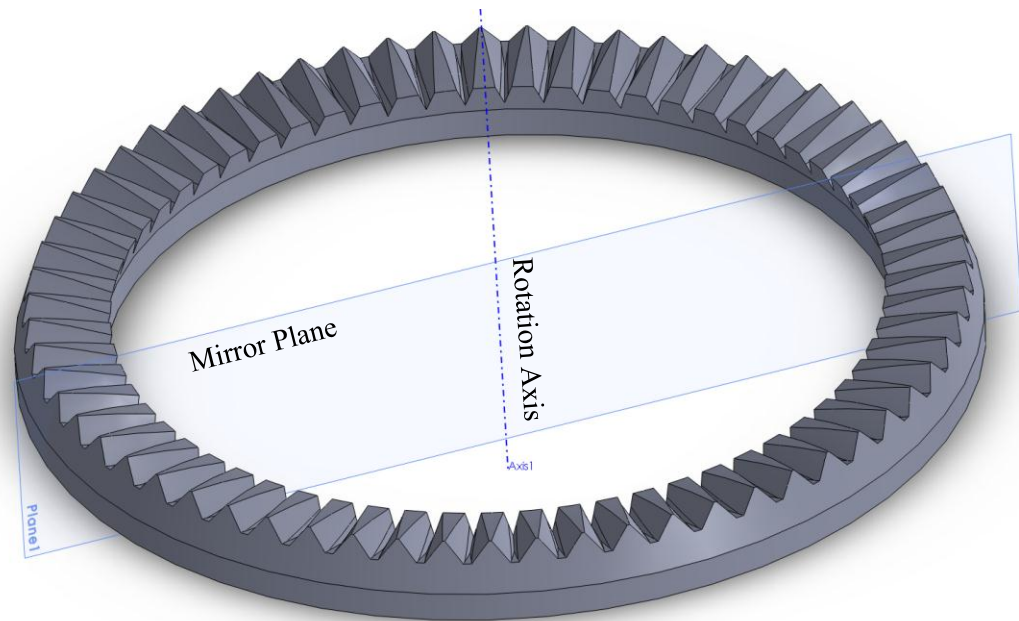


**Figure 17: The Resulting FG Model (Internal)**

### 3.4.1 Optional Feature Refinement

The FG model that results from this generation procedure has several functional features, such as a conjugate tooth surface, root geometry, and web. However, it lacks some of the features that are required for a truly operational component, such as root fillets and chamfers. This is an intentional omission intended to increase simulation performance, but can be easily addressed by applying the *Fillet* and *Chamfer* tools to all the sharp edges present on the addendum, dedendum, and root. In addition, it is useful to add fillets on the inner and outer FG radii to smooth the transition from web to tooth. These would be useful for more advanced simulations or prototype creation in the future. The regions of interest are best illustrated below, in Figure 18. The exact curvature of these features is left to the designer, and their appropriate sizing must be determined by application.

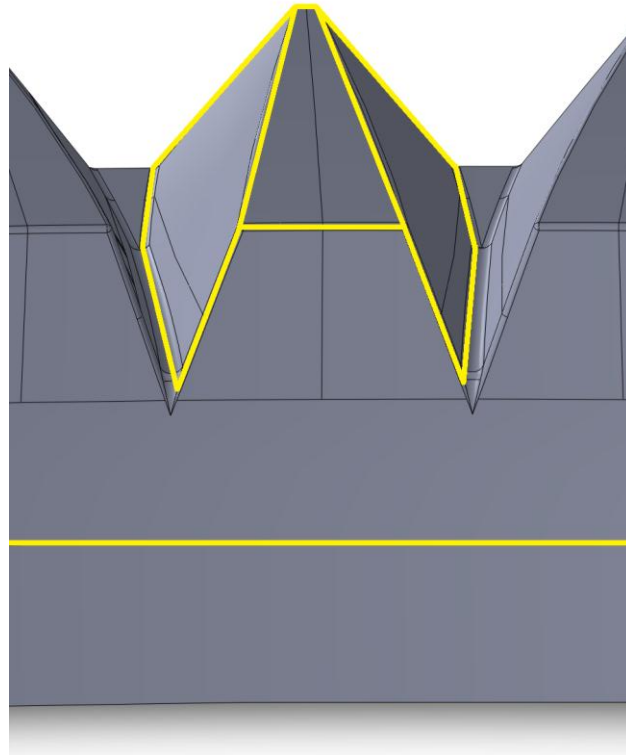


**Figure 18: Detailed View of Fillets and Chamfers (Outer FG Radii Not Shown)**

### 3.5 Summary

Over the course of this chapter, a detailed guide to FG model generation was compiled for the first time. This includes initial contact line import, face and root surface generation, tooth and web extrusion, as well as patterning. These are paired with descriptions of all necessary SolidWorks commands and reference geometry creation. In addition, the potential for feature refinement was briefly outlined. This procedure, taken as a whole, represents a specific set of instructions that facilitates accurate reproduction of the external and internal FG models. These fulfill part of the first stated objective related to implementing commercial software packages and will be the foundation for all research efforts that follow. In order to provide further support, Table 1 below encompasses a high-level listing of step number, action taken, SolidWorks menu items, and the following result.

**Table 1: Steps Taken to Construct a FG Model**

<b>Step Number</b>	<b>Action</b>	<b>SolidWorks Menu Item</b>	<b>Result</b>
<i>Step #1: Create Tooth Surface</i>	Import Contact Lines from MATLAB	Curve through XYZ Points	3D Sketch of the Contact Lines
	Create the opposite side of the tooth	Mirror	3D Sketch of the Contact Lines
	Join curves into a continuous geometry	Boundary Surface	Initial tooth faces have been formed
	Extend the existing surface	Ruled Surface	Basic tooth root geometry is present
<i>Step #2: Develop Tooth Features</i>	Fill the main tooth structure	Extruded Boss/Base	A raw tooth is now present
	Trim the working surface	Revolved Cut	The inner/outer radii and dedendum have been corrected
	Create the gear's support structure	Revolved Boss/Base	A section of the full gear has been realized
<i>Step #3: Generate Complete Gear</i>	Distribute the single tooth pattern	Circular Pattern	The overall form of a FG is now visible
	Remove parting lines and merge volumes	Combine	A single, continuous model is available
<i>Optional Feature Refinement</i>	Add realistic features to the teeth	Fillet/Chamfer	The FG is complete

## Chapter 4

### Face Gear Simulation Development

Now that a FG pair has been developed, the next step requires that they be tested for performance. This requires a FE package capable, at a minimum, of static analysis with significant nonlinear effects. Initially, SolidWorks Motion was considered, but after preliminary testing proved to be unreliable. Therefore, Abaqus 6.12-2 was chosen and pursued for all analysis required by this thesis. However, that decision was preceded by an initial test to determine the ability of Abaqus to capture TE. As a model, the work by Tharmakulasingam was reproduced locally and compared to published values [25]. The behavior of a spur gear pair was successfully reproduced, and therefore the system parameters used in this example were carried forward to guide the development of a FG case. For more detailed information on this proof of concept, see Appendix D.

The process of developing a simulation within Abaqus consists of eight steps, starting with model import and ending with job submission, as shown in Figure 19 below. Also, all the actions taken can be seen as part of the model tree in Appendix E and are complimented by associated menu images in Appendix F.

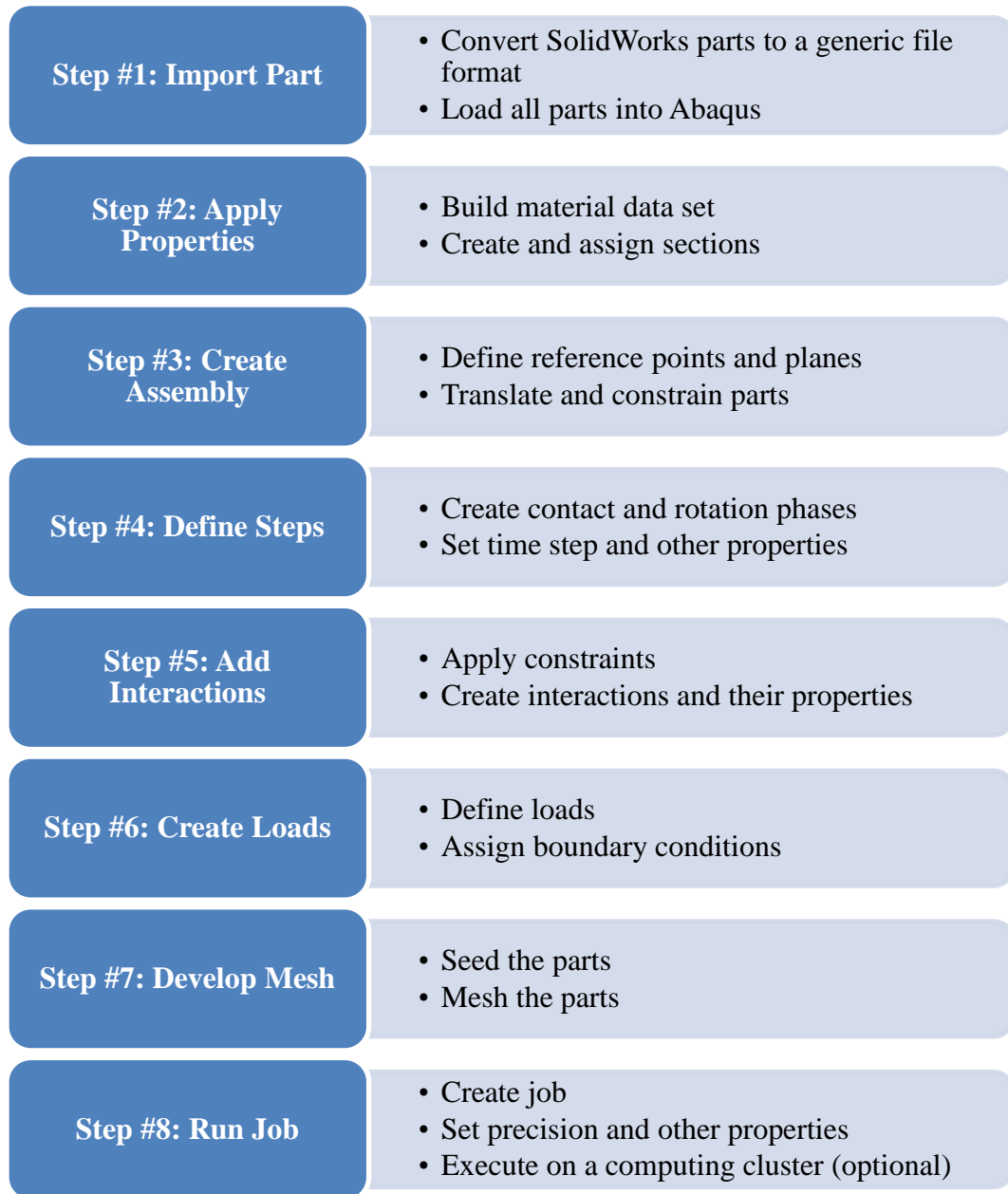


**Figure 19: Summary of Simulation Procedures Used for FG Generation in Abaqus**

#### **4.1 A Note on Abaqus Implementation**

When using Abaqus, there are a number of options presented to the user regarding the type of simulation to be performed. The major choices are Abaqus/Standard or Abaqus/Explicit,

which support either a static or dynamic analysis. Generally speaking, a standard (or implicit) simulation solves unknown values at a specific time using the current system information to iterate and check for convergence. On the other hand, an explicit simulation solves unknown values from system information already known and does not require iteration or checking for convergence. The following instructions will make it clear that a static, implicit analysis was used; however, Table 2 below provides some insight into the relative advantage or disadvantage of each approach in the context of this research.

**Table 2: Comparison between Abaqus/Standard and Abaqus/Explicit [45, 46]**

	<b>Abaqus/Standard</b> (Hilber-Hughes-Taylor operator)	<b>Abaqus/Explicit</b> (central-difference operator)
<i>Advantage(s)</i>	<ul style="list-style-type: none"> <li>- Complete FE library is available</li> <li>- Time increment is unconditionally stable, and therefore can be large</li> </ul>	<ul style="list-style-type: none"> <li>- Can handle complex contact conditions &amp; large deformations</li> <li>- Requires less disk space and memory when applied to large problems</li> </ul>
<i>Disadvantage(s)</i>	<ul style="list-style-type: none"> <li>- Inertial Effects ignored</li> <li>- Unable to use the general contact algorithm</li> <li>- Cannot handle discontinuities (i.e. impact, buckling, failure)</li> </ul>	<ul style="list-style-type: none"> <li>- Fewer FE types</li> <li>- Size of the time increment is limited (conditional stability), and therefore small</li> <li>- Can have long computation times depending on element size and material properties</li> </ul>
<i>Best Use</i>	- Static or quasi-static simulations	- Dynamic simulations

## 4.2 Step #1: Import Part

In order to bring the FG model developed in SolidWorks into the Abaqus environment, it must be converted from its proprietary SLDPRT format to another generic file type. This process poses certain challenges, which in the worst case results in the loss of geometric fidelity, and at best feature information. Some of these problems are acceptable, but it is important to choose a file type that minimizes their impact. For example, there is no need to modify the features of the part within Abaqus because SolidWorks is a much more robust modeling environment, so their absence will not impact the success of this procedure. Therefore, the STEP AP2014 format was chosen for its ability to preserve geometry, topology, colors, layers, geometric dimensioning/tolerance, and design intent [47]. The process for creating this file type is straightforward and readily detailed in the SolidWorks help files.

Another key factor to consider at this point is the nature of the geometry being imported. Looking forward to the operations that will be performed, the mesh creation phase (step number seven) is highly dependent on the model itself. Detailed features and parting lines will define the mesh seed behavior, and are highly likely to cause distorted elements. These can potentially result in simulation failures and inaccurate results. In addition, an increase in the number of elements that accompanies this case will demand higher memory and processing capabilities. In the interest of avoiding these issues, the simplified form of the FG models without optional feature refinements is used in this study.

To begin, with a new *Standard/Explicit Model Database* open, the *Import, Part* menu item can be used to bring in both the external and internal FG mentioned previously. The settings for this action can be left to their defaults, which will create an individual, 3D, deformable, and

original scale model. When this is completed, the workspace will display one of the two FG parts (depending on import order) as seen below in Figure 20.

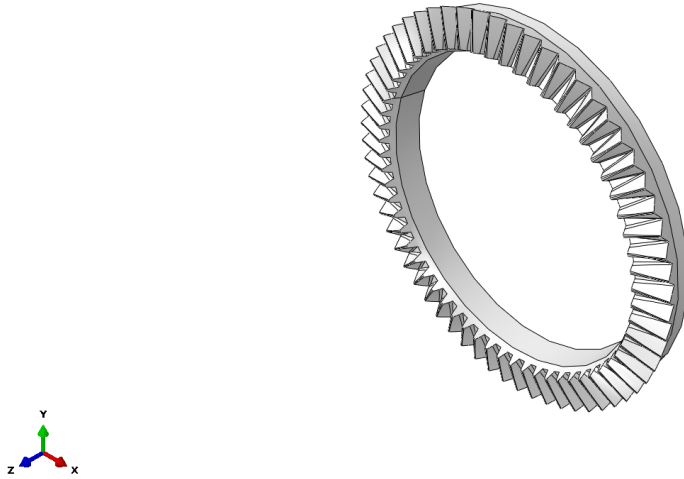


**Figure 20: Internal FG after Abaqus Part Import**

### **4.3 Step #2: Apply Properties**

Next, the *Module* can be switched to *Property*, which will allow materials to be assigned on a part by part basis. Through the *Create Material* feature, it is necessary to assign density and elastic properties. The specific values were set for common steel in the US unit system as shown below in Table 3.

**Table 3: Material Properties for the Simulation [48]**

<b>Parameter</b>	<b>Value</b>
Density (lbf·s <sup>2</sup> /in <sup>4</sup> )	0.000733
Young's Modulus (lbf/in <sup>2</sup> )	300·10 <sup>5</sup>
Poisson's Ratio	0.3

The issue of unit consistency is important to note since Abaqus does not have an inherent setting and once US or SI is selected at this stage, it must be used throughout the simulation. In addition, due to this flexibility, the units must agree with one another for accurate results (e.g. if density is in SI and elastic properties are US, the calculations will still take place despite being incorrect). For a summary of the units used, see Table 4 below. Once available, *Create Section* can be chosen with the category and type set to *Solid* as well as *Homogeneous*, respectively. Then, using *Assign Section*, the previously defined properties can be added to both the external and internal FG by switching between them through expanding the *Parts* category in the model tree and selecting *Make Current* for the desired component. Alternatively, the *Part* drop-down box can be set to the desired model.

**Table 4: Unit System Consistency**

<b>Quantity</b>	<b>SI (m)</b>	<b>SI (mm)</b>	<b>US Units (ft)</b>	<b>US Units (in)</b>
<i>Length</i>	m	mm	ft	inch
<i>Force</i>	N	N	lbf	lbf
<i>Mass</i>	kg	tonne (10 <sup>3</sup> kg)	slug	lbf·s <sup>2</sup> /in
<i>Time</i>	s	s	s	s
<i>Stress</i>	N/m <sup>2</sup> (Pa)	N/mm <sup>2</sup> (MPa)	lbf/ft <sup>2</sup>	lbf/in <sup>2</sup> (psi)
<i>Energy</i>	J	mJ (10 <sup>-3</sup> J)	lbf·ft	lbf·in
<i>Density</i>	kg/m <sup>3</sup>	tonne/mm <sup>3</sup>	slug/ft <sup>3</sup>	lbf·s <sup>2</sup> /in <sup>4</sup>

#### 4.4 Step #3: Create Assembly

Currently, both of the parts exist as separate entities, but if a successful simulation is to take place they must be brought together and their relationships defined. Therefore, once the module is switched to *Assembly*, both the external and internal FG can be pulled in via the *Instance Part* menu item and set to the *Dependent* instance type. In the interest of simple manipulation later, it is best to import the external FG first and then the internal FG using *Auto-Offset from Other Instances*. Now, it is necessary to set up the global datum points that will define the X, Y, Z positions of both gears. These are reflective of the positions produced by the MATLAB code and preserved during the SolidWorks modeling process. The first lies at the origin and serves as the most fundamental of three necessary for the system. The second represents a point at the center axis of the external FG, in plane with the base of the gear web. Furthermore, the third represents the center axis of the internal FG, also in plane with the base of the gear web. These points can be defined with the *Create Datum Point, Enter Coordinates* option and providing the X, Y, Z values listed below in Table 5.

**Table 5: Datum Point Coordinates**

<b>Dimension</b>	<b>Origin</b>	<b>External</b>	<b>Internal</b>
<i>X Value (in)</i>	0	0	0
<i>Y Value (in)</i>	0	-0.136	0
<i>Z Value (in)</i>	0	-1.565	-0.396

Next, two planes must be created to further help align the gears. The first of these will lie on the global X-Y plane and can be defined by using the *Create Datum Plane, Point and Normal* option. In this case, the Y-axis and origin can be used in combination to complete the action. This facilitates the creation of a second feature, which can be added by using *Create Datum Plane, Rotate from Plane* and selecting both the previously created plane along with the X-axis to induce a rotation equal to the nutation angle (in this case, negative five degrees).

The results of these actions are a total of five new features listed in the model tree, comprising three datum points and two planes. Now, it is necessary to make use of these as a tool to realistically align the previously imported FG pair in the simulation environment. Initially, it is possible to move them into position by using *Create Constraint, Coincident Point*, choosing the start point as the outermost center node of either the internal or external gear (indicated by an automatically provided yellow dot), and end point as the appropriate internal or external datum point. Here, the outermost point regarded as the start point coincides with the plane of the gear web, as shown as a green circle in Figure 21.

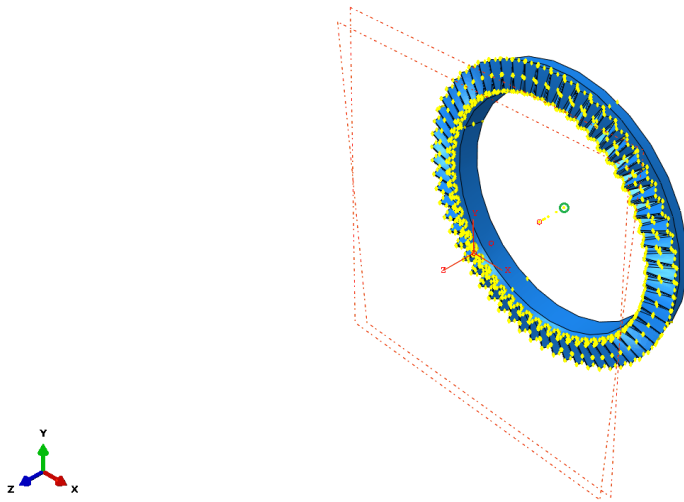


**Figure 21: Outermost Point of the External FG**

Then, the planes can be used to rotate the gears into a proper orientation and alignment. The key to this effort is to select the *Create Constraint, Parallel Face* tool, choose the outer edge of the gear web for the planar face of the movable instance, and then the appropriate plane for the fixed instance. Specifically, the external FG should be associated with the plane placed at the nutation angle, and the internal FG with the vertical plane. Note that the external FG will require the *Flip* option to be selected in this step, when prompted. As a result of these efforts, the system is complete with regard to the overall physical arrangement as seen in Figure 22. In addition, Figure 23 illustrates in greater clarity the relative position of the features created in this section by rendering the model hidden.

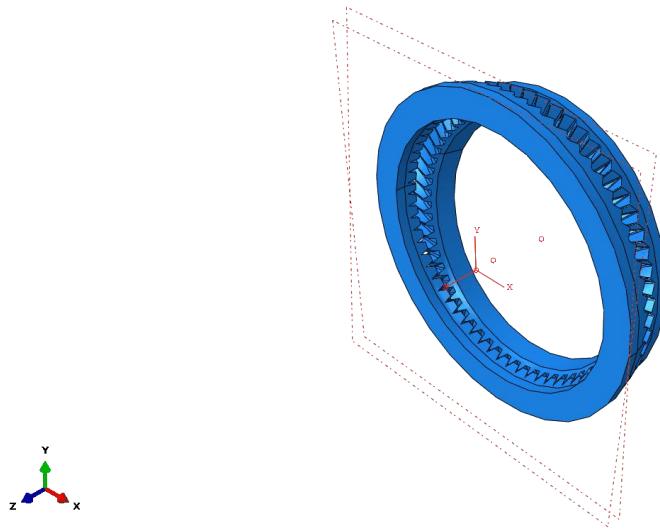


**Figure 22: Completed FG Assembly**

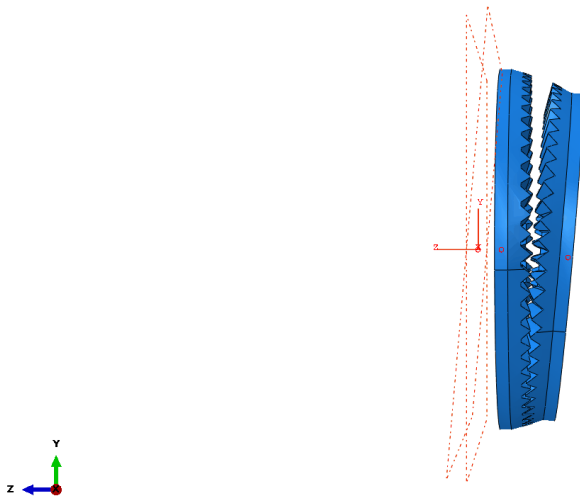


**Figure 23: Detail View of Assembly Features**

Lastly, a custom coordinate system is needed for use later in the simulation. Once *Create Datum CSYS, 3 Points* is selected the system type can be set to *Rectangular*, and then the point selection process can begin. The external FG datum point serves as the origin, and when

prompted for a point on the X-axis any arbitrary coordinate can be entered as long as it has the following characteristics: a positive value for X as well as the Y and Z displacement of the external gear itself. Finally, when prompted for a point on the X-Y plane, any of the points lying in the positive Y direction of the outer external FG web highlighted by Abaqus (again, indicated by yellow dots) will work. This idea is illustrated below with a green circle in Figure 24.

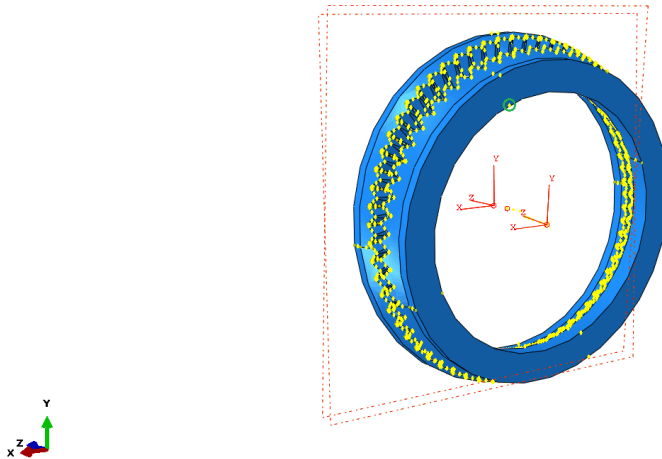


**Figure 24: Points Available for Selection**

#### **4.5 Step #4: Define Steps**

When conducting a simulation in Abaqus, the process is composed of several distinct sections, or steps. Each of these provides the opportunity to define different boundary conditions (BCs), loads, constraints, and more in the *Step* module. This ability is integral to creating a realistic situation, and therefore accurate performance data. In this particular case, there are three steps defined from beginning to end: initial, contact, and rotation. The purpose of the initial step is to define the necessary BCs that will form the fundamental motion of the system. Then, the

contact step ensures that the teeth of both the external and internal FG meet and become a firm pair before full motion occurs. This is achieved by holding the external FG in place and applying a specified torque to the internal FG. Lastly, the rotation step marks the beginning of the performance evaluation as the previous torque is held while a specified rotation is applied to the external FG in the opposite direction. Each of these can be produced with the *Create Step* option and the procedure type set to *Static, General*. This Abaqus/Standard approach was chosen instead of a dynamic representation due to static TE serving as the primary source of vibratory excitation in meshing gear pairs [49].

Also, the contact and rotation steps have a number of options that can be modified when *Edit Step* is accessed. With regard to the former, the *Basic* section has some specific settings that are integral to this particular case. These include non-linear geometry (Nlgeom) being set to *On*, and an automatic stabilization value of 0.0001 chosen through the *Specify Dissipated Energy Fraction* option. Also, adaptive stabilization must be activated with a value of 0.05 to complete the settings for this step. The *Incrementation* section should be the *Automatic* type, with the maximum number of increments set to 100,000. The increment size must have an initial value of 0.01 sec, minimum of  $2e-14$  sec, and maximum of 1 sec. As for Rotation, it too should have non-linear geometry set to *On*, however automatic stabilization is chosen to be *None*. Also, the maximum number of increments is again 100,000 but the increment size has changed to 0.0001 sec initial,  $2e-14$  sec minimum, and 0.0001 sec maximum. Note that the time periods for these steps found in the *Basic* section are essentially arbitrary due to the nature of a static simulation, but require a specified value nonetheless. In this particular case, 1 and 0.0628 sec were used for contact and rotation, respectively.

#### 4.6 Step #5: Add Interactions

The purpose of the *Interaction* module in Abaqus is to make the various models aware of each other, thus allowing realistic force and motion transfer to occur. The first step is to select *Create Interaction Property*, set the type to *Contact*, and then define both *Tangential Behavior* and *Normal Behavior*. The former can use the *Frictionless* formulation, whereas the latter should use “*Hard*” *Contact* pressure-overclosure. This “*Hard*” *Contact* setting minimizes the penetration of the slave surface into the master surface and does not allow the transfer of tensile stress across the interface. Next, in order to create the master and slave surfaces that are utilized by this setting, two groups must be created. The first, containing master surfaces, can be created under the *Tools* and *Surface* menu with the *Geometry* type setting. Now, it is necessary to select the two faces of every tooth present on either the external or internal FG; either of these can be chosen first without consequence. This procedure is manually intensive, but is necessary to complete accurately because missing a tooth, or even an individual face, would be detrimental to the simulation. The task can be simplified by using *Create Display Group* and selecting *Part Instances* to temporarily remove one of the gears for a better view. An image of this process, featuring the selection of several teeth, can be seen below in Figure 25.

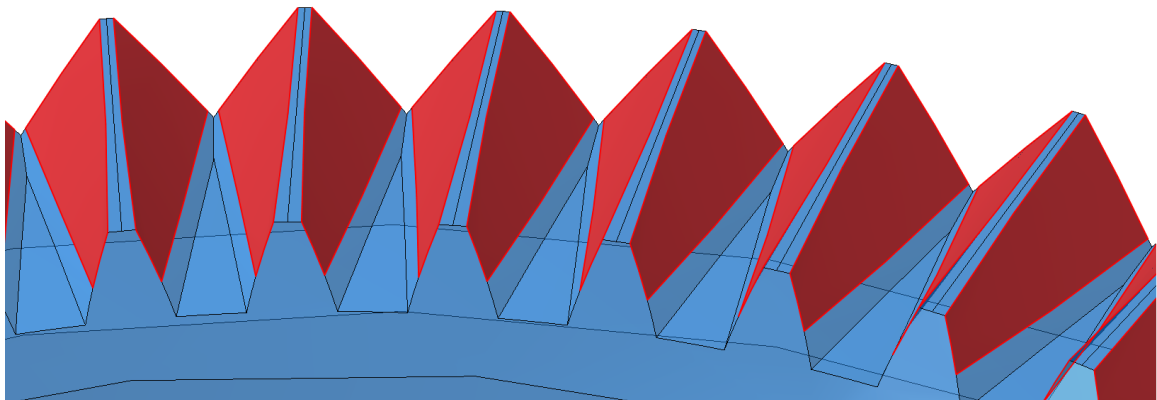
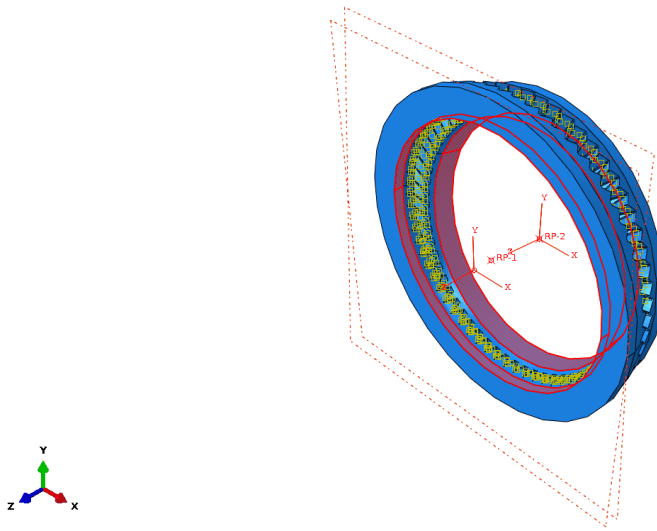


Figure 25: Selection of Tooth Face Surfaces

The result is a single macro surface that composes many individual surfaces across all the teeth. This procedure must be completed for the slave surfaces on the opposite gear, and can be performed in the same manner as described previously. The final task in ensuring the external and internal FG perform as expected is to use the *Create Interaction* option to apply a global *Surface-to-surface contact (Standard)* starting on the contact step. When chosen, Abaqus will prompt for a master surface selection, which can be done by selecting *Surfaces* and the appropriate set. This must be repeated for the slave surface, and then the *Edit Interaction* menu will appear. Lastly, the *Contact Interaction Property* should be set to the appropriate parameters defined earlier, which by default are contained in “IntProp-1”.

Another aspect that needs to be considered is the spatial relationships of the two gears. Namely, while they have been positioned previously, they need to be fixed in space to avoid rigid body motion. Before this can be applied, however, *Reference Points* are required that are coincident with both the external and internal FG datum points. These can be added by the *Create Reference Point* option and selecting the datum points required. In addition, two new sets of geometry need to be assigned for use in the following step. By selecting *Tools* and *Set* in the menu, these can be assigned to the inner bore of both gears. When the sets are selected, the system appears as it does below in Figure 26.



**Figure 26: Selection of the FG Bore**

Once in place, these reference points and sets can be used with the *Create Constraint* option and *MPC Constraint* type. Specifically, the *MPC Control Point* is the reference point and the slave nodes are the bore set of either the external or internal FG, respectively. Also, within this tool the MPC type should be set to *Beam* to ensure the reference point and slave nodes share all displacements and rotations. This will ensure that any forces acting on the reference point will be effectively transferred to the gear body, allowing the simulation to take place. At this point, overall assembly of the FG system is complete, and will appear as shown below in Figure 27.

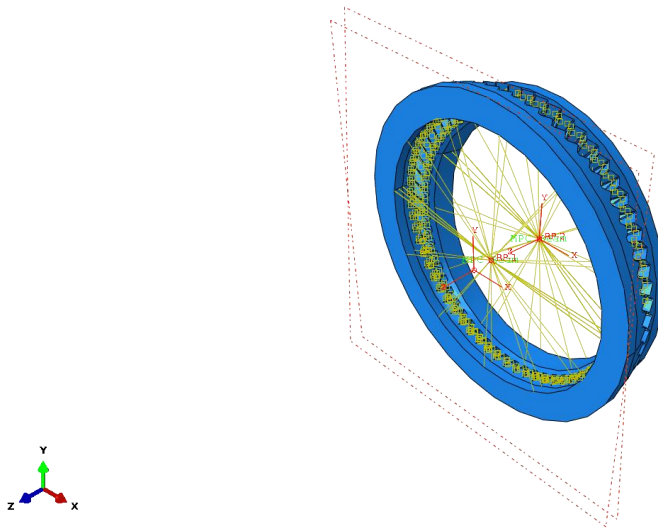


**Figure 27: Final Form of the FG System**

#### **4.7 Step #6: Create Loads**

The two primary tasks associated with the *Load* module are to apply loads and BCs to the previously created reference points. First, the *Create Load* option with the step set to *Contact*, category assigned to *Mechanical*, and type selection of *Moment* will provide the force needed to bring the two gears into contact. In this particular example, when prompted to decide on a location for the load, the *Sets* option should be used to select the internal FG reference point. This type of assignment indicates that the internal FG will act as the driven part, whereas the external FG will be the driver. Additionally, the load should approximate that experienced by a typical helicopter gearbox. Considering the classic Kaman K-Max, a value of 50,000 lbf-in was used, which by default will be applied uniformly with a ramped nature.

Next, the *Create Boundary Condition* option can be selected with the *Initial* step, *Mechanical* category, and *Displacement/Rotation* type. When prompted to select a region for the

BC, the *Sets* option allows access to the previously created reference points. The first state of the system should be achieved by setting both the external and internal FG to zero linear displacement as well as zero rotational displacement. However, since internal FG can be considered the driven gear, it will be allowed to rotate in the Z-direction. Note that checking the box for a given direction indicates that value is fully constrained. Furthermore, it is important to make use of the alternative coordinate system created earlier for the external gear when assigning its particular boundary conditions. The X, Y, and Z constraints must be in this frame of reference due to the nutation angle, which modifies the way in which forces are resolved.

These particular BC and load settings will be propagated across all three steps created earlier, but where the *Rotation* step is concerned the BC on the external FG will need to be modified. This allows it to oppose the previously created torque load, and induce rotation in the system. For this modification, a specific angular displacement in the Z-direction should be chosen according to amount of simulation data required. In this case, a rotation totaling  $2\pi$  radians was used due to computational considerations. A summary of the BC and load settings can be found below in Table 6.

**Table 6: Summary of Loads and Boundary Conditions**

<b>Gear Property</b>	<b>Initial</b>	<b>Contact</b>	<b>Rotation</b>
<i>External FG Loads</i> ( <i>lbf·in</i> )	N/a	N/a	N/a
<i>Internal FG Loads</i> ( <i>lbf·in</i> )	N/a	CM1 = CM2 = 0 CM3 = -50,000	CM1 = CM2 = 0 CM3 = -50,000
<i>External FG BCs</i> ( <i>rad</i> )	U1 = U2 = U3 = 0 UR1 = UR2 = UR3 = 0	U1 = U2 = U3 = 0 UR1 = UR2 = UR3 = 0	U1 = U2 = U3 = 0 UR1 = UR2 = 0 UR3 = $2\pi$
<i>Internal FG BCs</i> ( <i>rad</i> )	U1 = U2 = U3 = 0 UR1 = UR2 = 0 UR3 = free	U1 = U2 = U3 = 0 UR1 = UR2 = 0 UR3 = free	U1 = U2 = U3 = 0 UR1 = UR2 = 0 UR3 = free

#### 4.8 Step #7: Develop Mesh

One of the key components of a successful simulation is an appropriate FE mesh. The practical considerations are as follows: assigning elements, seeding the parts, and meshing them. Before any of these can be addressed, it is necessary to set the object considered to part, rather than assembly, mode. This option can be found in the Abaqus toolbar, and is required because the external and internal FG were originally imported as dependent instances and must be modified on an individual basis. Once this change is made, a single part will be shown and the *Assign Element Type* option can be selected. This will allow the global settings to be adjusted, which should consist of *Quadratic, Tetrahedral* elements. These can be found under the *Standard* element library and within the *3D Stress* family. This assignment should be applied to both gears using *Assign Mesh Controls* with the element shape set to *Tetrahedral*. An entity for these mesh

controls will be requested, and the part of interest should be chosen. Next, the *Seed Part* option can be used; for the purposes of this study, an approximate global size of 0.06 was used in combination with a maximum deviation factor of 0.1. In addition, the minimum size control as a fraction of global size was also equal to 0.1. Again, this procedure needs to be used for both parts. Lastly, selecting *Mesh Part* for both the external and internal FG will complete this effort and result in an assembly ready for simulation. The final form will appear as shown below in Figure 28, and Table 7 summarizes the mesh statistics. It is important to acknowledge two critical factors associated with this step: number of elements across the width and length of the tooth as well as mesh convergence. It was important to maximize the detail present on the tooth in order to achieve quality results, so that was balanced with computational cost in this case. As for checking convergence, which ensures that results are not influenced by FE density, a combination of the current mesh quality and computational time meant that this was not pursued.

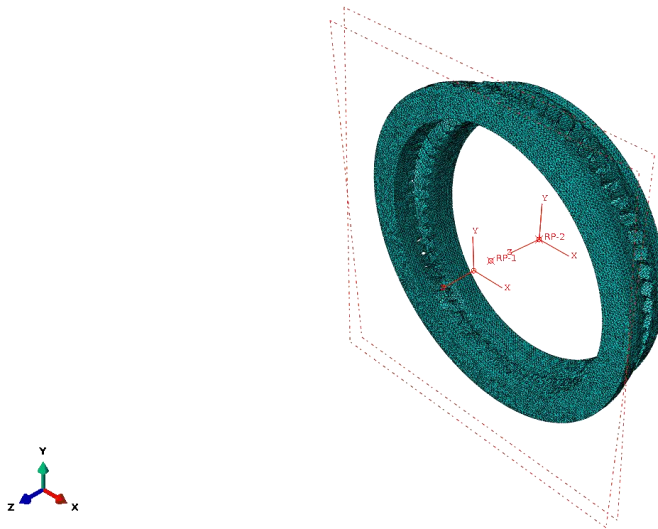


**Figure 28: The Fully Meshed FG Assembly**

Table 7: Mesh Characteristics

	<b>External FG</b>	<b>Internal FG</b>
<i>Nodes</i>	266,406	261,329
<i>Elements</i>	176,513	175,438
<i>Type</i>	C3D10	C3D10

#### 4.9 Step #8: Run Job

The process for executing the simulation begins with the selection of *Create Job*, which will then provide a series of options under *Edit Job*. The majority of these can be left to their defaults, but a section of interest is *Precision*. Essentially, this determines the rate of error accumulation as a result of iterating to a solution. The nodal output precision is typically set to *Single*, but for this case *Full* (or double precision) was used to ensure fidelity. Next, the *Job Manager* option can be used to *Submit* the job previously created. While this is running, the *Monitor* tool is useful to observe the current simulation progress and troubleshoot any warnings or errors. Note that warnings are fairly typical, especially concerning a limited number of distorted elements, and are non-fatal. It is up to the user to determine if these issues are serious enough to compromise the validity of the simulation, but with the settings described up to this point that is not the case. Finally, once complete, the *Results* tool allows the *Output Database* to be viewed and any relevant performance characteristics to be plotted and exported for further analysis.

#### 4.9.1 Optional Cluster Simulation

Given the complexity of the FG geometry, as well as the large FE number (with current settings there are over 350,000 between both models), the memory and processor requirements are significant. Typically these exceed the capability of a standard desktop computer within a reasonable solution time, but Abaqus has the ability to capitalize on multiple processors across a number of machines. This makes it a prime candidate for distributed parallel processing, where available. In the case of this research, the Lion-X clusters at PSU were extensively used to facilitate solutions when possible. Specifically, the Lion-LSP cluster was the tool of choice due to its ability to allocate memory on request, which is critical in order to prevent a simulation from being interrupted prematurely. The specifications of this cluster can be found below, in Table 8.

**Table 8: Lion-LSP Specifications [50]**

<b>Server</b>	<b>Quantity</b>	<b>Processor</b>	<b>Number of Processor Cores</b>	<b>Memory (GB)</b>
<i>Dell PowerEdge R810</i>	1	Intel Xeon E7- 8837 Eight-Core 2.66 GHz	16	256
<i>Dell PowerEdge E910</i>	1	Intel Xeon E7- 8837 Eight-Core 2.66 GHz	32	512
<i>Dell PowerEdge E910</i>	1	Intel Xeon E7- 8837 Eight-Core 2.66 GHz	32	1024

In order to make use of this system, two files are necessary: the Abaqus input file (.inp) and a Portable Batch System (PBS) file. The input file is a self-contained resource that holds all the model information, ranging from geometry, loads, BCs, constraints, and more. This is created every time a user decides to *Submit* a job and is found in the Abaqus root directory by default; alternatively, it can be produced by choosing to *Write Input* from the *Job Manager* menu. Using this data, the host system can accurately recreate and execute the simulation. As for the PBS file, it is a script that loads the input file on the cluster and defines resource allocation as well as data transfer. A commented and customized version, based on examples provided by Research Computing at PSU, can be found in Appendix G for reference [51, 52].

One of the questions that arises when using distributed computing is the accuracy of the results due to this architecture. For the uninitiated, this can appear to be an arbitrary assumption, and therefore an accuracy test was conducted. This involved a disk, with the same steel properties as defined for the FG, suspended in the simulation environment and allowed to freely rotate about the Z axis without friction. These constraints were achieved using the same methods described previously which made use of a *Reference Point* and *MPC Beam* constraint. It was then exposed to a moment and the angular acceleration, angular velocity, and angular displacement values were collected in a dynamic implicit step. This was done both on a distributed cluster similar to Lion-LSP, called HAMMER, as well as computer analytically via MATLAB using dynamics fundamentals. Further details on the system parameters can be found in Appendix H, including an image of the model. The difference between these results was then computed, and found to be within 4% in the worst case with transient effects present, and less than 1.5% once steady state was reached. This can be seen below, in Figure 29.

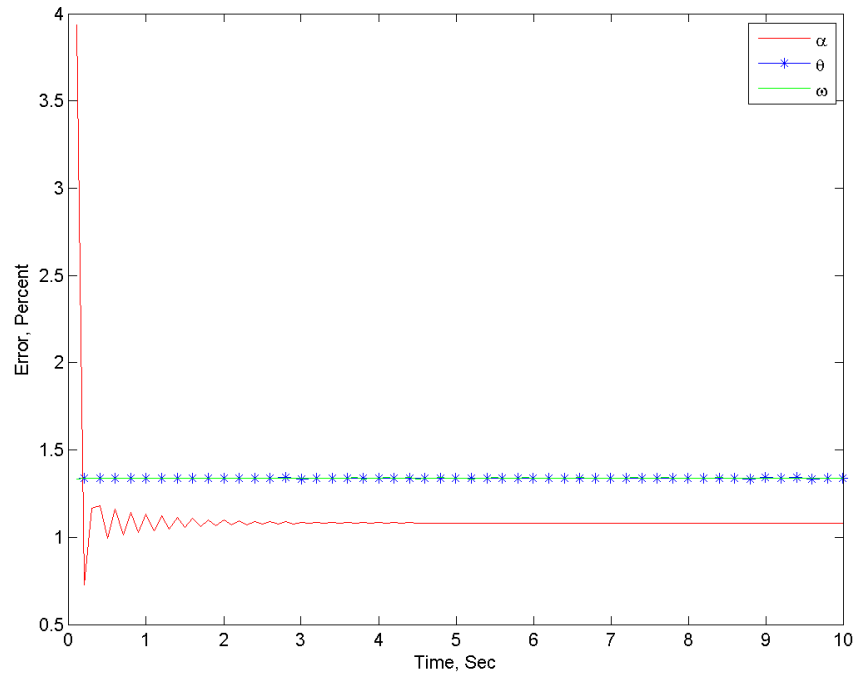


**Figure 29: Plot of Percent Error between Abaqus Distributed Solution and MATLAB Analytical Solution**

In light of these results, it was concluded that while there was some accuracy cost using distributed simulation capabilities, this is within commonly accepted engineering limits. In addition, it is important to keep in mind that these losses will be even less in the case of a static, rather than dynamic, simulation where transient effects do not play a role.

#### 4.10 Summary

This chapter presents the development of a simulated FG system with the intention of running it to produce static TE data. Original contributions regarding the modeling methods and necessary parameter values were outlined, which embodies the first attempt at such a task in literature. To that end, the contents cover the full range of part import, application of material

properties, assembly, step creation, interaction and load definition, mesh population, as well as job execution. Like Chapter 3, this achieves the first objective of exploring and documenting the commercial software packages integral to further FG pair research. For a review of actions taken to complete this task, a summary can be found below in Table 9. Also, when an Abaqus model is created, all the parameters required to recreate that system are recorded in a journal file (.jnl). These commands are in the form of Python code, and can be loaded with the *Run Script* command. The result is a reconstruction of the necessary model features, loads, boundary conditions, and more. Due to its size, this code is on file with the relevant parties at PSU for future research and development rather than included in this document.

**Table 9: Steps Taken to Set Up an Abaqus Simulation**

<b>Step Number</b>	<b>Action</b>	<b>Abaqus Menu Item</b>	<b>Result</b>
<i>Step #1: Import Part</i>	Import STEP model file	File, Import, Part	Both the external and internal FG are loaded
<i>Step #2: Apply Properties</i>	Define material properties	Create Material	A new material is available in the database
	Set material type	Create Section	The material is ready for assignment
	Choose the part to be associated with the material	Assign Section	The external and internal FG have mechanical properties
<i>Step #3: Create Assembly</i>	Import Abaqus model	Instance Part	External and internal FGs are present

	Define X, Y, Z positions of the gears	Create Datum Point, Enter Coordinates	The origin and center points of the gears are visible
	Insert a vertical plane coincident with the X-Y plane	Create Datum Plane, Point and Normal	A plane to align the internal FG is now available
	Define a plane at the nutation angle	Create Datum Plane, Rotate from Plane	A plane to align the external FG is now available
	Move the gears into place	Create Constraint, Coincident Point	The external and internal FG are associated with their datum points
	Fix the gears in their proper angular position	Create Constraint, Parallel Face	The external and internal FG are now aligned correctly
	Set up a coordinate system that is aligned with the external FG	Create Datum CSYS, 3 Points	A new coordinate system can now be used to assign BCs
<i>Step #4: Define Steps</i>	Establish the primary simulation components	Create Step	Three steps are defined for the system
	Set the necessary step parameters	Edit Step	All steps are ready for execution

<i>Step #5: Add Interactions</i>	Define how surfaces will interact with one another	Create Interaction Property	Realistic physics are now possible
	Prepare the regions which will experience contact	Tools, Surface, Create	All the gear teeth are recognized as master or slave surfaces
	Activate contact	Create Interaction	Both surface sets are aware of one another
	Produce an anchor point for the gears	Create Reference Point	Two references exist for use
	Define the surface of the external and internal FG bore that will be constrained	Tools, Set, Create	Two sets are available for assignment
	Tie the reference points and their associated FG bore together	Create Constraint	The gears can support loads and BCs
<i>Step #6: Create Loads</i>	Define the torque acting on the system	Create Load	The required moment to bring the gear teeth into contact is present
	Fix the gears in space and define their rotation	Create Boundary Condition	Appropriate motion of the system is possible

<i>Step #7: Develop Mesh</i>	Decide on the appropriate element to use	Assign Element Type	The proper element properties will be applied
	Assign element type to the part	Assign Mesh Controls	The external and internal FG will use the appropriate element type
	Produce a global element size and density	Seed Part	Both gears are seeded with the desired parameters
	Create the elements that will fill the part	Mesh Part	The external and internal FG are ready for simulation
<i>Step #8: Run Job</i>	Generate the file to run the simulation	Create Job	The simulation can be executed
	Change the settings related to precision	Edit Job	The data output will be more accurate
	Commit the job to the solver	Submit	The simulation is run
	View the outcome of the simulation	Results	Graphs and raw data are available
<i>Optional Cluster Simulation</i>	Prepare an input file for simulation	Write Input	An input file is written to the Abaqus root directory

## Chapter 5

### Post Processing and Results

Once the Abaqus simulation completes, which for the previously mentioned hardware took approximately 22 hours, an Output Database (ODB) file will be produced. This contains results for a range of parameters, including a visual representation of the system's motion. In order to access this data the ODB file should be opened, which immediately activates the *Visualization* module with the undeformed shape of the FG system present. By using a combination of *Animate Time History*, *Plot Contours on Deformed Shape* and the *Field Output Drop-Down* menu it is possible to examine the stresses on the gear teeth. Initially, looking at the overall assembly, it is clear that there is a significant stress field being produced in the mesh during rotation. In Figure 30 below, the results are shown from inside the hub of the system at one rotation, which has a maximum von Mises stress of 491 Ksi. Generally speaking, it can be seen that the teeth on the periphery of the mesh region are more lightly loaded than those at the center, and exhibit a clear point of contact. This stress propagates through the dedendum of the tooth and into the gear web, where the maximum value occurs. A result of this magnitude is relatively high and outside the normal material limits for steel, but these FGs haven't been optimized for the current load. Future iterations can address this by modifying the design accordingly, taking into account the feature refinements suggested in Chapter 3.

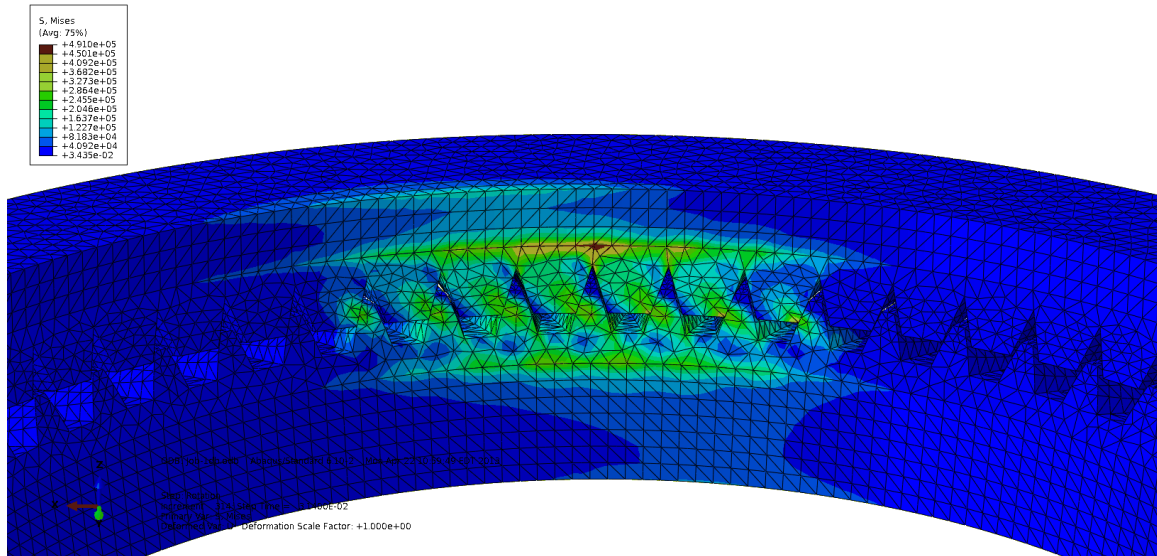


**Figure 30: Overall von Mises Stresses**

By removing one of the FG parts using the *Create Display Group* option, it is possible to examine these stresses at the same time step in detail. Looking at the external FG in Figure 31, several unique observations can be made, foremost of these regarding the point of contact on the inner radius. There is a clear load concentration in this area, which increases towards the center of the mesh region. Also, it can be seen that the load is more uniform across the face of the tooth according to this trend as well. Overall, the von Mises stress reaches a maximum of 333.7 Ksi in this situation, which is generally acceptable for steel.



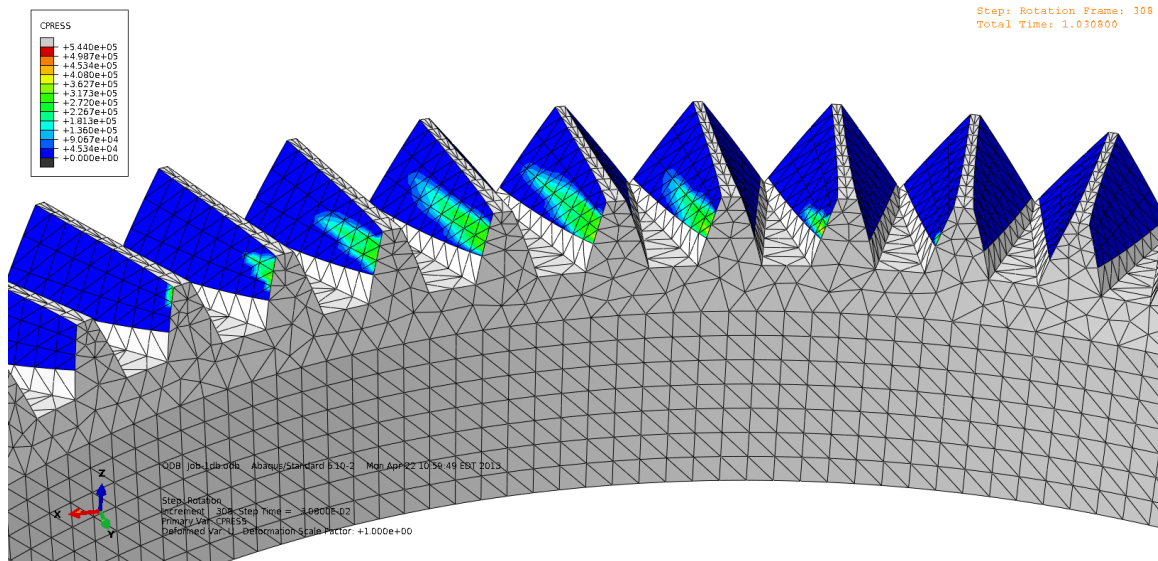


**Figure 32: Closeup of Contact Pressure**

Next, the system's angular displacement (UR) can be considered, which is of particular interest due to its fundamental relationship with TE. Using the *Create XY Data* option, the source can be set to *ODB Field Output* and position set to *Unique Nodal*. This allows *UR: Rotation Displacement Magnitude* to be selected, which will output the relevant components. Next, by switching to the *Elements/Nodes* tab, the *Reference Points* created earlier can be designated as the nodes of interest by changing the method to *Node Sets* and choosing the appropriate set for the external and internal FG. Once saved, the next task is to go under the *Report* menu, select *XY*, and choose all the listings present for export. However, before confirming this action, it is important that the data has an appropriate number of significant digits to ensure precision. This can be checked under the *Setup* tab, where number of significant digits should be set to nine and the number format *Scientific*. Then, these will be written as an "abaqus.rpt" file to the root program directory by default, much like the one shown in Appendix I. This data demonstrates both the final simulation values as well as the format used for subsequent calculations. Note that these

numbers have been truncated to save space, and the order in which the columns appear may vary due to the sequence of *Reference Point* creation and *Node Set* selection.

Next, it is necessary to process this raw data and apply the equations governing TE in order to understand the behavior of this FG system. Also, from this point forward, SI units will be used for more direct comparison to literature. With that objective in mind, a MATLAB code was developed which loads the output file and processes it as required; for reference, this code is available in Appendix J. Before examining these final results, however, it is useful to consider the magnitude of the internal and external FG angular position over time ( $\theta_1$  and  $\theta_2$  respectively). These are the fundamental measured quantities, and their difference can provide an initial glimpse into the system's TE. The equation governing this relationship is the following:

$$TEA = \theta_1 - \theta_2$$

**Equation 2: Angular Difference Representation of Transmission Error**

While basic, it is possible to observe that the contact and rotation steps are acting as intended in Figure 33. Furthermore, the data captured after rotation indicates that within two revolutions the angular difference maximizes at 0.2025 rad or 11.60 deg, as seen in Figure 34.

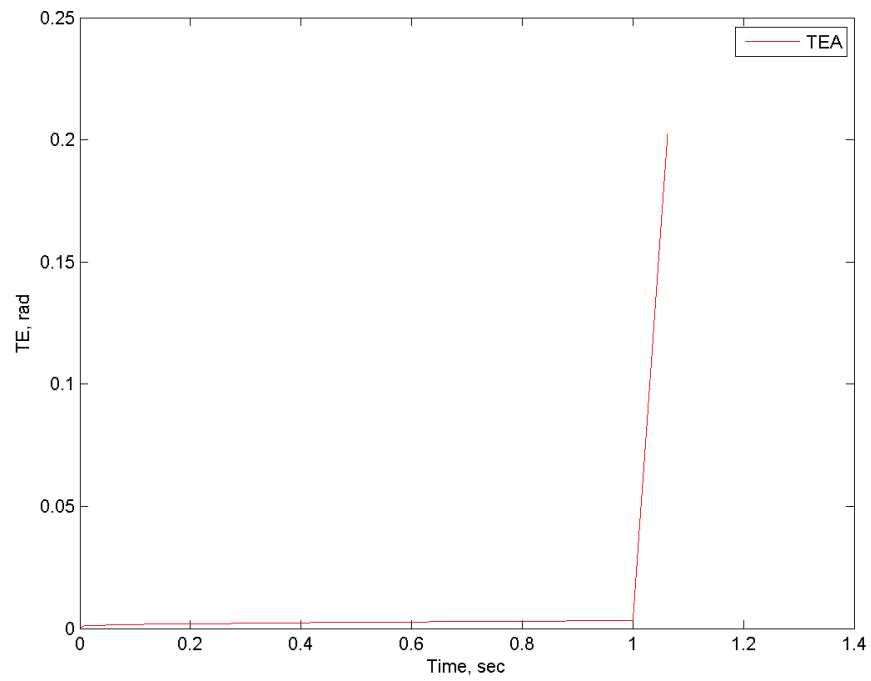


**Figure 33: Difference in Angular Position vs. Time**

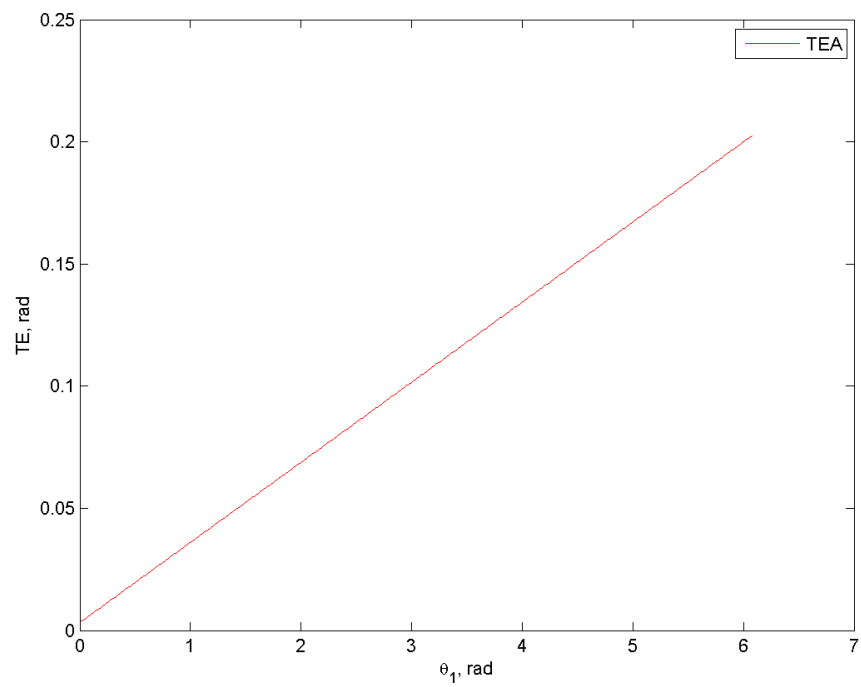


**Figure 34: Difference in Angular Position vs. Rotation**

Now, considering TE in the classic form represented by Equation 1, there are two graphs of interest. The first, Figure 35, represents TE over the course of the entire simulation. Initially, it rapidly gains value within the contact step, and reaches more than 75  $\mu\text{m}$  in 0.01 seconds. However, the slope diminishes as it approaches the point of rotation, eventually achieving a maximum of 205.87  $\mu\text{m}$  by one second of simulation time. This behavior is due to the elastic deformation of the gear teeth while the system is stationary and under a torque load. The value, however, is relatively high compared to typical TE in literature. Unfortunately, the reason for this is currently unknown, and will hopefully be resolved with future improvement of the model.

Next, after one second the system's input gear (represented by the external FG) begins to turn and introduces the unique behavior seen in Figure 36, which has a maximum, minimum, and range of 206.12  $\mu\text{m}$ , 205.69  $\mu\text{m}$  and 0.43  $\mu\text{m}$  respectively. On a per tooth basis, as shown in Figure 37, these values reach a maximum, minimum, and range of 25.77  $\mu\text{m}$ , 25.71  $\mu\text{m}$  and 0.06  $\mu\text{m}$  respectively.

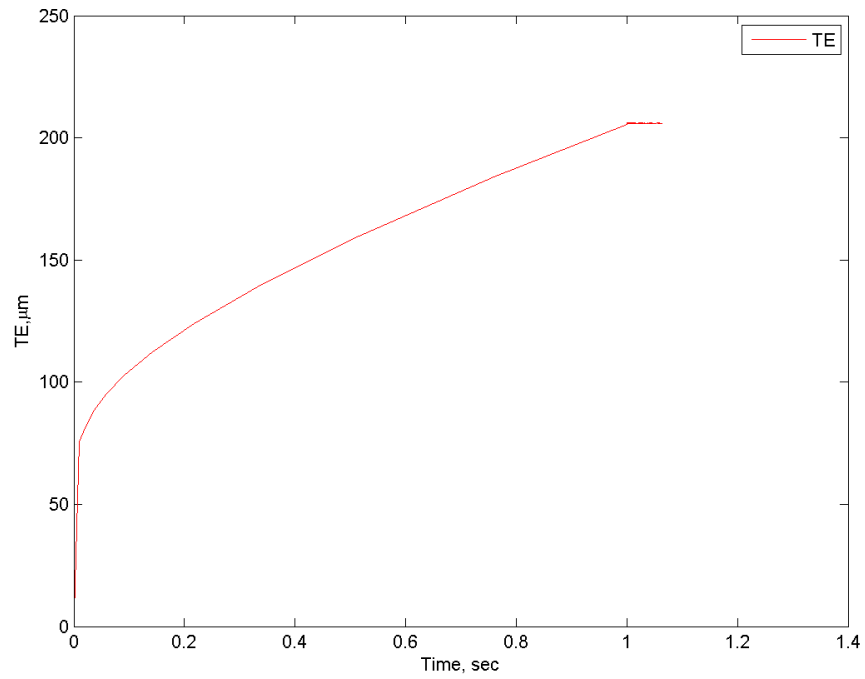


**Figure 35: TE vs. Time**

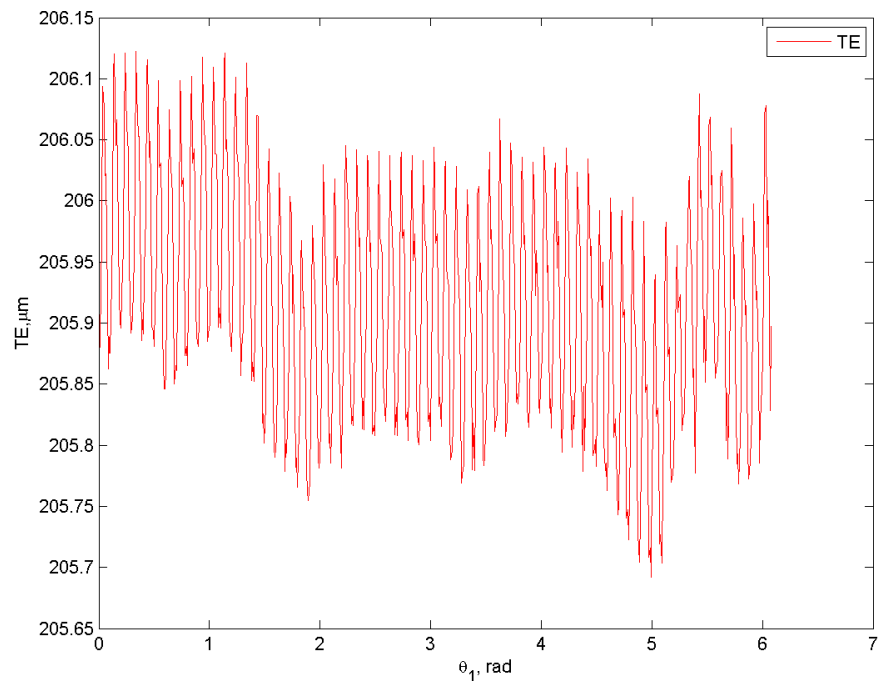


**Figure 36: TE vs. Rotation**

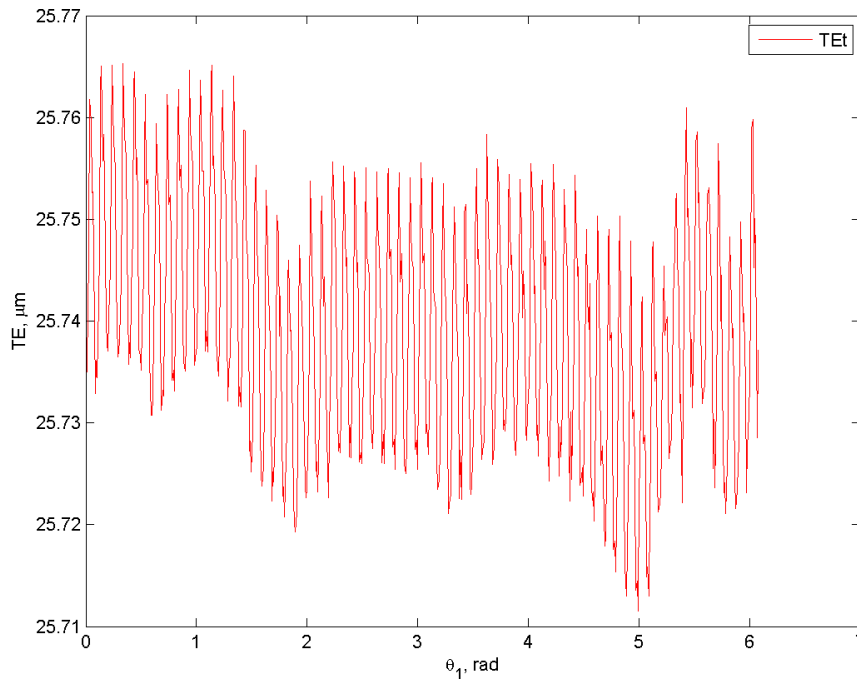


**Figure 37: TE vs. Rotation, per Tooth**

To complement the classic TE equation that generated these graphs, another unique approach was considered as well. This involved thinking of the system from a 3D perspective, where the pitch circle radius and FG angular displacements can be represented as X, Y, Z position vectors. Specifically, the pitch circle vector (represented by the variable  $rpV$ ) would have its origin at the pitch cone apex and terminate at a common mesh point that lies on the plane of the pitch circle of both the external and internal FG. In this particular case the pitch cone angle for the internal FG is 107.77 degrees, resulting in a pitch circle vector length of 2.71 inches. This concept can be seen below, in Figure 38 and Figure 39.

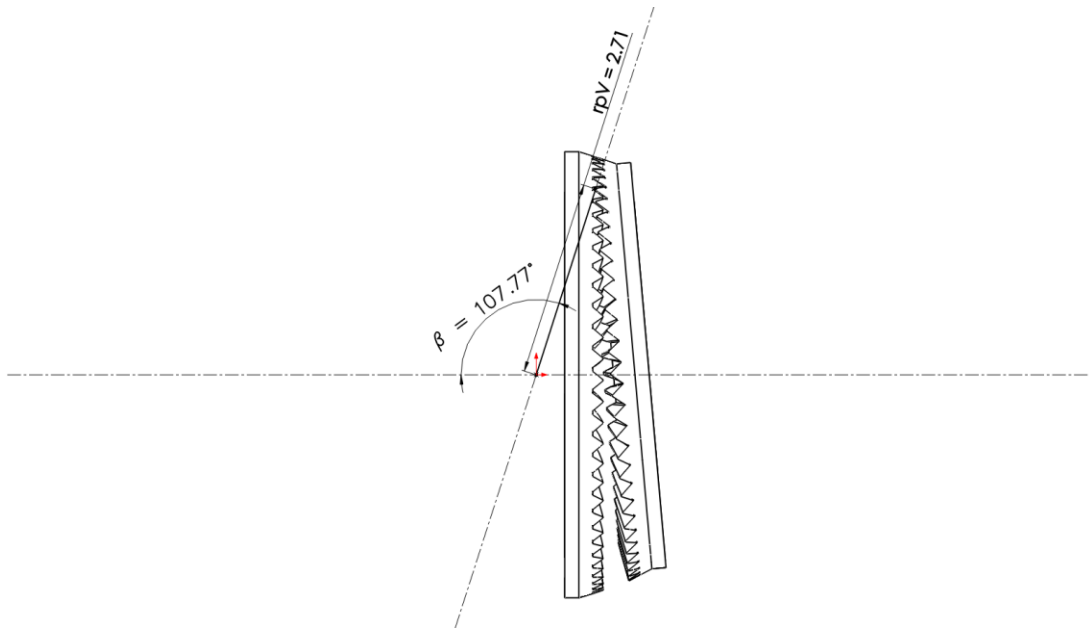


**Figure 38: Transmission Error Vector Geometry**

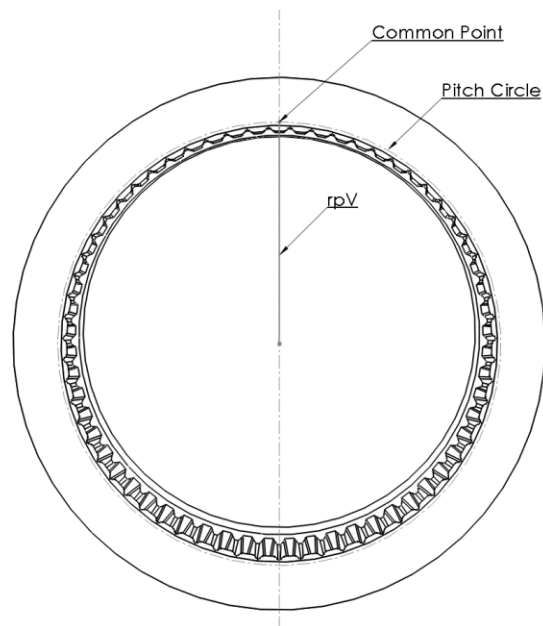


**Figure 39: Pitch Circle and Associated Relations**

Mathematically, this idea can be represented by a magnitude cross product between the new position vector and the system's angular displacement. In that case, the latter would be

composed of the difference between the X, Y, and Z rotation of both FGs. Such an approach is represented by Equation 3, which is a unique expression of TE and a new concept for FG analysis.

$$TEVM = |rpV \times \Delta\theta_{12}| = \left\| \begin{bmatrix} rp_x \\ rp_y \\ rp_z \end{bmatrix} \times \begin{bmatrix} \theta_{1x} - \theta_{2x} \\ \theta_{1y} - \theta_{2y} \\ \theta_{1z} - \theta_{2z} \end{bmatrix} \right\|.$$

**Equation 3: Vector Representation of Transmission Error**

Once applied to the data for the system, both mesh and individual tooth TE values were produced in much the same manner as done previously. In Figure 40 the overall behavior can be seen, which rapidly gains value before reducing its slope up to the point of rotation, again maximizing at 205.87  $\mu\text{m}$ . Next, Figure 41 illustrates the behavior after rotation, which is increasing over time and therefore does not present a viable maximum or minimum. This is an interesting outcome that could be explored with further data, but since the processing ability, memory capacity, and simulation time of the computer systems used approached their capacity this was not addressed.

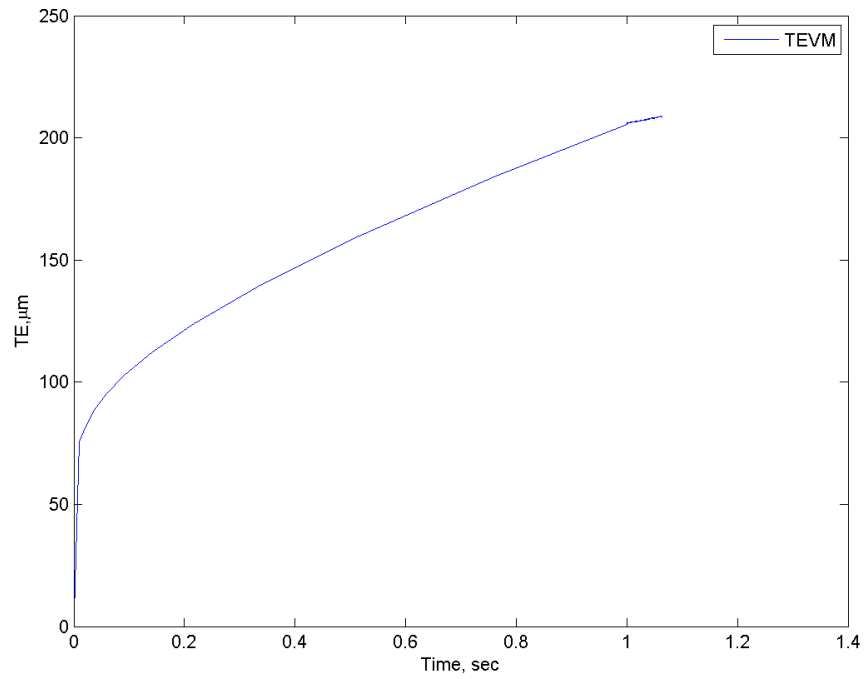


Figure 40: TEVM vs. Time

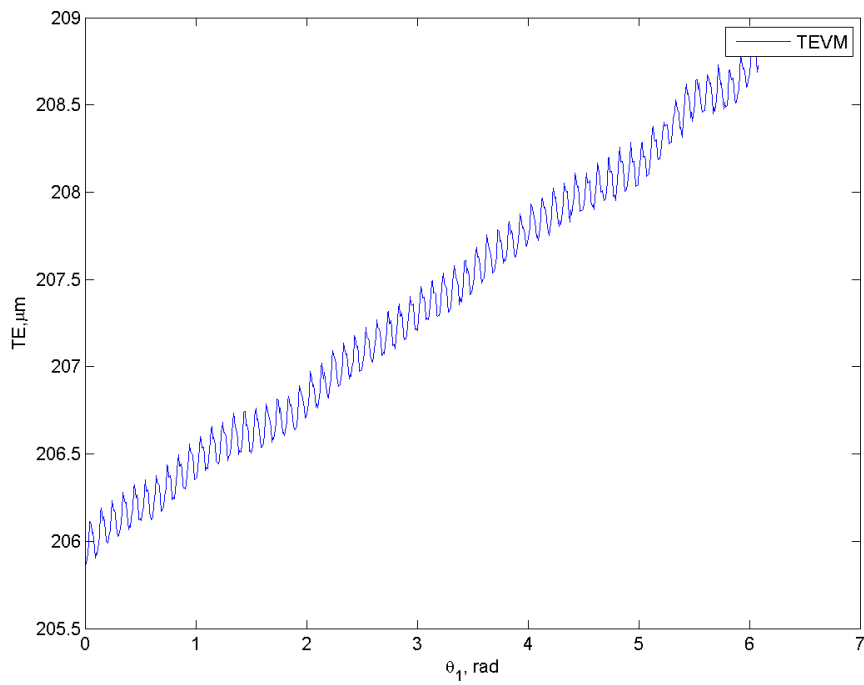
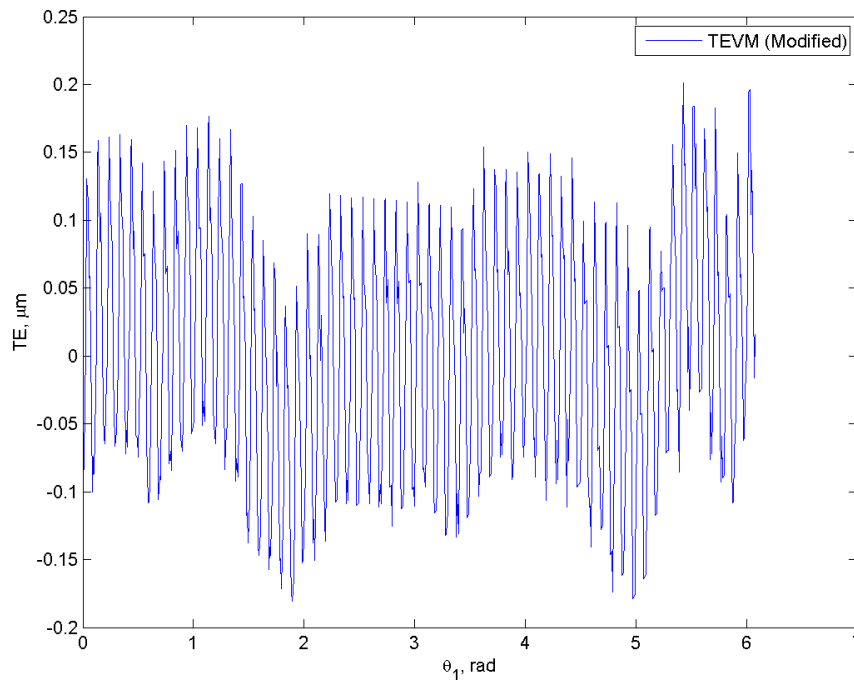
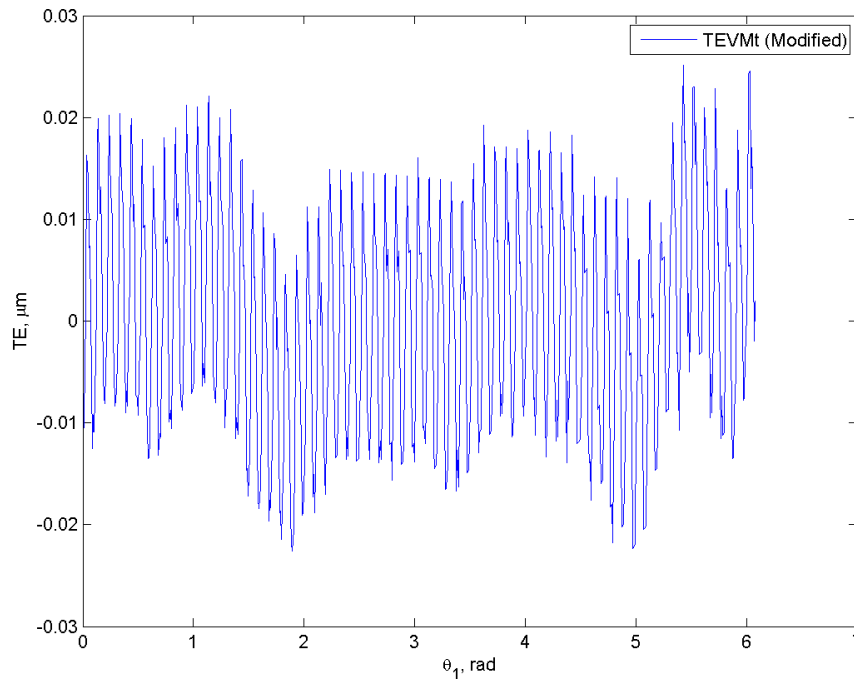


Figure 41: TEVM vs. Rotation

In order to further evaluate this phenomenon, the function was corrected to remove its slope and intercept, which had the effect seen in Figure 42. Here, it is possible to observe that the maximum, minimum, and range for the mesh are  $0.201\ \mu\text{m}$ ,  $-0.181\ \mu\text{m}$ , and  $0.382\ \mu\text{m}$  respectively. Again, it is valuable to look at this on a per tooth basis in Figure 43, which has a maximum, minimum, and range of  $0.0251\ \mu\text{m}$ ,  $-0.0226\ \mu\text{m}$ , and  $0.0477\ \mu\text{m}$  respectively.



**Figure 42: TEVM (Modified) vs. Rotation**



**Figure 43: TEVM (Modified) vs. Rotation, per Tooth**

### 5.1 Analysis

The von Mises stress and contact pressure results produced by the simulation provide a number of key insights that both confirm and enhance current FG theory. The first of these is the previously noted stress on the inner radius of the FG when in a loaded state, which was predicted by Saribay and can now be directly observed [13]. Using this knowledge, it is possible to optimize the FG design and generation procedure in the future. In addition, the contact pressure plots reveal the fundamental presence of line contact between the external and internal FG. This is apparent during the contact step, when a gradual load is applied and the various pairs of gear teeth begin to mate and deflect accordingly. For example, Figure 44 below is at the beginning stages of contact, Figure 45 is a relative midpoint, and Figure 46 occurs immediately before

rotation. Over the course of these three stages the contact pressure region becomes noticeably wider and longer, which is an indicator of higher quality interaction.

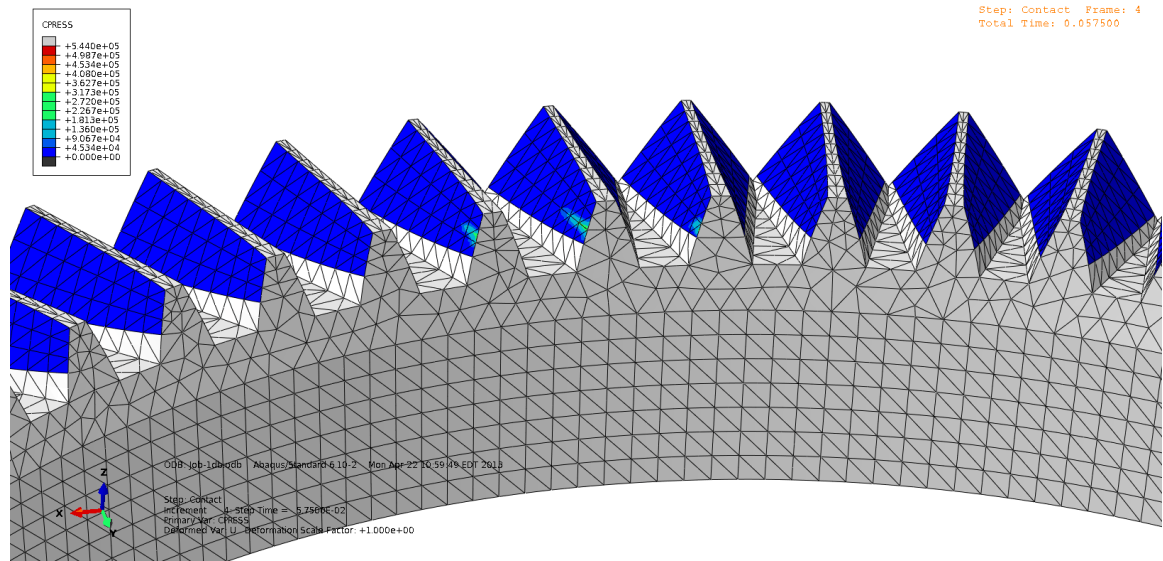


Figure 44: Closeup of Contact Pressure, Early

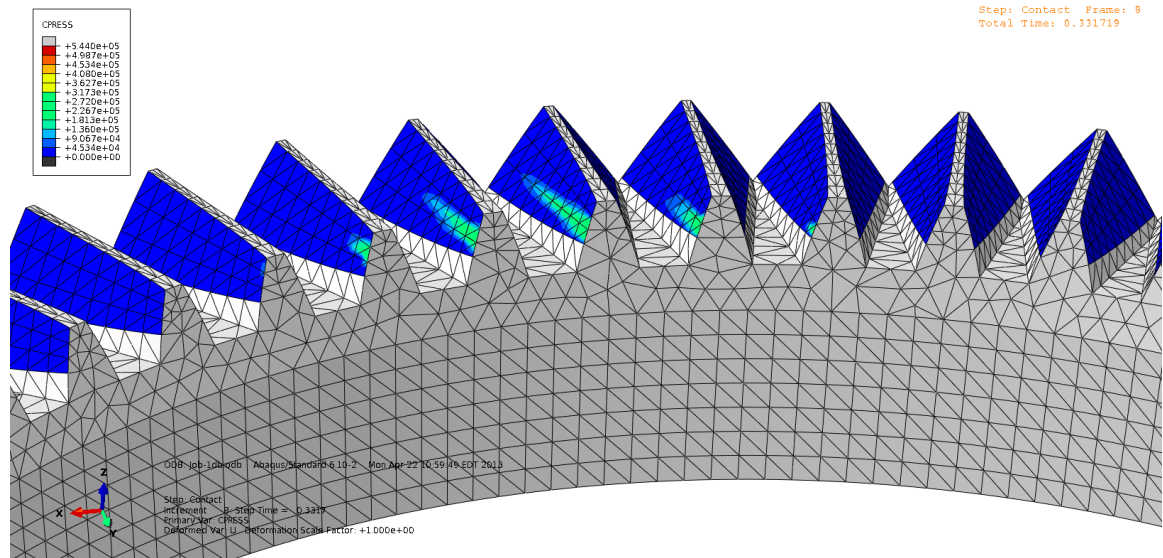
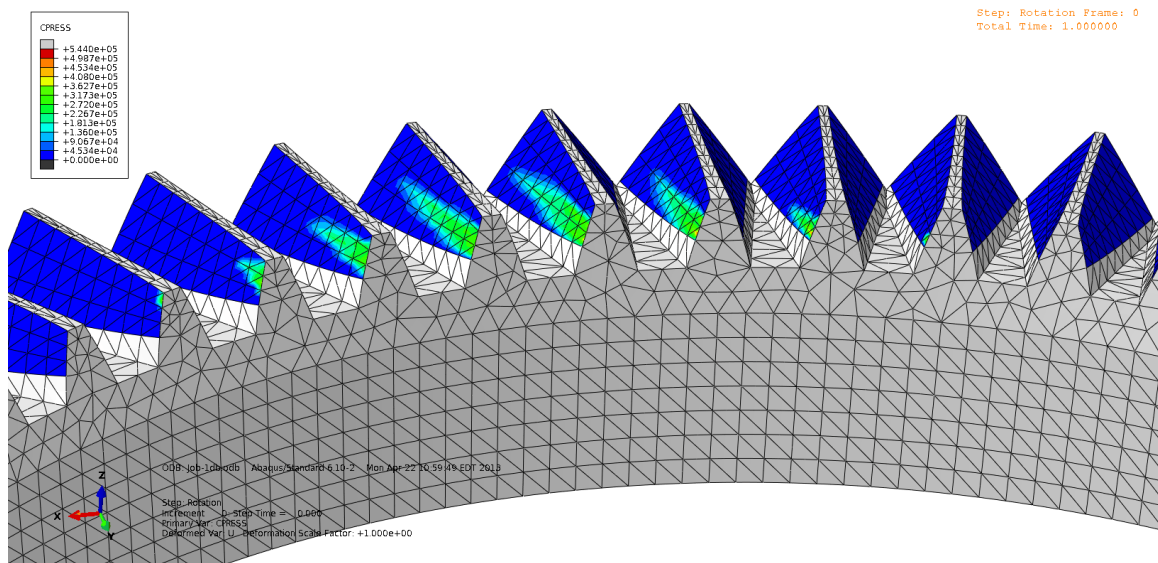
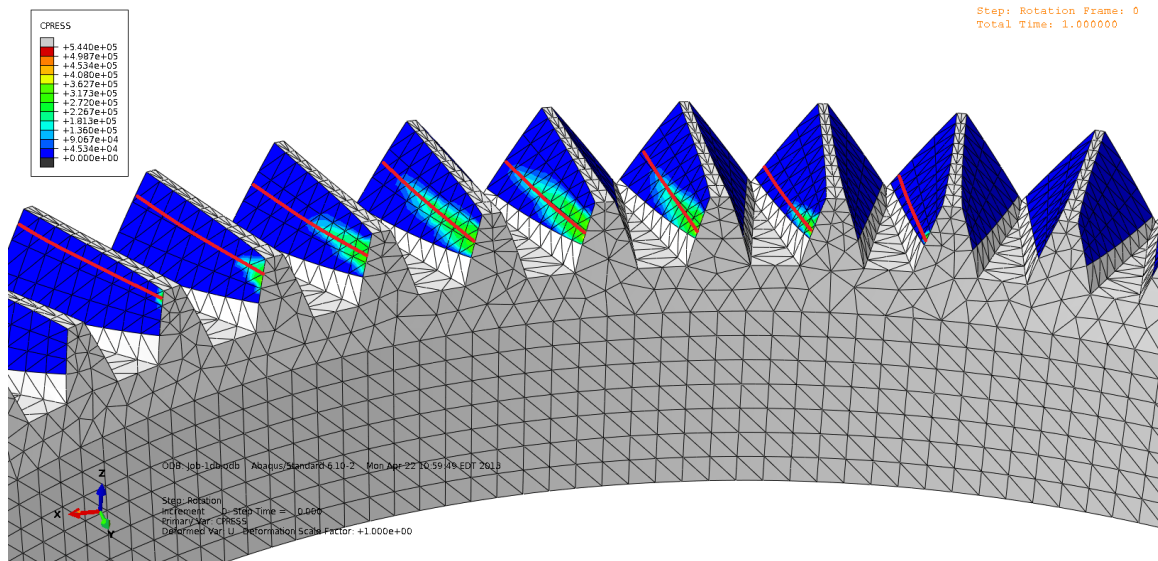


Figure 45: Closeup of Contact Pressure, Midpoint



**Figure 46: Closeup of Contact Pressure, Late**

Lastly, there is a distinct progression in the location of the contact line across each tooth face in the mesh region. As demonstrated by Figure 47, it begins in the addendum of the leftmost tooth, and progresses between teeth until it ends up in the dedendum of the rightmost tooth. This indicates that within the mesh region there is a plane of contact, which is analogous to the bevel gear behavior originally predicted and described by Mark [53].



**Figure 47: Closeup of Contact Line Progression**

At this stage, it is important to examine the behavior present in the data, which encompasses three different expressions: TEA, TE, and TEVM. The first, which considers the angular deviation of the external and internal FG, indicates there is a distinct difference between the two simulation steps. This is expected, with the angular difference growing slowly over the contact step, and then a noted increase occurring after one second when the rotation step is active. During the contact step, the external FG is being held in place as the internal FG is pressing up against it, causing the teeth to deflect and allow for limited angular displacement. Then, once rotation occurs, the external FG rotates  $2\pi$  radians and drives the internal FG as prescribed. To further explore this idea, it is possible to compare the simulated and calculated rotation of the external FG with the expectation that these would be the same in an ideal system. In particular, the calculated value is fundamentally governed by the gear ratio of the FG pair (represented by the variable  $mp$ ), which in the case of a 61 tooth external FG and 63 tooth internal FG is 0.968. By taking the internal FG angular displacement as provided by the simulation, and dividing by this value, it is possible to produce the calculated values for the external FG according to basic

gear theory. The graph of these two values, seen below in Figure 48, illustrates the agreement between the different approaches due to the overlap between their values.

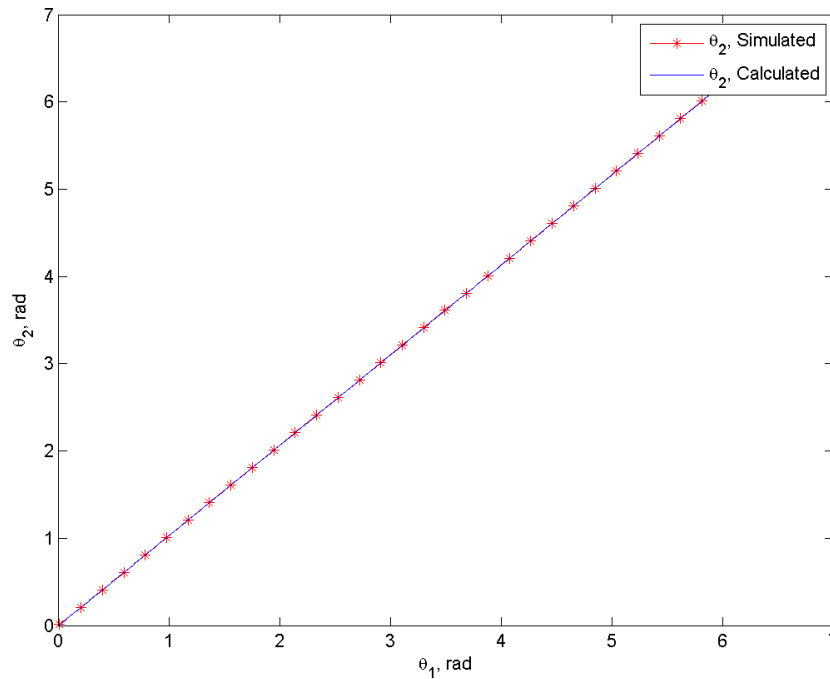


**Figure 48: Simulated and Calculated Angular Position vs. Rotation**

Despite the visual consistency seen in the previous graph, it is important to examine the values more rigorously to confirm that their deviation is within reasonable bounds. This comparison is expressed by Equation 4 below, and once applied produces the data seen in Figure 49. The deviation has a maximum, minimum and range of 0.003248 rad, 0.003242 rad and 0.000006 rad respectively. This discrepancy can be considered very small and confirms that the system is performing as expected.

$$\Delta\theta_2 = \theta_{2,simulated} - (\theta_{1,simulated}/mp)$$

**Equation 4: Angular Rotation Analysis of the External FG**

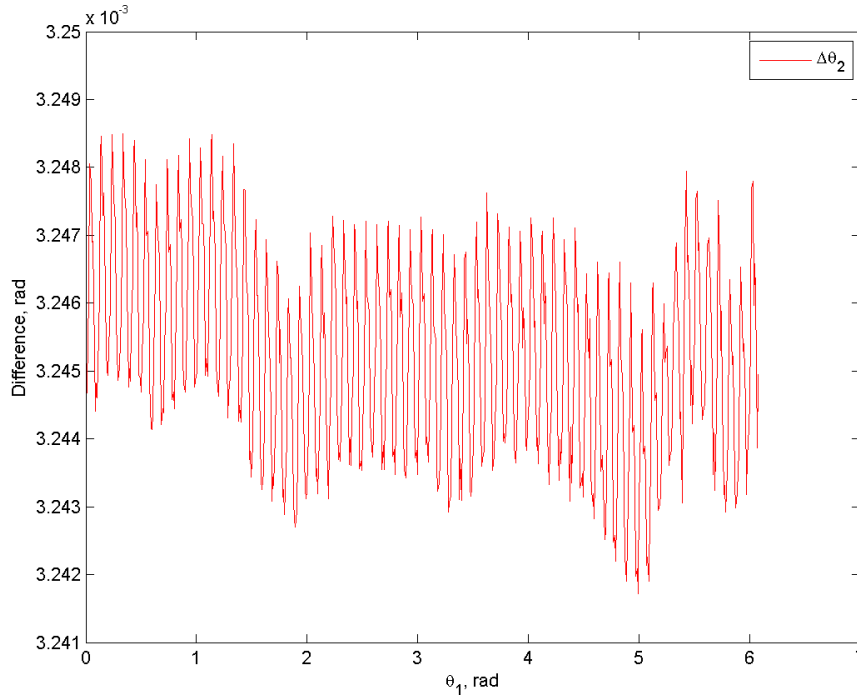


**Figure 49:  $\Delta\theta_2$  vs. Rotation**

Next, turning to the TE and TEVM values, it is first important to consider if their overall behavior is convincing and agrees with expectations. The region of greatest interest is after rotation begins, which exhibits a periodic fluctuation that is characteristic of TE across all the literature sources. Theoretically, this is due to the individual teeth entering and leaving the mesh at a rate dependent on the angular velocity of the system, which causes variations in the mesh stiffness. If the peaks and valleys of this system's TE and TEVM graphs share this relationship, that represents a confirmation of the physics of the simulation. This is indeed the case, and when plotting vertical lines at the period at which teeth enter or leave the mesh the result can be seen

below in Figure 50 and Figure 51. Note that in this case, the period of mesh is total rotation divided by the number of teeth on the driving gear, which results in 0.0997 rad per tooth. Also, only a selection of the total rotation is shown to highlight the detail present in the individual peaks.

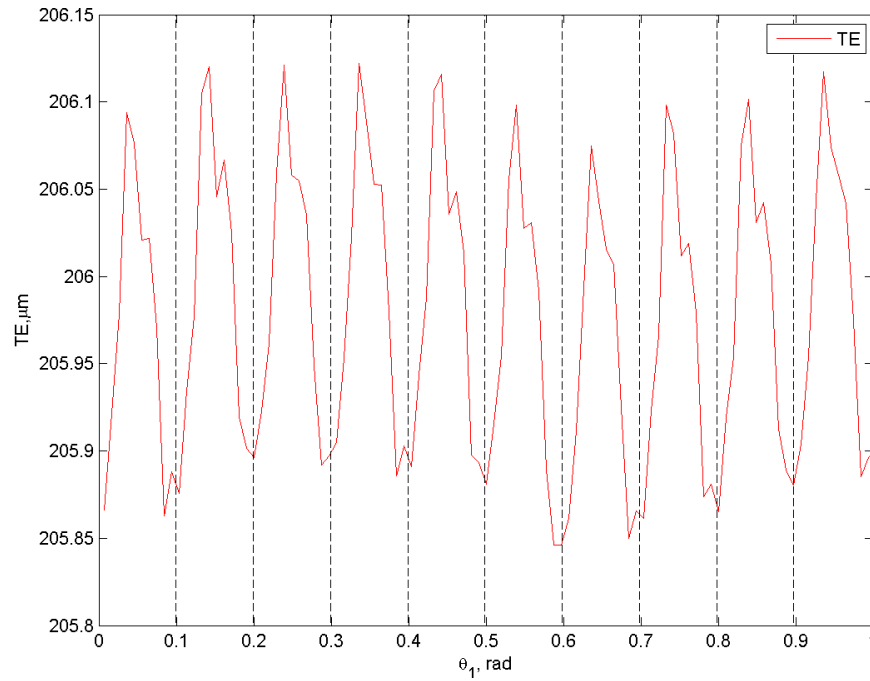


**Figure 50: TE vs. Rotation with Tooth Period Indicators**

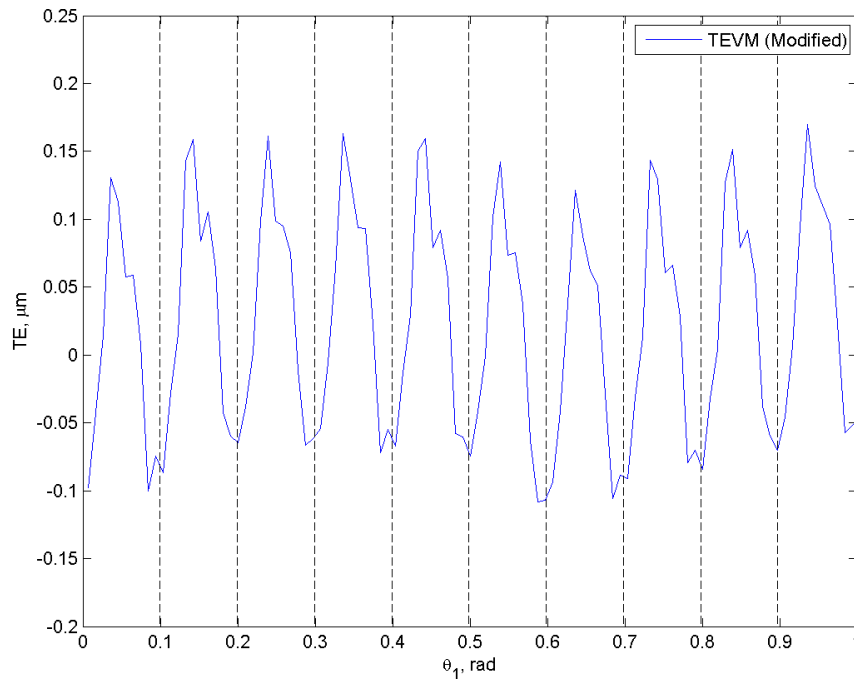


**Figure 51: TEVM (Modified) vs. Rotation with Tooth Period Indicators**

Furthermore, the median value of both TE and TEVM changes as the system rotates, which represents a form of drift in the data. This is likely a result of the contact algorithm being used as part of the sliding formulation, or the normal/tangential behavior of the contact interaction definition. All of these were based on the assumption of frictionless and finite sliding, which may not be the case. Additionally, there are a number of avenues where error could have been introduced to the simulation, as detailed below in Table 10. Resolving these problems was outside the scope of this work, and will be recommended for future investigation.

**Table 10: Overview of Error Sources**

<b>Potential Source of Error</b>	<b>Reason</b>
Importing contact lines into SolidWorks and creating a surface	To create the geometry between lines, SolidWorks must interpolate the values
Converting the SolidWorks part to a generic file format (STEP)	The geometry is processed and approximated to generate a non-native output
Meshing the part geometry	Nodes form tetrahedral FE shapes that approximate the geometry according to density

In addition to the general behavior, it is important to consider the specific values that are being produced. While no experimental data exists for a conjugate meshing FG pair, the theoretical work presented in Chapter 2 provides some guidelines and insight. Based on the expressions for single tooth and mesh deflection by DeSmidt and Zhao [54], and taking into account the parameters of this particular FG system, a MATLAB code was developed and provided for reference in Appendix K. Using this method, which relies upon a series and parallel spring model, the single tooth deflection was estimated at 41.5  $\mu\text{m}$  while the mesh deflection was 83  $\mu\text{m}$ . Assuming perfect teeth without geometric errors/modifications, these deflections are considered analogous to those produced by the Abaqus simulation. Using that as the basis for comparison, the FG pair TE featured a lower single tooth deflection of 25.77  $\mu\text{m}$  but a higher mesh deflection of 206.12  $\mu\text{m}$ . On the other hand, using the TEVM representation, much lower values were seen for both the single tooth and mesh, which were 0.201  $\mu\text{m}$  and 0.0251  $\mu\text{m}$  respectively. Another possible opportunity for comparison is the peak-to-peak TE value for the mesh, which is 0.43  $\mu\text{m}$  for the classic TE equation and 0.382  $\mu\text{m}$  for TEVM. These are both less than the common standard of 1  $\mu\text{m}$  peak-to-peak TE for a precision gear pair [25], and indicates the FG system is effective.

## 5.2 Summary

Throughout this chapter, the results of the previously outlined simulation were presented with emphasis on physical phenomena and key TE values. Initially, the overall von Mises stress present in the FG mesh provided some visual clues to the behavior of the system. It was clear that there was a range of stress throughout the teeth, with the outer edges of the mesh experiencing less than the center. Also, it was visible that the root and gear web of the tooth carried some of the stress as well. By looking at the external FG individually, this was confirmed further, along with another important observation. Namely, the inner radius of those teeth experienced the highest stress, which was predicted by previous literature. In addition, switching from von Mises stress to contact pressure revealed the distinct presence of contact lines between the two FGs, as expected. This followed the same behavior as the stress, with the contact lines being shorter on the outside of the mesh and increasing towards the center across eight teeth. These also accurately reflected the torque load on the system, visibly increasing in length during the contact step. Even more revealing was their orientation, which progressed throughout the mesh from the upper tooth face on one end to the lower tooth face on the other. This indicated a plane of contact was present, confirming another behavior detailed in the literature.

Next, turning to the graphs of TE, the first to be considered was TEA. This provided insight into the rotational behavior of the system and validated that the contact and rotation steps were performing as expected. This was further confirmed with a graph of the theoretical and simulated rotation of the external FG, which agreed with one another. Using the classic TE equation, another graph was created which illustrated the system's stationary tooth deflection up until the point of rotation, and then produced fluctuating values afterwards that represented the change in stiffness as teeth entered and exited the mesh. In fact, the minimum of each fluctuation

coincided with the angular period for a tooth, closely reflecting results seen in literature for spur gears. However, it was relatively high and an alternative vector expression known as TEVM was developed with the hope of more accurately representing a three dimensional system. This was a unique contribution that proved to be successful in producing a TE value that aligned with, and was in fact an improvement on, the performance of a precision gear. Like the traditional TE, this agreed with the angular period for the teeth interacting with the mesh. These graphs and the subsequent analysis they facilitated were the result of fulfilling the final two objectives for this work, which included gathering TE data for a FG pair, exploring alternate expressions of TE, and understanding the mesh and tooth dynamics.

## Chapter 6

### Conclusion

Currently, vertical lift technologies touch every aspect of our society, ranging from the way that we are transported in a medical emergency, how we respond in a natural disaster, and the tools available to our armed forces. Over time, these sectors will only expand and evolve to fill more roles with increasingly demanding performance requirements. In addition, future applications which are outside any current considerations will surely develop. These opportunities, and challenges, require innovative technologies that push the envelope of what is possible. One of the most promising possibilities is PMT technology, which has the potential to be the definitive next-generation drivetrain component by reducing weight, part count, overall size, and maintenance costs. In order to support the viability of this concept, this work has attempted to develop fundamental tools and results related to a FG pair. Primary contributions include:

1. Documenting the modeling process
2. Developing and documenting the simulation process
3. Computationally obtaining TE data for a FG pair
4. Exploring a novel TE expression for FG applications
5. Creating original TE analysis code
6. Computationally exploring the physics of FG performance and comparing to what is available in the literature

The initial two results fulfill the first research objective, which sought to implement commercial software packages in order to address the problem of robust evaluation tools.

Contributions three, four, and five accomplish the second objective intended to understand static TE in the FG pair. This was in response to the second research problem that required comprehensive performance knowledge to be developed. Finally, the sixth contribution resolved the third objective to explore mesh and tooth dynamics in order to confirm previously predicted behavior.

In detail, the modeling process contained in Chapter 3 will serve as a basis for producing future FG variations consistently and reliably. This will be exceedingly important as the theoretical and computational efforts that complement FG analysis mature. With regard to the simulation process, the detailed step and parameter information provided in Chapter 4 represents a fundamental development in the ability to understand the performance of a FG system. Using this methodology, additional data and complimentary performance metrics can be gathered to ensure the long term viability of this project. In addition, derivative system configurations can be pursued with relative ease, allowing the design space of a FG system to be explored further. Also, the generation of TE data for a FG pair and development of a novel mathematic expression in Chapter 5 represents a first of its kind effort which has not been attempted before. This information provides insight into the performance of the current generation FG model, and a baseline for further development. Using the corrected vector expression of TE as the method of choice reveals that a peak-to-peak value of  $0.382 \mu\text{m}$  is possible, which when compared to an average of  $5 \mu\text{m}$  for standard gears and  $1 \mu\text{m}$  for their high performance counterparts is an exceptional achievement [25]. Lastly, these calculations were made possible by code outlined in Appendix J, which serves as the bridge between the simulation and the graphs necessary to understand its behavior. This can be leveraged in the future to efficiently process TE data and serve as a modular framework for other metrics.

Taken as a whole, these various contributions represent a robust package for the development and analysis of a FG pair, and have been developed from the ground up to suit this purpose. It is expected that they will benefit the ongoing FG research at PSU, as well as the gearbox community as a whole going forward.

### **6.1 Future Work**

The potential for the PMT and conjugate meshing FGs is significant, and therefore the research scope is likely to expand rapidly over time. Some opportunities are particularly apparent at this point, foremost among them the experimental validation of the tools and methodologies that have been developed. The capabilities of the computational tools and hardware have been pushed to their limits in the course of this investigation, and unless the fundamental results are tested against a physical prototype it will be difficult to progress further. In particular, the TE and TEVM values should be examined closely for both the accuracy of their overall behavior and actual numerical value. However, once validated, it will be possible to further refine the simulation and data analysis code to more accurately represent reality. When these two efforts have converged, a powerful tool will be available to support the case for adoption of FG technology and the PMT. Currently, a test rig has been assembled and a FG pair has been released for quotation, which puts this task on track for completion in 2014. Another high priority objective would be the execution of a parameter study which explores the impact of various loads, reduction ratios, and nutation angles on FG performance. All of these factors are likely to affect overall TE and tooth stresses, but the extent of that impact should be quantified to understand the system relationships on a more fundamental level. This should be relatively straightforward now that the simulation process is understood and outlined in detail. On a related note, approaches to designing an optimum root fillet need to be considered due to the importance

of this geometric feature to the operation of a realistic gear. This was only outlined as a consideration previously, but must be systematically pursued. Next, it would be useful to explore the load sharing properties of the FG pair, which will play a role in the overall PMT design. Finally, all of the analysis up to this point has been focused on a static TE case, but this should be complimented by a dynamic analysis as well. Some efforts were made in that direction during this research, but were eventually set aside in favor of maintaining a specific focus.

This list is by no means exhaustive, and should only serve as a starting point for future investments. However, it is likely that as each of these fundamental issues are addressed the confidence in FG technology will grow exponentially. Ultimately, it is hoped that this document encourages discussion and interest in an exciting invention that has the potential to make a positive impact in the helicopter industry.

## Appendix A

### SolidWorks: FeatureManager Design Tree

Within SolidWorks, the FeatureManager Design Tree serves to record all modeling and sketching activities that take place. In this case, Figure 52 shows the typical steps taken to create an internal or external FG. In addition, the three steps first outlined in Figure 8 are indicated along with their relevant actions.

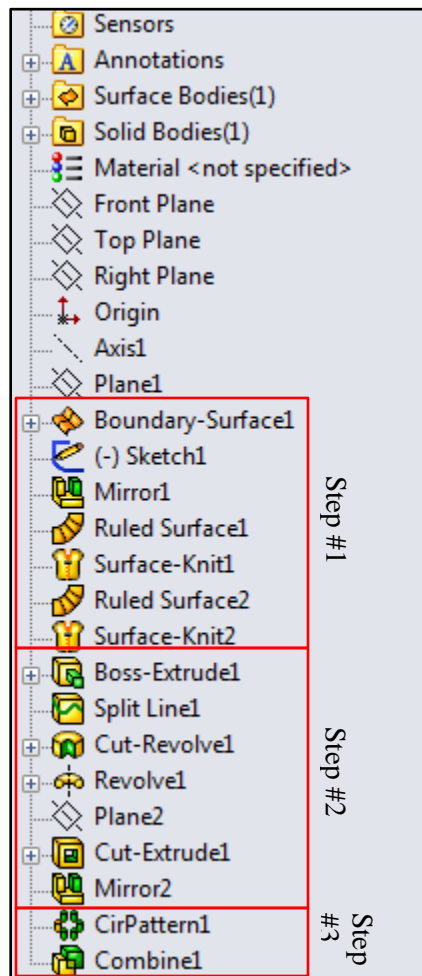


Figure 52: SolidWorks FeatureManager Design Tree for FG Generation

## Appendix B

### SolidWorks: Detailed Menu Items

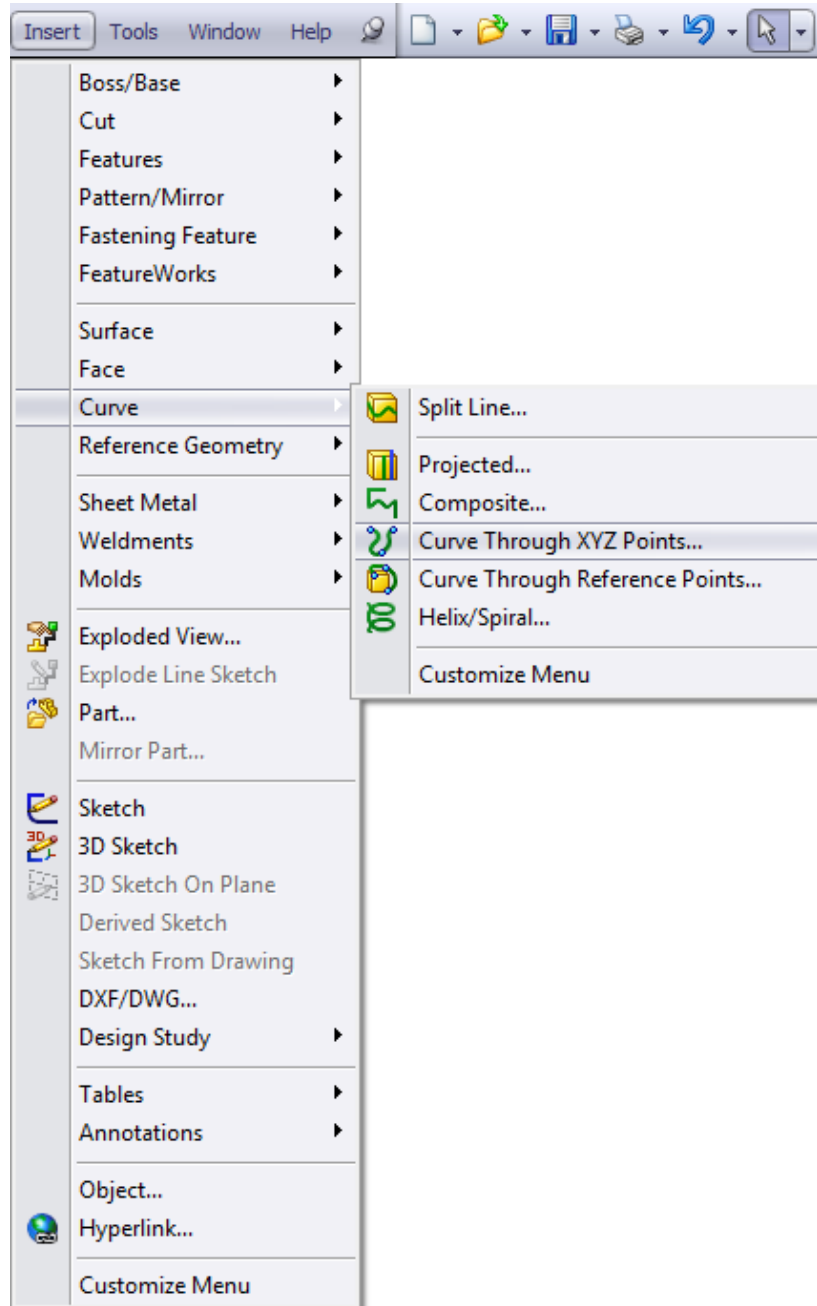


Figure 53: Curve Import Menu Item

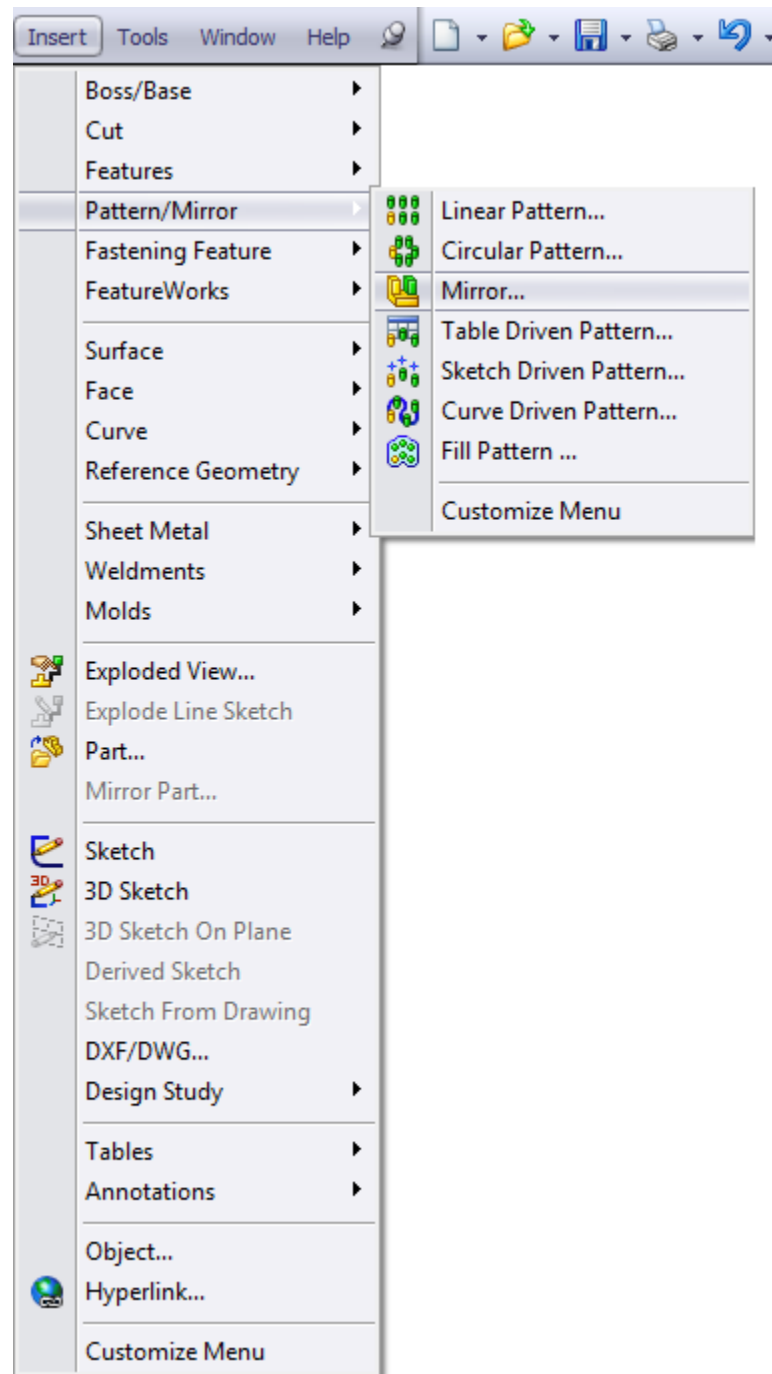


Figure 54: Mirror Menu Item

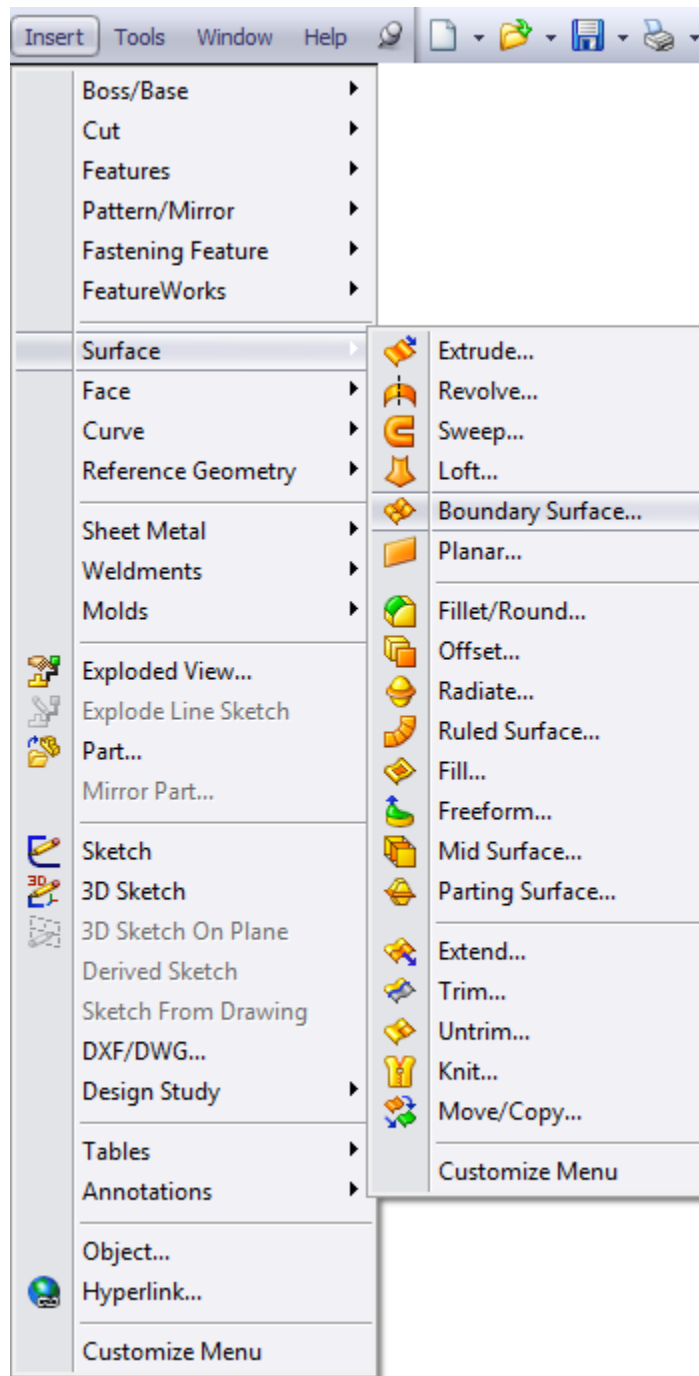


Figure 55: Boundary Surface Menu Item

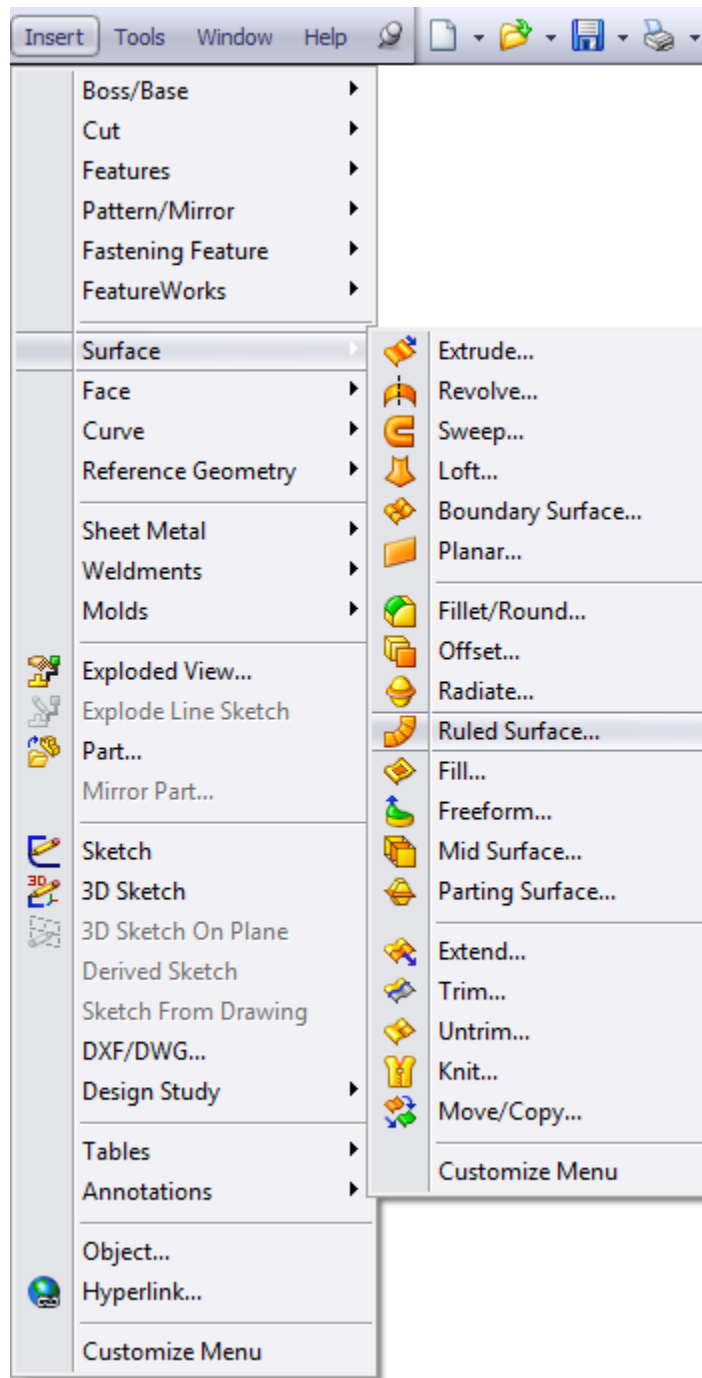


Figure 56: Ruled Surface Menu Item

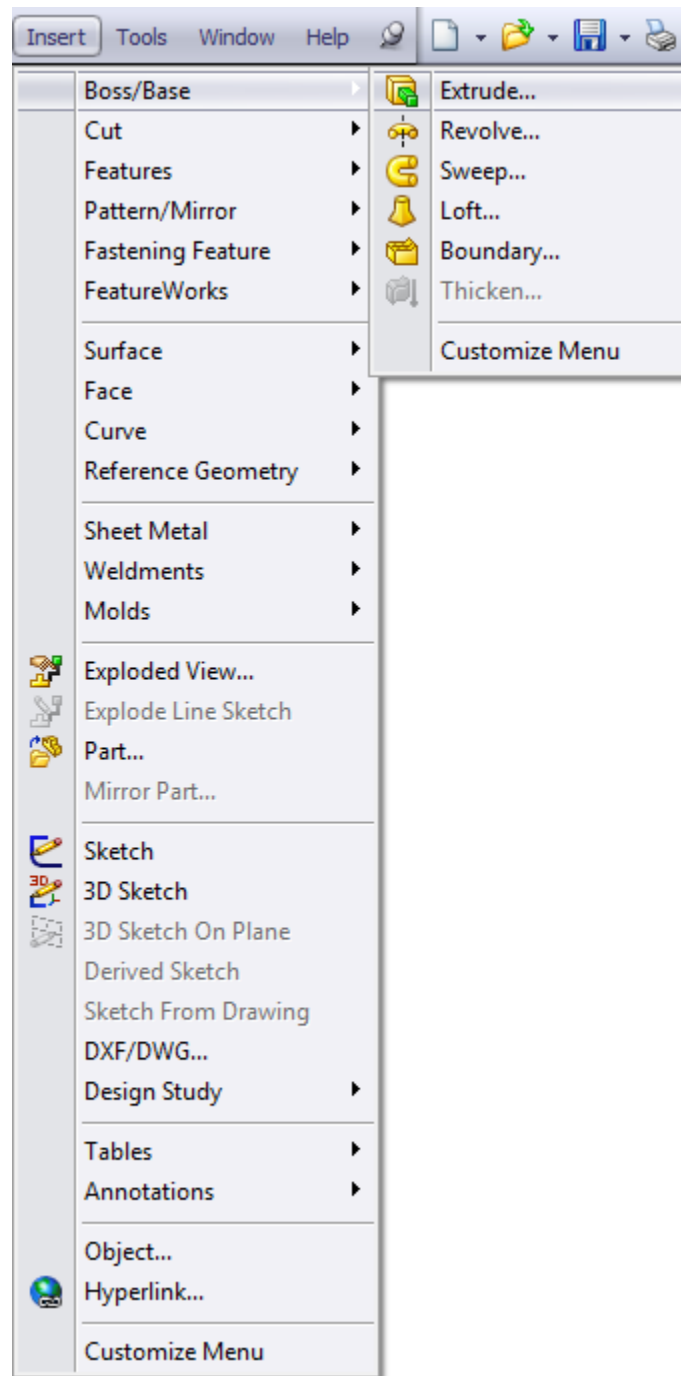


Figure 57: Extrude Menu Item

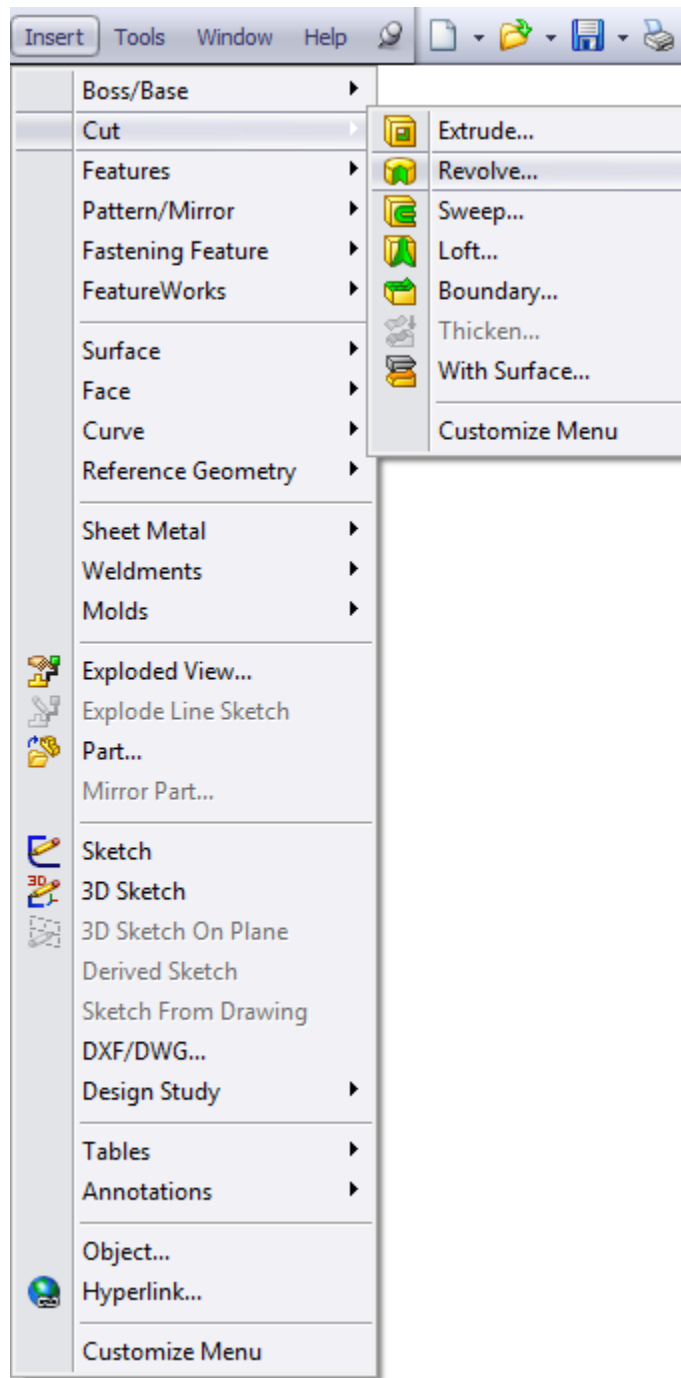


Figure 58: Cut Menu Item

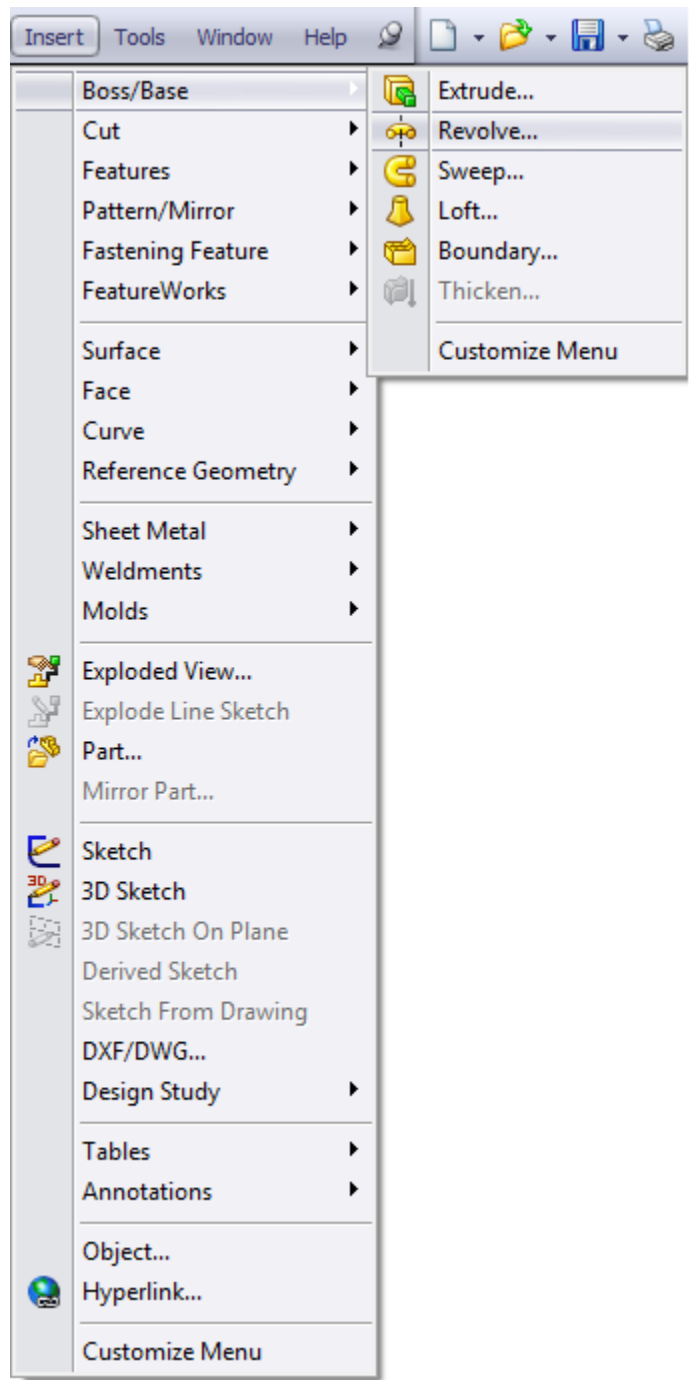


Figure 59: Revolved Boss/Base Menu Item

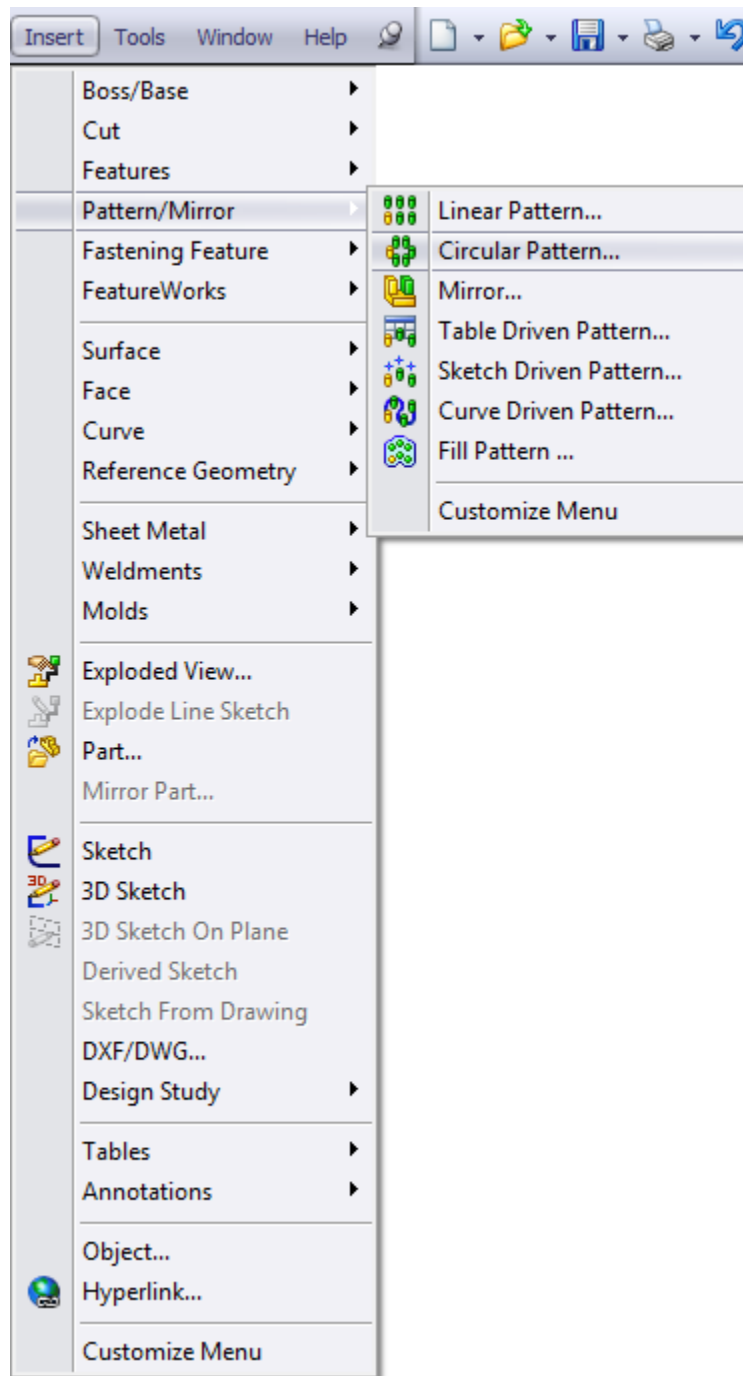


Figure 60: Circular Pattern Menu Item

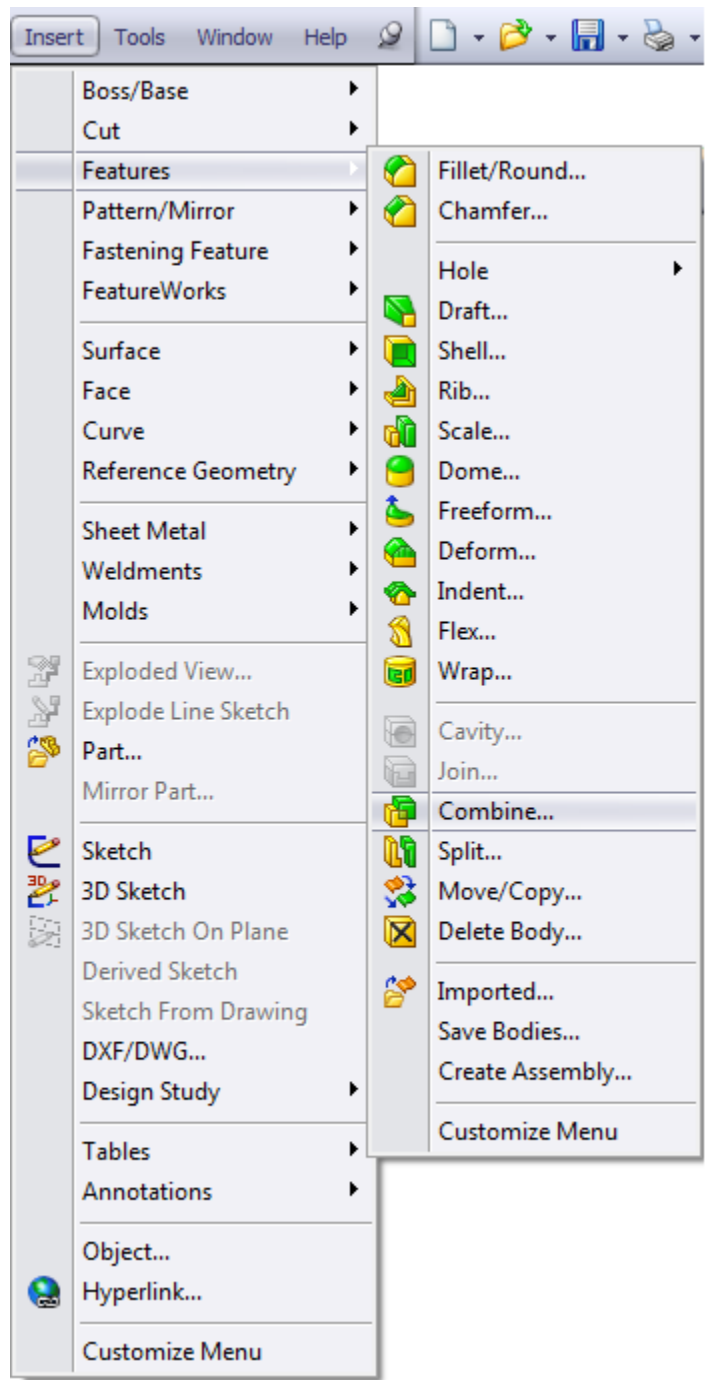


Figure 61: Combine Menu Item

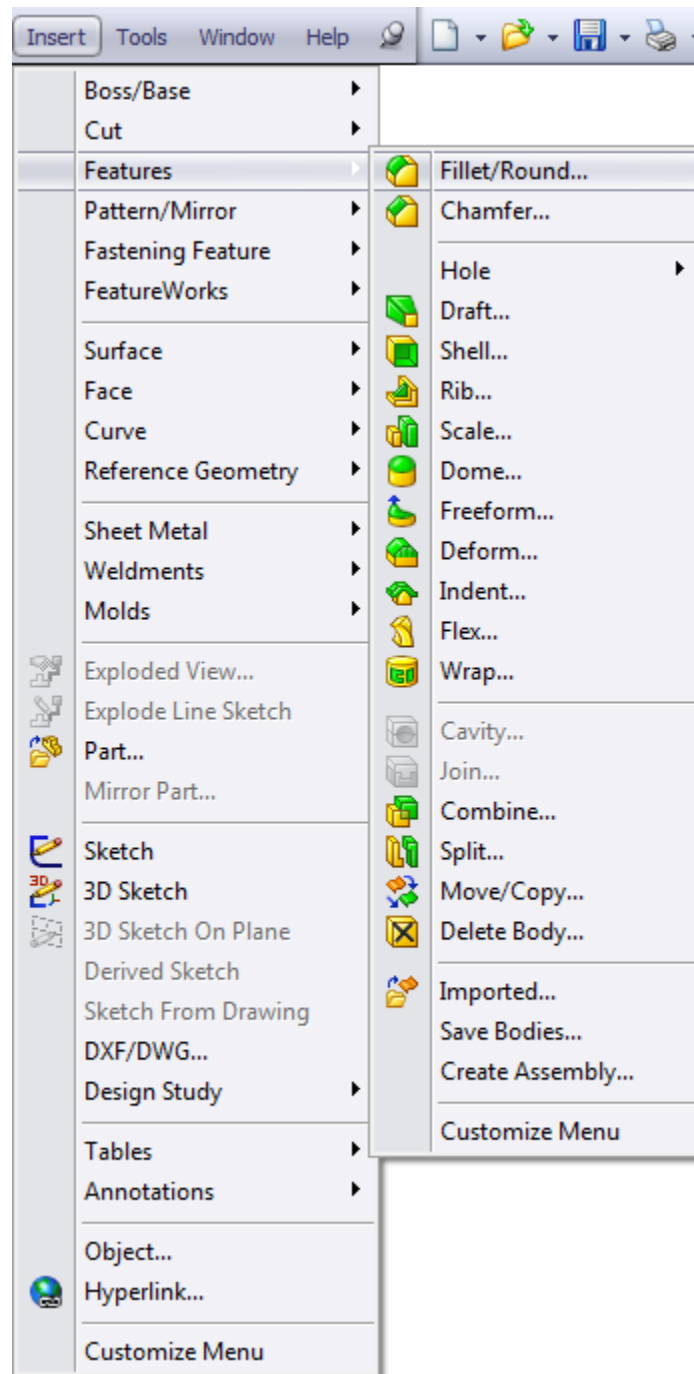


Figure 62: Fillet/Chamfer Menu Item

## Appendix C

### FG Design Parameters

**Table 11: External FG Data**

Category	Value
AGMA Quality	12
Number of Teeth	61
Inner Radius ( <i>in</i> )	4.56
Outer Radius ( <i>in</i> )	5.64
Diametral Pitch ( <i>1/in</i> )	12.2
Mean Pressure Angle ( <i>degrees</i> )	25
Pitch Diameter ( <i>in</i> )	5
Mean Whole Depth ( <i>in</i> )	0.184
Face Width ( <i>in</i> )	0.5303
Tooth to Tooth Composite Tolerance ( <i>in</i> )	0.0004
Total Composite Tolerance ( <i>in</i> )	0.0011
Average Backlash with Mate ( <i>in</i> )	0.004
Shaft Angle ( <i>degrees</i> )	175
Surface Roughness of Functional Profile ( $\mu\text{in}$ )	25 $\mu\text{in}$ (ground, soft) or 15 $\mu\text{in}$ (ground, hard)
Pitch Cone Angle ( <i>degrees</i> )	67.22
Number of Teeth	63

Table 12: Internal FG Data

Category	Value
AGMA Quality	12
Number of Teeth	63
Inner Radius ( <i>in</i> )	5.08
Outer Radius ( <i>in</i> )	6.19
Diametral Pitch ( <i>1/in</i> )	12.2
Mean Pressure Angle ( <i>degrees</i> )	25
Pitch Diameter ( <i>in</i> )	5.16
Mean Whole Depth ( <i>in</i> )	0.184
Face Width ( <i>in</i> )	0.5303
Tooth to Tooth Composite Tolerance ( <i>in</i> )	0.0004
Total Composite Tolerance ( <i>in</i> )	0.0011
Average Backlash with Mate ( <i>in</i> )	0.004
Shaft Angle ( <i>degrees</i> )	175
Surface Roughness of Functional Profile ( $\mu in$ )	25 $\mu in$ (ground, soft) or 15 $\mu in$ (ground, hard)
Pitch Cone Angle ( <i>degrees</i> )	107.77
Number of Teeth	61

## Appendix D

### Spur Gear Test

As part of the literature review and tool validation effort, Tharmakulasingam's work was closely examined. In particular, the Python code listed in the appendix of the referenced document provided an opportunity to test Abaqus' capabilities first hand. As a result of running this code, the full Model Tree was available as well, providing insight into some of the "best practice" simulation methodologies [25]. The outcome of this effort can be found below, with Figure 63 showing the overall spur gear system and Figure 64 showing a detail view of the von Mises stress results. Additionally, Figure 65 depicts the TE values produced locally by the simulation, which closely match the behavior in both Tharmakulasingam's thesis and actual spur gear pairs.

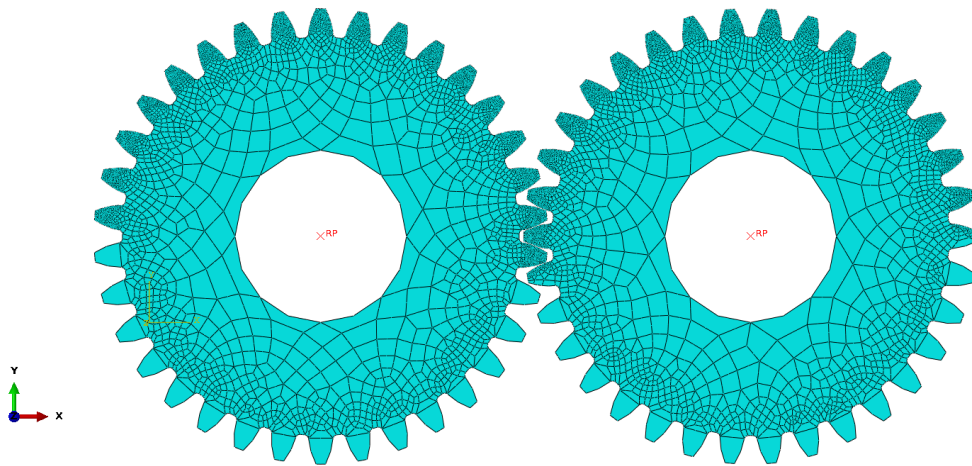


Figure 63: Spur Gear System, Test Code

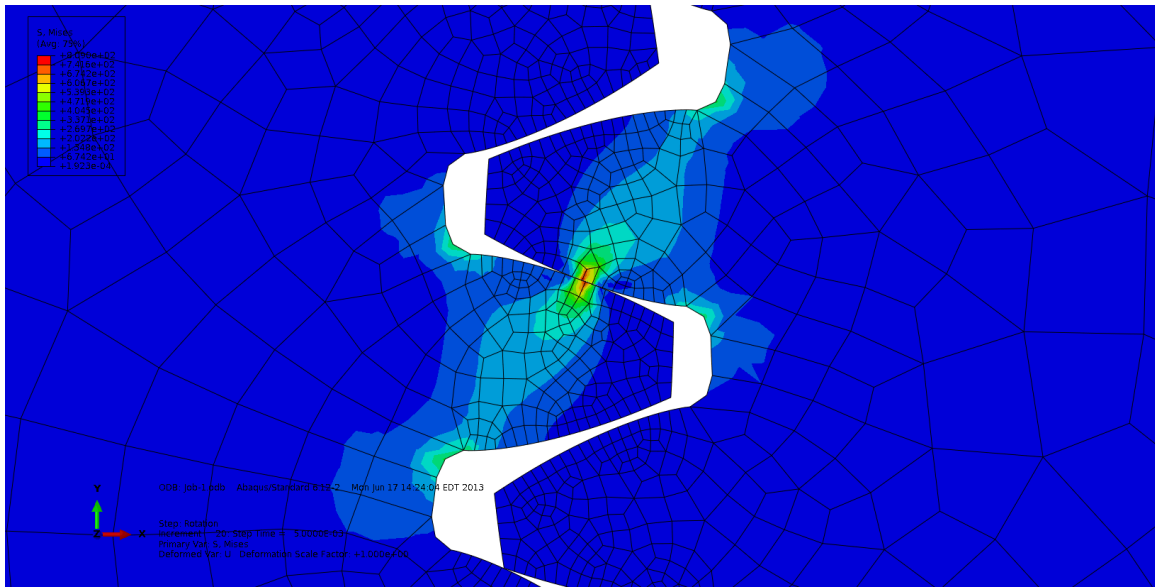


Figure 64: Von Mises Stress, Test Code

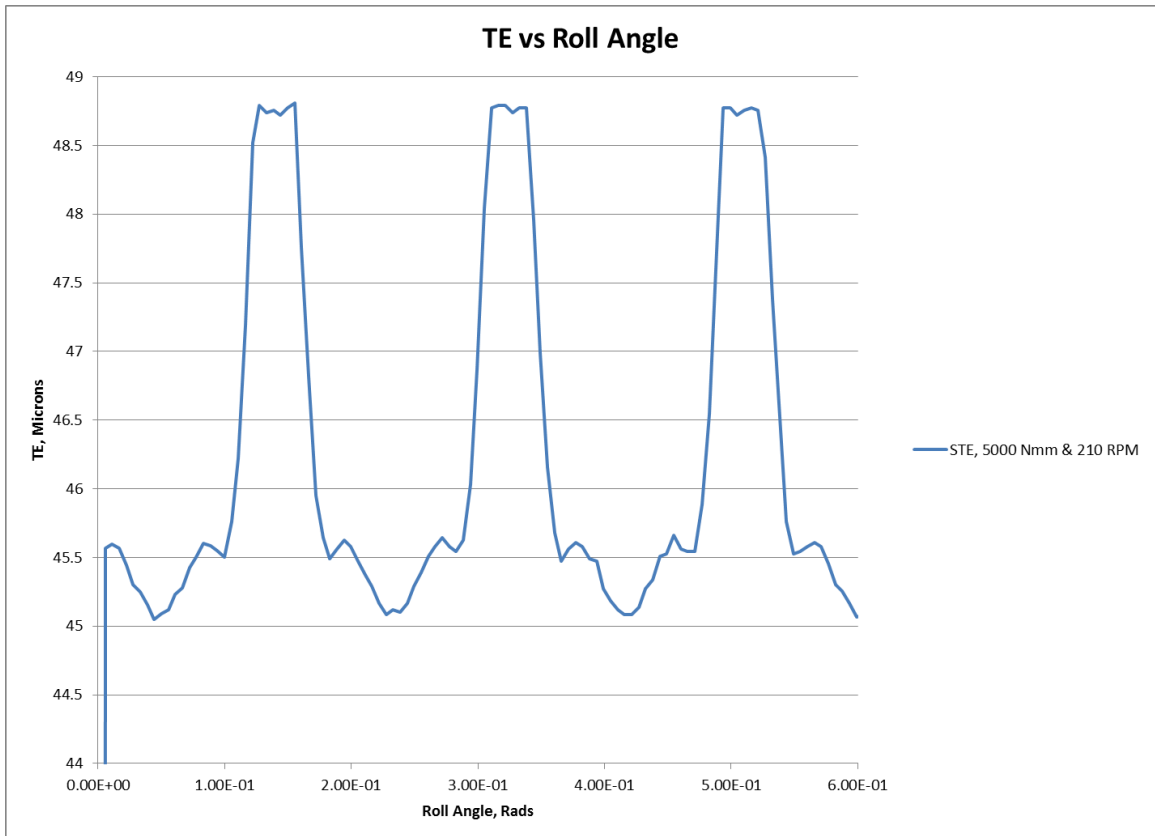


Figure 65: TE Data, Test Code

## Appendix E

### Abaqus: Model Tree

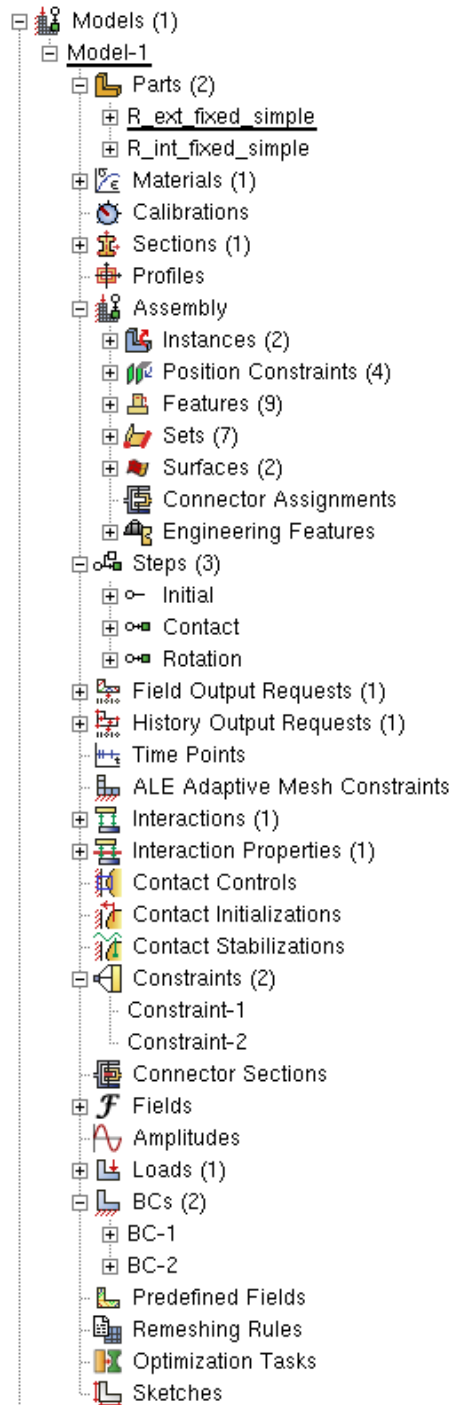


Figure 66: Abaqus Model Tree for FG Generation

## Appendix F

### Abaqus: Detailed Menu Items

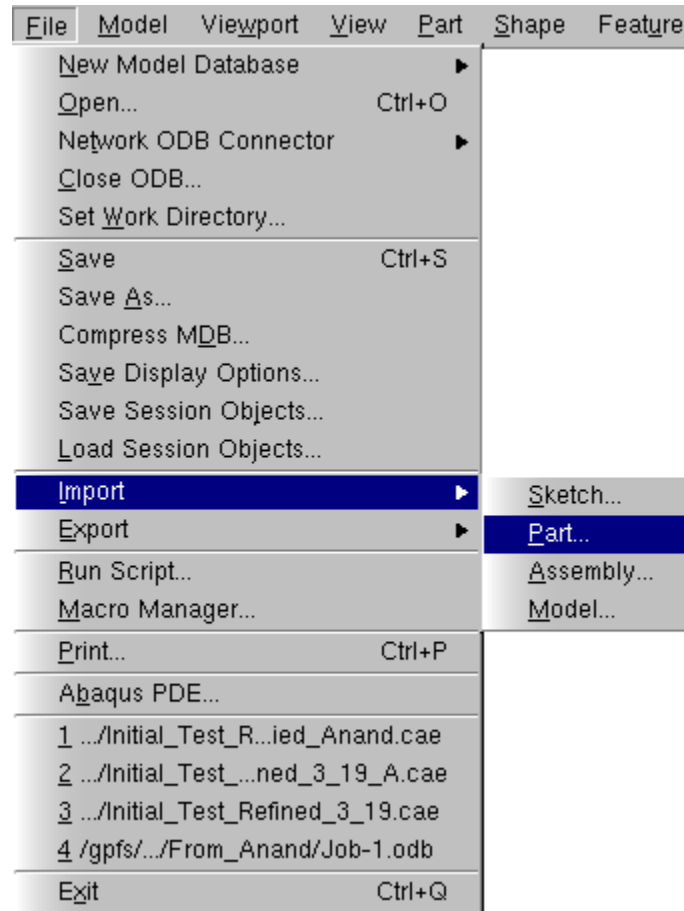


Figure 67: Import Part Menu Item

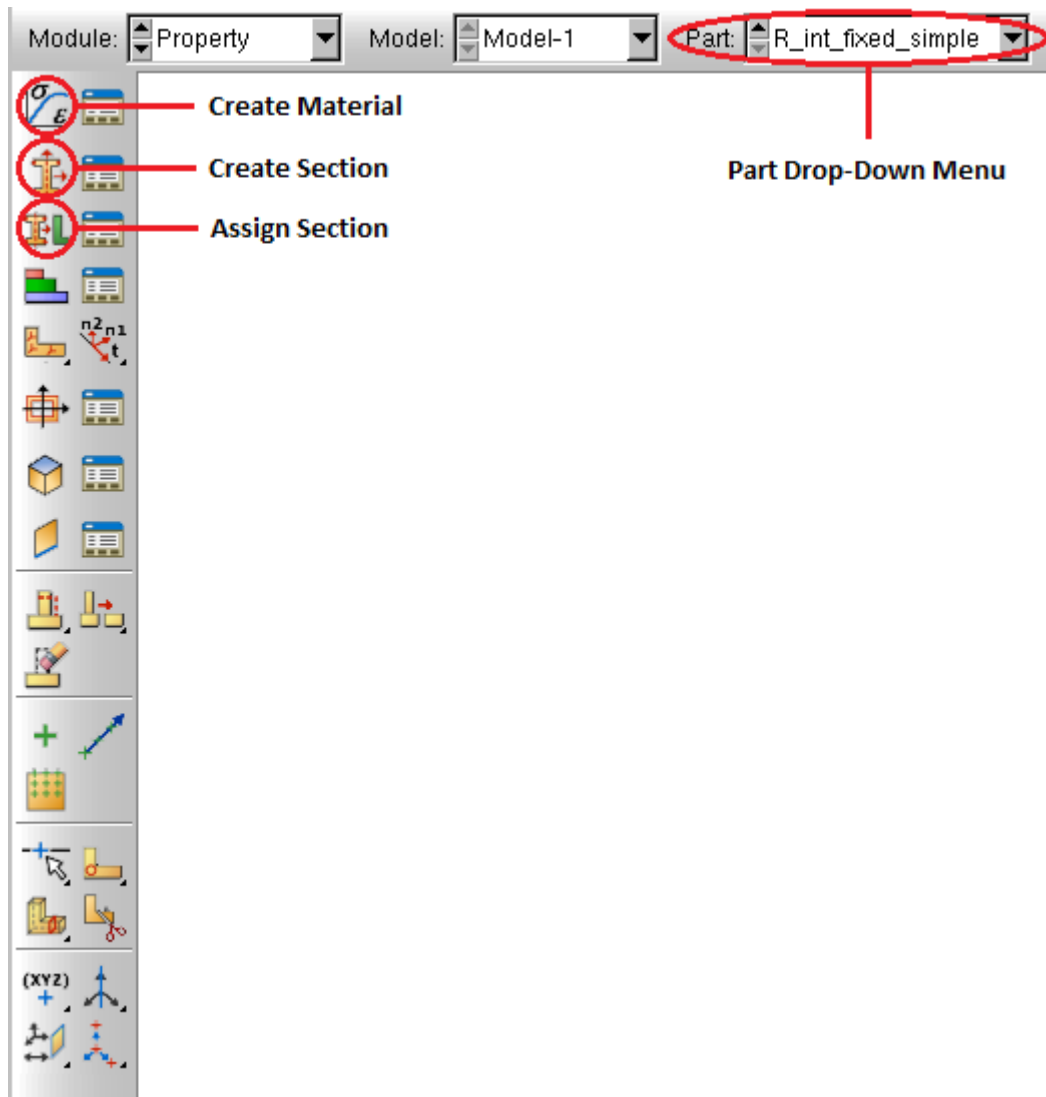


Figure 68: Sequence for Applying Properties

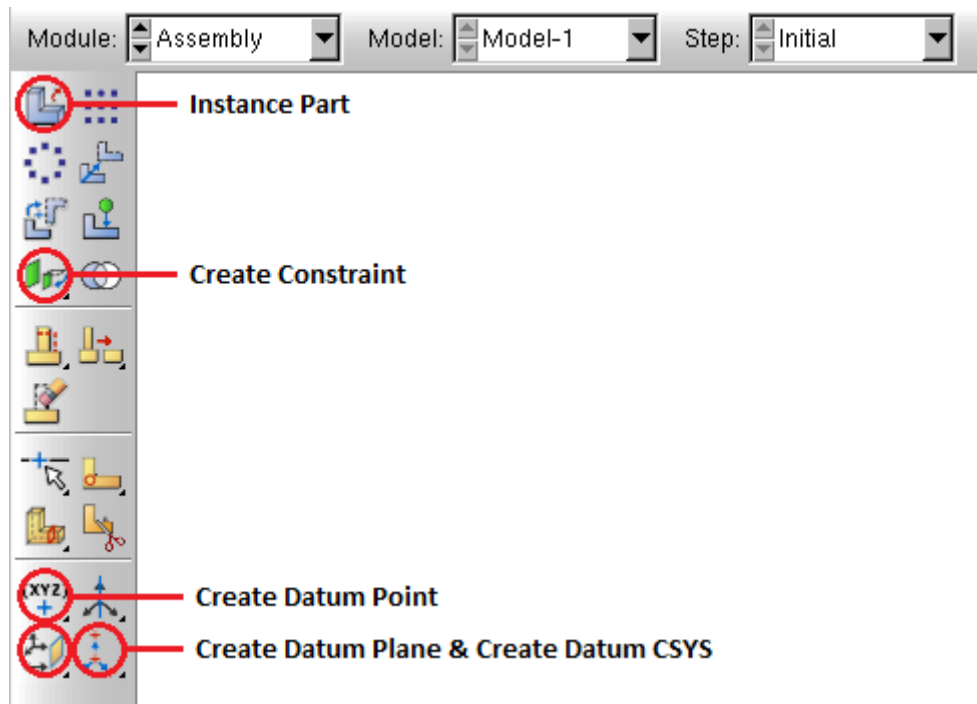


Figure 69: Sequence for Creating an Assembly

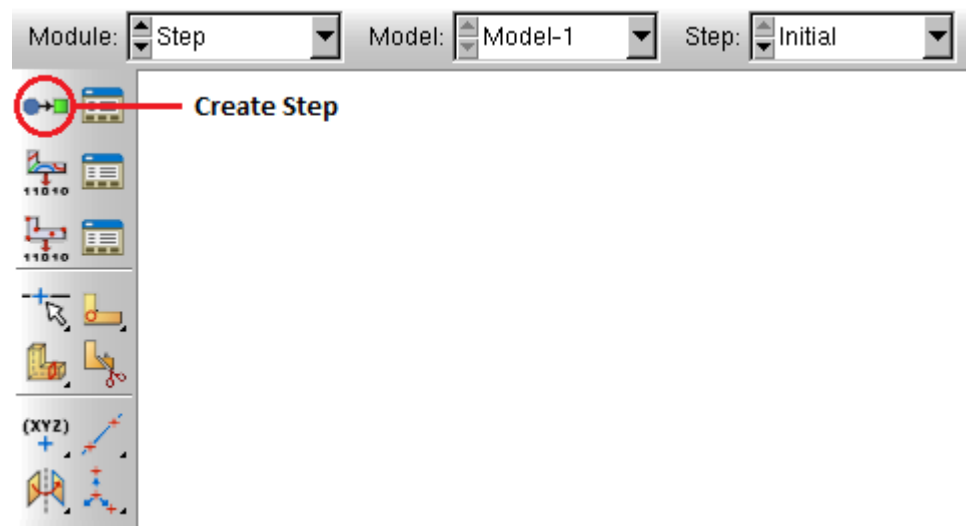


Figure 70: Sequence for Defining Steps

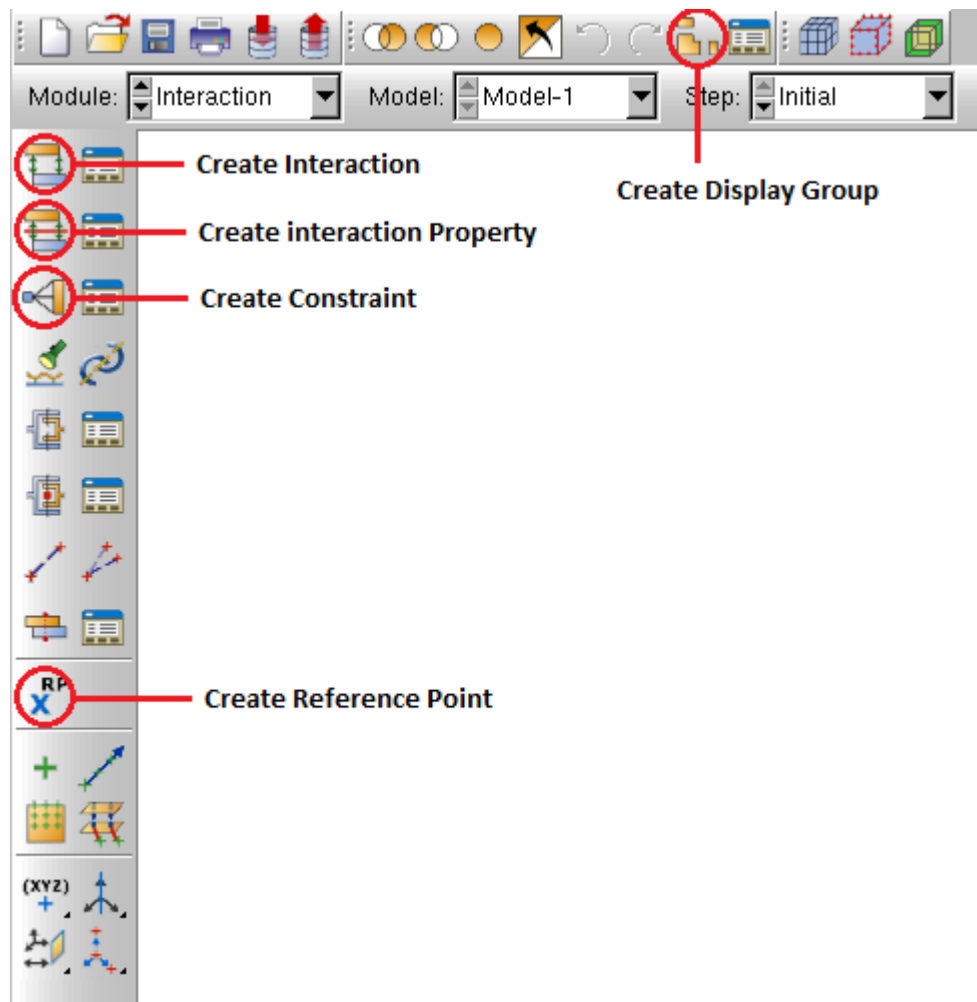
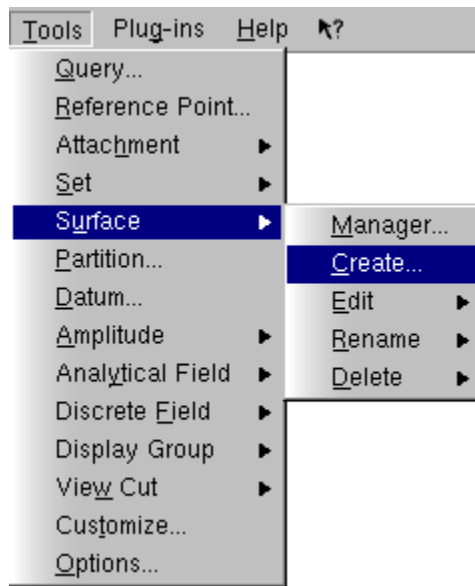
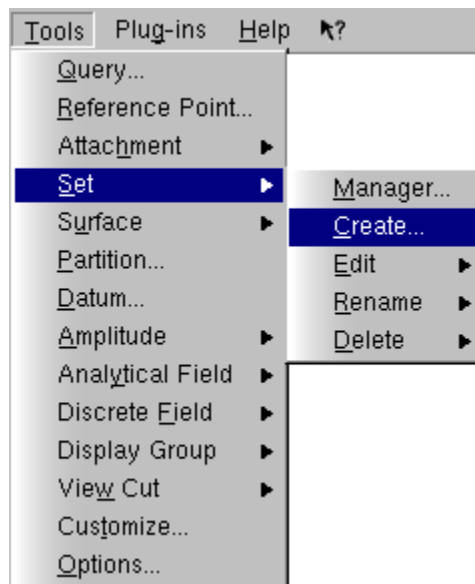


Figure 71: Sequence to Add Interactions



**Figure 72: Create Surface Menu Item**



**Figure 73: Create Set Menu Item**

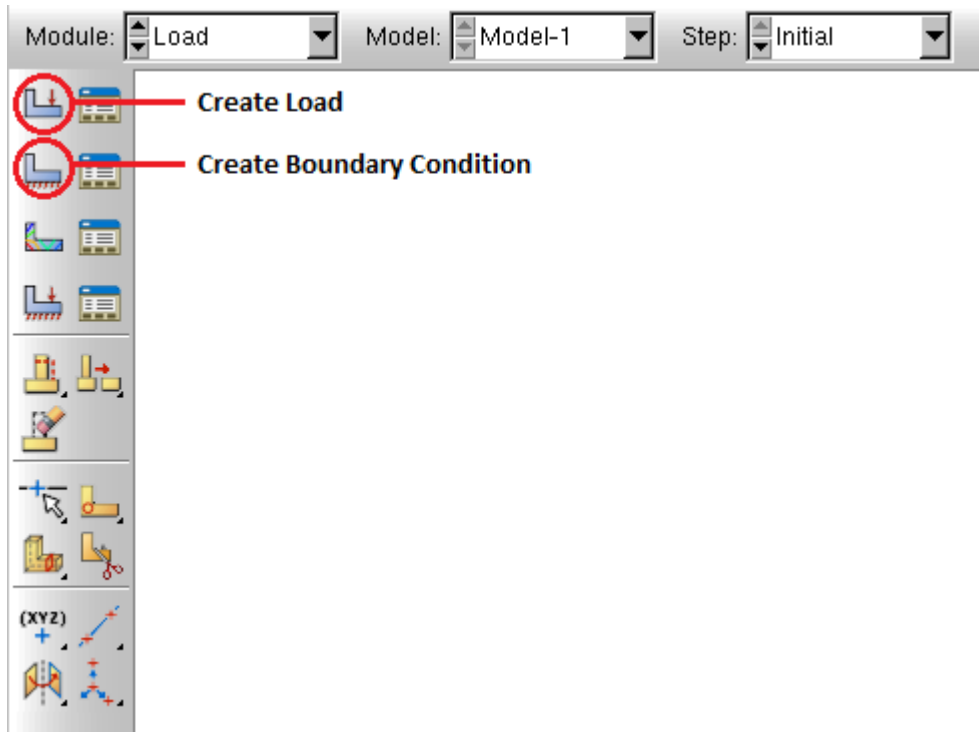


Figure 74: Sequence to Create Loads

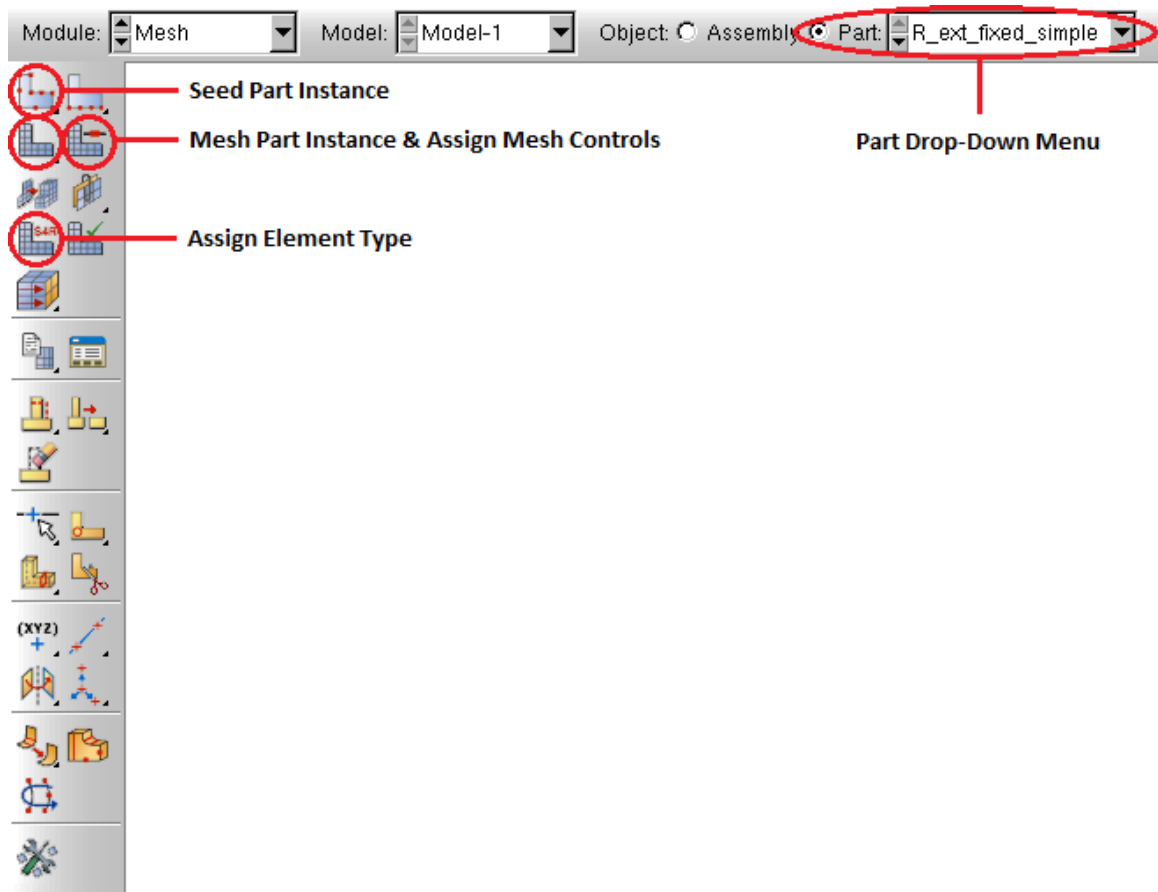


Figure 75: Sequence to Develop Mesh

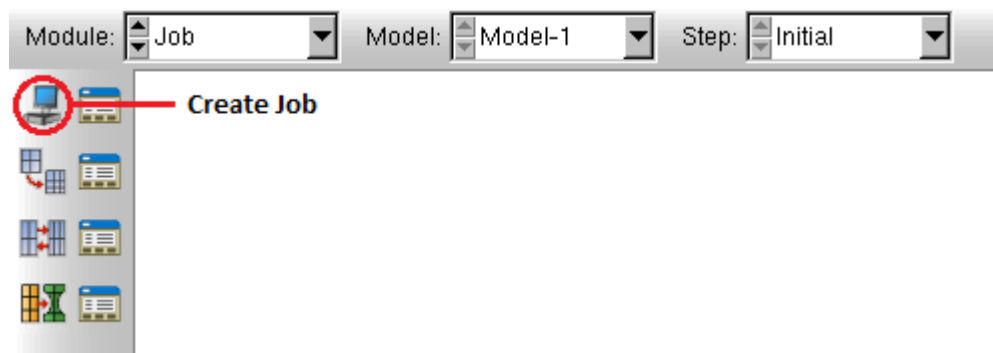


Figure 76: Sequence to Run Job

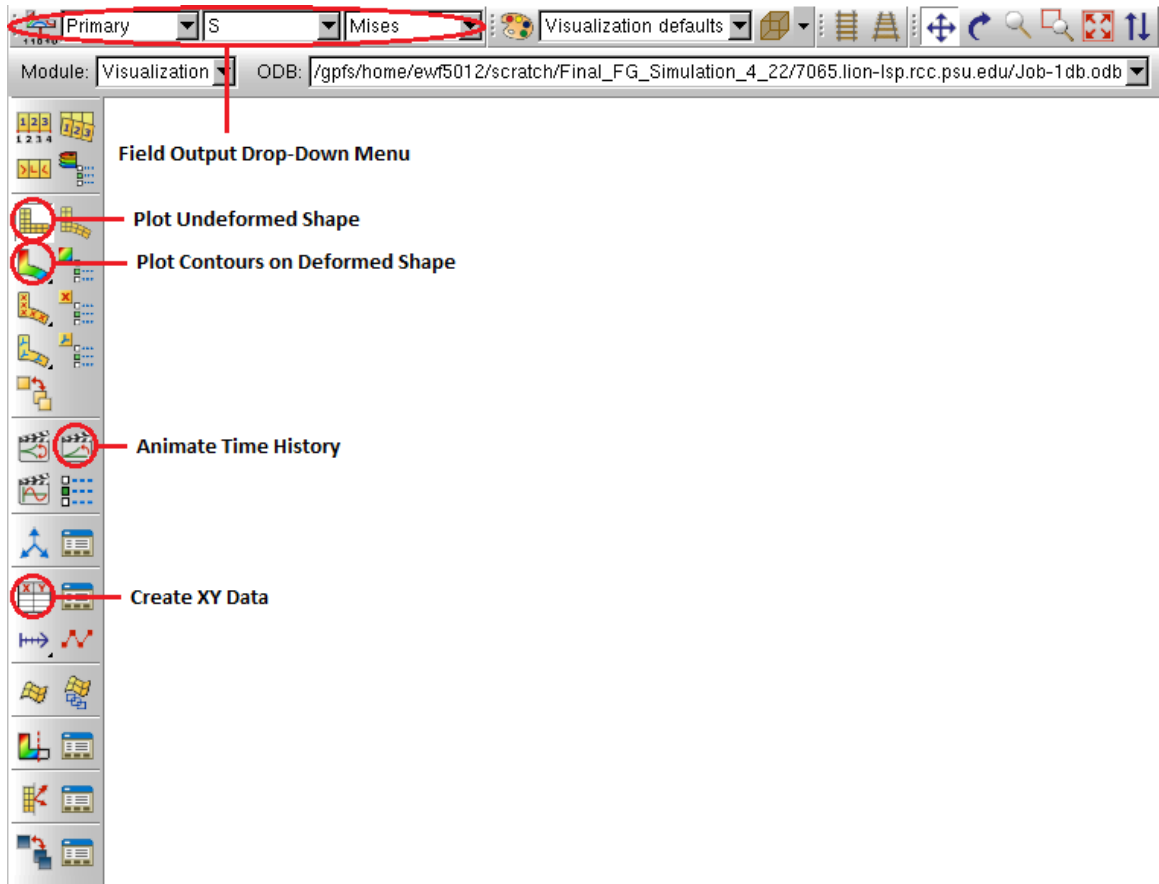


Figure 77: Sequence to Post Processing



Figure 78: Report XY Menu Item

## Appendix G

### PBS Script

```
# This is a PBS script to execute the FG simulation. It will request 16 processors on one node for
# 48 hours.
#
# Request 16 processors on one node.
#
# PBS -l nodes=1:ppn=16
#
# Request 48 hours of walltime. Note that this is likely excessive.
#
#PBS -l walltime=48:00:00
#
# Request that regular output and terminal output go to the same file.
#
#PBS -j oe
#
# Request 300 GB of memory per process. Note that this is likely excessive.
#
#PBS -l mem=300gb
#
# The following is the body of the script. By default, PBS scripts execute in your home directory,
# not the directory from which they were submitted. The following line places you in the
# directory from which the job was submitted.
#
cd $PBS_O_WORKDIR
#
# Copy input files to TMPDIR and then change working directory
cp Job-1db.inp $TMPDIR
cd $TMPDIR
#
# load module and then run abaqus
module load abaqus
abaqus job=Job-1db cpus=16 interactive
#
# Copy output files back to your working directory and clean up $TMPDIR
cp -r $TMPDIR $PBS_O_WORKDIR
rm -rf $TMPDIR
```

## Appendix H

### Computational Comparison Model and Parameters

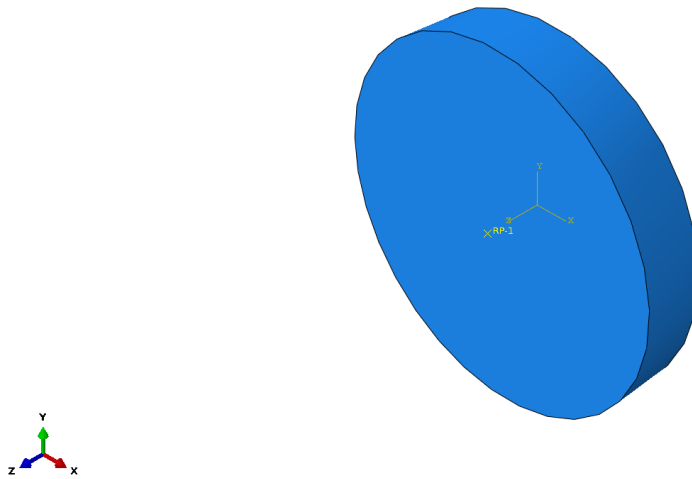


Figure 79: Model Used for Simulation

Table 13: Disk Parameters

Parameter	Value
Diameter ( <i>in</i> )	6
Thickness ( <i>in</i> )	1
Loads ( $lb_f \cdot in$ )	CM3 = 10
Boundary Conditions	$U1 = U2 = U3 = 0$ $UR1 = UR2 = 0$ $UR3 = \text{free}$



## Appendix J

### MATLAB Transmission Error Analysis Code

```

clear all
close all
clc

%% Import Simulation Data from Abaqus
FGData = xlsread('Face_Gear_Data.xlsx');

%% FG Dimensional Parameters
n1 = 63; %internal FG
n2 = 61; %external FG
mp = n2/n1; %ratio, output/input

dmp1 = 5.16*25.4*1000; %mean pitch diameter of the internal FG, [microns]
rmp1 = dmp1/2; %mean pitch radius of the internal FG, [microns]

dmp2 = dmp1*mp; %mean pitch diameter of the external FG, [microns]
rmp2 = dmp2/2; %mean pitch radius of the external FG, [microns]

rpV = [0;2.58;-0.8269]*25.4*1000; %this is the position vector at a contact along the pitch cone
wrt pitch cone apex in global frame, [microns]
rpVy = abs(rpV(2,1)); %y-component of the position vector

%% Load FG Data
t = FGData(:,1); %time, seconds
theta1V = FGData(:,[5 7 9]); %x,y,z components of the internal FG rotation, [radians]
theta2V = FGData(:,[4 6 8]); %x,y,z components of the external FG rotation, [radians]

theta1M = FGData(:,3); %magnitude of the internal FG rotation, [radians]
theta2M = FGData(:,2); %magnitude of the external FG rotation, [radians]

%% Calculate FG Transmission Error

%primary values
TE = abs(theta1M*rmp1 - theta2M*rmp2); %standard method of (driver*r1-driven*r2),
[microns]
TEt = TE/8; %standard method per tooth, [microns]

TEA = abs(theta1M - theta2M); %compute angular displacement difference, [radians]
TEAt = TEA/8; %compute angular displacement difference per tooth, [radians]

%secondary values
rpV = repmat(rpV,1,length(t)); %new vectorized approach begins by creating position matrix,
[microns]
theta12V = (theta1V-theta2V); %compute vector difference matrix by (driver-driven), [radians]

```

```

TEV = cross(abs(rpV),theta12V); %compute vectorized TE matrix by r*cross*(delta_theta),
[microns]
TEVM = sqrt((TEV(:,1).^2)+(TEV(:,2).^2)+(TEV(:,3).^2)); %compute vector magnitude of TE
matrix, [microns]
TEVMt = TEVM/8; %compute vector magnitude of TE matrix per tooth, [microns]

%check TEV/TEVM calculations
TEa = ((rpV(:,2).*(theta2V(:,3)-theta1V(:,3)))-(rpV(:,3).*theta2V(:,2))); %cross product by hand,
[microns]

%supporting calculations
index1 = max(find(t==1))+1:1:length(t); %find times occurring after FG rotation, [seconds]

coeff = polyfit(t(index1),TEVM(index1),1); %determine slope and y-intercept of TEVM
LT = polyval(coeff,t(index1)); %create a line of best fit

coefft = polyfit(t(index1),TEVMt(index1),1); %determine slope and y-intercept of TEVMt
LTt = polyval(coefft,t(index1)); %create a line of best fit

%% FG Plots
figure(100) %plot angular difference vs. time

subplot(2,1,1:2)
plot(t,TEa,'r-'), hold on
title('Difference in Angular Position between Gear and Pinion vs. Time')
xlabel('Time, sec')
ylabel('TE, rad')
legend('TEa')
%export_fig Data.pdf -pdf -append
%saveas(gcf,'TEA_Time.png')

%check TEV/TEVM calculations
%subplot(2,1,2)
%plot(t,TEVM,'r-'), hold on
%plot(t,TEa,'b-'), hold on
%title('Vectorized Transmission Error vs. Time')
%xlabel('Time, sec')
%ylabel('TE,\mum')
%legend('TEVM','TEa')
%export_fig Data.pdf -pdf -append

figure(110) %plot TE values vs. time

subplot(3,1,1)
plot(t,TE,'r-'), hold on
plot(t,TEVM,'b-'), hold on
title('Transmission Error vs. Time')
xlabel('Time, sec')

```

```

ylabel('TE,\mum')
legend('TE','TEVM')

subplot(3,1,2)
plot(t,TE,'r-'), hold on
title('Transmission Error vs. Time')
xlabel('Time, sec')
ylabel('TE,\mum')
legend('TE')
%saveas(gcf,'TE_Time.png')

subplot(3,1,3)
plot(t,TEVM,'b-'), hold on
title('Transmission Error vs. Time')
xlabel('Time, sec')
ylabel('TE,\mum')
legend('TEVM')
%saveas(gcf,'TEVM_Time.png')
%export_fig Data.pdf -pdf -append

figure(120) %plot angular difference vs. angular displacement

subplot(2,1,1:2)
plot(theta1M,TEA,'r-'), hold on
title('Difference in Angular Position between Gear and Pinion vs. Angular Displacement')
xlabel('\theta_1, rad')
ylabel('TE, rad')
legend('TEA')
%export_fig Data.pdf -pdf -append

%check TEV/TEVM calculations
%subplot(2,1,2)
%plot(theta1M,TEVM,'r-'), hold on
%plot(theta1M,TEa,'b-'), hold on
%title('Vectorized Transmission Error vs. Angular Displacement')
%xlabel('\theta_1, rad')
%ylabel('TE,\mum')
%legend('TEVM','TEa')
%export_fig Data.pdf -pdf -append

figure(130) %plot TE values vs. angular displacement

subplot(3,1,1)
plot(theta1M,TE,'r-'), hold on
plot(theta1M,TEVM,'b-'), hold on
title('Transmission Error vs. Angular Displacement')
xlabel('\theta_1, rad')
ylabel('TE,\mum')
legend('TE','TEVM')

```

```

subplot(3,1,2)
plot(theta1M,TE,'r-'), hold on
title('Transmission Error vs. Angular Displacement')
xlabel('\theta_1, rad')
ylabel('TE,\mum')
legend('TE')

subplot(3,1,3)
plot(theta1M,TEVM,'b-'), hold on
title('Transmission Error vs. Angular Displacement')
xlabel('\theta_1, rad')
ylabel('TE,\mum')
legend('TEVM')
%export_fig Data.pdf -pdf -append

figure(140) %plot angular difference vs. time after rotation

subplot(2,1,1:2)
plot(t(index1),TEA(index1),'r-'), hold on
title('Difference in Angular Position between Gear and Pinion vs. Time After Rotation')
xlabel('Time, sec')
ylabel('TE, rad')
legend('TEA')
%export_fig Data.pdf -pdf -append

%check TEV/TEVM calculations
%subplot(2,1,2)
%plot(t(index1),TEVM(index1),'r-'), hold on
%plot(t(index1),TEa(index1),'b-'), hold on
%title('Vectorized Transmission Error vs. Time After Rotation')
%xlabel('Time, sec')
%ylabel('TE,\mum')
%legend('TEVM','TEa')
%export_fig Data.pdf -pdf -append

figure(150) %plot TE values vs. time after rotation

subplot(3,1,1)
plot(t(index1),TE(index1),'r-'), hold on
plot(t(index1),TEVM(index1),'b-'), hold on
title('Transmission Error vs. Time After Rotation')
xlabel('Time, sec')
ylabel('TE,\mum')
legend('TE','TEVM')

subplot(3,1,2)
plot(t(index1),TE(index1),'r-'), hold on
title('Transmission Error vs. Time After Rotation')
xlabel('Time, sec')

```

```

ylabel('TE,\mum')
legend('TE')

subplot(3,1,3)
plot(t(index1),TEVM(index1),'b-'), hold on
title('Transmission Error vs. Time After Rotation')
xlabel('Time, sec')
ylabel('TE,\mum')
legend('TEVM')
%export_fig Data.pdf -pdf -append

figure(160) %plot angular difference vs. angular displacement after rotation

subplot(2,1,1:2)
plot(theta1M(index1),TEA(index1),'r-'), hold on
title('Difference in Angular Position between Gear and Pinion vs. Angular Displacement After
Rotation')
xlabel('\theta_1, rad')
ylabel('TE, rad')
legend('TEA')
%export_fig Data.pdf -pdf -append
%saveas(gcf,'TEA_Rotation_After.png')

%check TEV/TEVM calculations
%subplot(2,1,2)
%plot(theta1M(index1),TEVM(index1),'r-'), hold on
%plot(theta1M(index1),TEa(index1),'b-'), hold on
%title('Vectorized Transmission Error vs. Angular Displacement After Rotation')
%xlabel('\theta_1, rad')
%ylabel('TE,\mum')
%legend('TEVM','TEa')
%export_fig Data.pdf -pdf -append

figure(170) %plot TE values vs. angular displacement after rotation

subplot(3,1,1)
plot(theta1M(index1),TE(index1),'r-'), hold on
plot(theta1M(index1),TEVM(index1),'b-'), hold on
title('Transmission Error vs. Angular Displacement After Rotation')
xlabel('\theta_1, rad')
ylabel('TE,\mum')
legend('TE','TEVM')

subplot(3,1,2)
plot(theta1M(index1),TE(index1),'r-'), hold on
vline(0:(2*pi()/63):t(==1),'k-'), hold on %plot lines for every tooth contact
title('Transmission Error vs. Angular Displacement After Rotation')
%axis([0 1 205.8 206.15])
xlabel('\theta_1, rad')

```

```

ylabel('TE,\mum')
legend('TE')
%saveas(gcf,'TE_Rotation_After.png')
%saveas(gcf,'TE_Rotation_After_Per_Tooth_Lines.png')

subplot(3,1,3)
plot(theta1M(index1),TEVM(index1),'b-'), hold on
vline(0:((2*pi())/63):t(t==1),'k--'), hold on %plot lines for every tooth contact
title('Transmission Error vs. Angular Displacement After Rotation')
xlabel('\theta_1, rad')
ylabel('TE,\mum')
legend('TEVM')
%saveas(gcf,'TEVM_Rotation_After.png')
%export_fig Data.pdf -pdf -append

figure (180) %plot TE values (per tooth) vs. angular displacement after rotation

subplot (3,1,1)
plot(theta1M(index1),TEAt(index1),'r-'), hold on
title('Difference in Angular Position between Gear and Pinion (per tooth) vs. Angular Displacement After Rotation')
xlabel('\theta_1, rad')
ylabel('TE, rad')
legend('TEAt')

subplot (3,1,2)
plot(theta1M(index1),TEt(index1),'r-'), hold on
vline(0:((2*pi())/63):t(t==1),'k--'), hold on %plot lines for every tooth contact
title('Transmission Error (per tooth) vs. Angular Displacement After Rotation')
xlabel('\theta_1, rad')
ylabel('TE, \mum')
legend('TEt')
%saveas(gcf,'TE_Rotation_After_Per_Tooth.png')

subplot (3,1,3)
plot(theta1M(index1),TEVMt(index1),'b-'), hold on
vline(0:((2*pi())/63):t(t==1),'k--'), hold on %plot lines for every tooth contact
title('Vectorized Transmission Error (per tooth) vs. Angular Displacement After Rotation')
xlabel('\theta_1, rad')
ylabel('TE, \mum')
legend('TEVMt')
%export_fig Data.pdf -pdf -append

figure(190) %plot other values

subplot(4,1,1)
plot(theta1M(index1),TEVM(index1)-LT,'b-'), hold on
vline(0:((2*pi())/63):t(t==1),'k--'), hold on %plot lines for every tooth contact
title('Vectorized Transmission Error vs. Time After Rotation')

```

```

% axis([0 1 -0.2 0.25])
xlabel('\theta_1, rad')
ylabel('TE, \mum')
legend('TEVM (Modified)')
%saveas(gcf,'TEVM_Rotation_After_Corrected.png')
%saveas(gcf,'TEVM_Rotation_After_Corrected_Lines.png')

subplot(4,1,2)
plot(theta1M(index1),TEVMt(index1)-LTt,'b-'), hold on
vline(0:(2*pi()/63):t==1),'k--'), hold on %plot lines for every tooth contact
title('Vectorized Transmission Error (per tooth) vs. Angular Displacement After Rotation')
xlabel('\theta_1, rad')
ylabel('TE, \mum')
legend('TEVMt (Modified)')
%saveas(gcf,'TEVM_Rotation_After_Corrected_Per_Tooth.png')

subplot(4,1,3)
plot(theta1M(index1),theta2M(index1),'r-'), hold on
plot(theta1M(index1),theta1M(index1)/mp,'b-'), hold on
title('Measured and Theoretical Pinion Rotation vs. Angular Displacement After Rotation')
xlabel('\theta_1, rad')
ylabel('\theta_2, rad')
legend('\theta_2, Simulated', '\theta_2, Calculated')
%saveas(gcf,'Theta_Rotation_After_Comparison.png')

subplot(4,1,4)
plot(theta1M(index1),theta2M(index1)-(theta1M(index1)/mp),'r-'), hold on
title('Difference between Measured and Theoretical Pinion Rotation vs. Angular Displacement
After Rotation')
xlabel('\theta_1, rad')
ylabel('Difference, rad')
legend('\Delta\theta_2')
%saveas(gcf,'Theta_Rotation_After_Difference.png')
%export_fig Data.pdf -pdf -append

```

## Appendix K

### MATLAB Stiffness Analysis Code

```

clear all
close all
clc

%% Define Variables

%taken from FG technical details Excel sheet

%SI
E = 2.10*10^5; %Young's Modulus, [N/mm^2]
fw = 13.47; %face width, [mm]. Converted from .5303 [in]
pc = 25.4*(pi/12.2); %circular pitch, [mm]. Converted from 12.2 [1/in] diametral pitch
th = 4.67; %tooth height, [mm]. Converted from .184 [in]
alpha = 25*(pi/180); %mean pressure angle, [rads]
nt = 8; %number of teeth in contact.
T = 5649241.45; %torque, [N*mm]. Converted from 50,000 [lbf*in]
rp = 63.5; %pitch circle radius, [mm]. Converted from 2.5 [in]

%% Equation

kt1 = (E*fw*(pc^3))/(32*(th^3)*cos(alpha)); %single tooth stiffness, [N*mm]
kt2 = kt1;

kmi = nt*(1/((1/kt1)+(1/kt2))); %total mesh stiffness, [mm]

x = 1000*((T/rp)/kmi); %total displacement, [microns]
xs = 1000*(((T/8)/rp)/kt1); %single tooth displacement, [microns]

```

## References

1. Leishman, J.G. *A History of Helicopter Flight*. [cited 2013; Available from: <http://terpconnect.umd.edu/~leishman/Aero/history.html>.
2. *Air Medical Services: Critical Component of Modern Healthcare Systems*. 2011, MedEvac Foundation International. p. 36.
3. Parsons, D. *Future Helicopter Technology Remains Up in the Air*. 2012 [cited 2013; Available from: <http://www.nationaldefensemagazine.org/archive/2012/April/Pages/FutureHelicopterTechnologyRemainsUpintheAir.aspx>.
4. *JMR-FVL: The US Military's Future "Helicopters"?* 2013 [cited 2013; Available from: <http://www.defenseindustrydaily.com/jmr-fvl-the-us-militarys-future-helicopters-014035/>.
5. Saribay, Z.B. and R.C. Bill, *Design Analysis of Pericyclic Mechanical Transmission System*. Mechanism and Machine Theory, 2013. **61**: p. 102-122.
6. *The Involute Curve and Involute Gearing*. 6 ed. 1955: The Fellows Gear Shaper Company.
7. Dudley, D.W., *The Evolution of the Gear Art*. 1969: American Gear Manufacturers Association.
8. Buckingham, E., *Analytical Mechanics of Gears*. Dover ed. 1963: McGraw-Hill.
9. *Spur Gears*. [cited 2013; Available from: [http://www.roymech.co.uk/Useful\\_Tables/Drive/Gears.html](http://www.roymech.co.uk/Useful_Tables/Drive/Gears.html).
10. Litvin, F., et al., *Design and Geometry of Face-Gear Drives*. Journal of Mechanical Design, 1992. **114**: p. 642.
11. Litvin, F.L., et al., *Handbook on Face Gear Drives with a Spur Involute Pinion*. 2000, DTIC Document.
12. Lemanski, A.J., *Variable Speed Power Transmission*, U.S.P. Office, Editor. 2006: United States of America.
13. Saribay, Z.B., *Analytical Investigation of the Pericyclic Variable-Speed Transmission System for Helicopter Main-Gearbox*, in *Aerospace Engineering*. 2009, The Pennsylvania State University. p. 364.
14. Litvin, F., et al., *Application of Face-Gear Drives in Helicopter Transmissions*. Journal of mechanical design, 1994. **116**: p. 672.
15. Bossler, R. and G. Heath. *Advanced Rotorcraft Transmission (ART) Program Status*. in *Rotary Wing Propulsion Specialists' Meeting, Williamsburg, VA*. 1990.
16. Litvin, F., *Development of Face-Gear Technology for Industrial and Aerospace Power Transmission*. NASA/CR-2002-211320.
17. Saribay, Z.B., et al., *Elastohydrodynamic Lubrication Analysis of Conjugate Meshing Face Gear Pairs*. Journal of the American Helicopter Society, 2012. **57**(3): p. 1-10.
18. Saribay, Z.B., et al., *Geometry and Kinematics of Conjugate Meshing Face-Gear Pairs*. Vertical Lift Research Center of Excellence. p. 36.
19. Saribay, Z.B., *Tooth Geometry and Bending Stress Analysis of Conjugate Meshing Face-Gear Pairs*. Proceedings of the Institution of Mechanical Engineers, Part C: Journal of Mechanical Engineering Science, 2012.
20. Mark, W.D., *Analysis of the Vibratory Excitation of Gear Systems: Basic Theory*. The Journal of the Acoustical Society of America, 1978. **63**: p. 1409.
21. Åkerblom, M., *Gear Noise and Vibration: A Literature Survey*. 2001.

22. Dudley, D.W. and D.P. Townsend, *Dudley's Gear Handbook*. 1991: McGraw-Hill Companies.
23. Munro, R., *A Review of the Theory and Measurement of Gear Transmission Error*. Gearbox noise and vibration, 1990: p. 3-10.
24. Smith, J.D., *Gears and Their Vibration: A Basic Approach to Understanding Gear Noise*. 1983: M. Dekker.
25. Tharmakulasingam, R., *Transmission Error in Spur Gears: Static and Dynamic Finite-Element Modeling and Design Optimization*, in *School of Engineering and Design*. 2009, Brunel University: United Kingdom. p. 261.
26. Mark, W.D., *Elements of Gear Noise Prediction*. Noise and Vibration Control Engineering: Principles and Applications, 1992: p. 735-770.
27. Litvin, F.L. and J. Zhang, *Spur Gears: Optimal Geometry, Methods for Generation and Tooth Contact Analysis (TCA) Program*. 1988, DTIC Document.
28. Chang, S., R. Huston, and J. Coy. *A Finite Element Stress Analysis of Spur Gears Including Fillet Radii and Rim Thickness Effects*. 1983. ASME.
29. Muthukumar, R. and M. Raghavan, *Estimation of Gear Tooth Deflection by the Finite Element Method*. Mechanism and Machine Theory, 1987. **22**(2): p. 177-181.
30. Lee, C.H., *Non-Linear Contact Analysis of Meshing Gears*. 2009.
31. Sommer, A., J. Meagher, and X. Wu, *An Advanced Numerical Model of Gear Tooth Loading from Backlash and Profile Errors*, in *Rotating Machinery, Structural Health Monitoring, Shock and Vibration, Volume 5*. 2011, Springer. p. 191-201.
32. Li, S., *Finite Element Analyses for Contact Strength and Bending Strength of a Pair of Spur Gears with Machining Errors, Assembly Errors and Tooth Modifications*. Mechanism and machine theory, 2007. **42**(1): p. 88-114.
33. Lin, T., H. Ou, and R. Li, *A Finite Element Method for 3D Static and Dynamic Contact/Impact Analysis of Gear Drives*. Computer methods in applied mechanics and engineering, 2007. **196**(9): p. 1716-1728.
34. Wang, J.D. and I.M. Howard, *Error Analysis on Finite Element Modeling of Involute Spur Gears*. Journal of Mechanical Design, 2006. **128**: p. 90.
35. Rigaud, E. and D. Barday. *Modelling and Analysis of Static Transmission Error - Effect of Wheel Body Deformation and Interactions between Adjacent Loaded Teeth*. in *4th World Congress on Gearing and Power Transmission*. 1999.
36. Wang, J. and I. Howard, *Finite Element Analysis of High Contact Ratio Spur Gears in Mesh*. Journal of tribology, 2005. **127**(3): p. 469-483.
37. Wei, Z., *Stresses and Deformations in Involute Spur Gears by Finite Element Method*. 2004, University of Saskatchewan.
38. Prášil, L. and J. Mackerle, *Finite Element Analyses and Simulations of Gears and Gear Drives: A Bibliography 1997-2006*. Engineering computations, 2008. **25**(3): p. 196-219.
39. Barone, S., L. Borgianni, and P. Forte, *CAD/FEM Procedures for Stress Analysis in Unconventional Gear Applications*. International Journal of Computer Applications in Technology, 2002. **15**(4): p. 157-167.
40. Barone, S., L. Borgianni, and P. Forte. *CAD/FEM Analysis of Teeth Contact Stress and Load Share in Face Gears*. in *ASME 27th Design Automation Conference, Pittsburgh*. 2001.
41. Guingand, M., J.-P. De Vaujany, and C.-Y. Jacquin, *Quasi-Static Analysis of a Face Gear Under Torque*. Computer methods in applied mechanics and engineering, 2005. **194**(39): p. 4301-4318.
42. Guingand, M., J.P. De Vaujany, and Y. Icard, *Analysis and Optimization of the Loaded Meshing of Face Gears*. Journal of Mechanical Design, 2005. **127**: p. 135.

43. Litvin, F., et al., *Application of Finite Element Analysis for Determination of Load Share, Real Contact Ratio, Precision of Motion, and Stress Analysis*. Journal of Mechanical Design, 1996. **118**: p. 561.
44. Barone, S., L. Borgianni, and P. Forte, *Evaluation of the Effect of Misalignment and Profile Modification in Face Gear Drive by a Finite Element Meshing Simulation*. Journal of Mechanical Design, 2004. **126**: p. 916.
45. *Abaqus 6.11: Analysis User's Manual*, in *Volume II: Analysis*. Dassault Systèmes.
46. *Overview of Abaqus/Explicit*. Abaqus, Inc.
47. McHenry, K. and P. Bajcsy, *An Overview of 3D Data Content, File Formats and Viewers*. 2008, Technical Report ISDA08-002.
48. *Consistent Units*. [cited 2013; Available from: <http://www.dynasupport.com/howtos/general/consistent-units>.
49. Beranek, L.L. and I.L. Vér, *Noise and Vibration Control Engineering: Principles and Application*. 1992: John Wiley & Sons, Inc.
50. *Lion-LSP System Information*. [cited 2013; Available from: <https://rcc.its.psu.edu/resources/hpc/lion-lsp/>.
51. *PBS User Guide*. [cited 2013; Available from: [http://rcc.its.psu.edu/user\\_guides/system\\_utilities/pbs/](http://rcc.its.psu.edu/user_guides/system_utilities/pbs/).
52. *Abaqus Usage Instructions*. [cited 2013; Available from: <http://rcc.its.psu.edu/resources/software/abaqus/>.
53. Mark, W.D., *The Generalized Transmission Error of Spiral Bevel Gears*. Journal of Mechanisms, Transmission, and Automation in Design, 1987. **109**: p. 275-282.
54. DeSmidt, H. and J. Zhao, *Extension-Twist Coupled Graphite/Epoxy Composite Driveshafts for Gear-Mesh Vibration Suppression*, in *American Helicopter Society 66th Annual Forum*. 2010, American Helicopter Society International, Inc.: Phoenix, AZ.